Nuclear structure observables calculated with Gogny energy density functionals

Tomás R. Rodríguez

ISOL-France Workshop IV

March 11th, 2022

CIAFF
Centro de Investigación Avanzada en Física Fundamental

UAM Universidad Autónoma de Madrid

Universidad Autónoma de Madrid
Departamento de Física Teórica

Outline

Outline

Introduction

The nuclear many-body problem is… a **huge** problem!

- The nuclear interaction is problematic

- The quantum *A*-body system is problematic

We rely on models!

personal note: even in the *ab initio* world

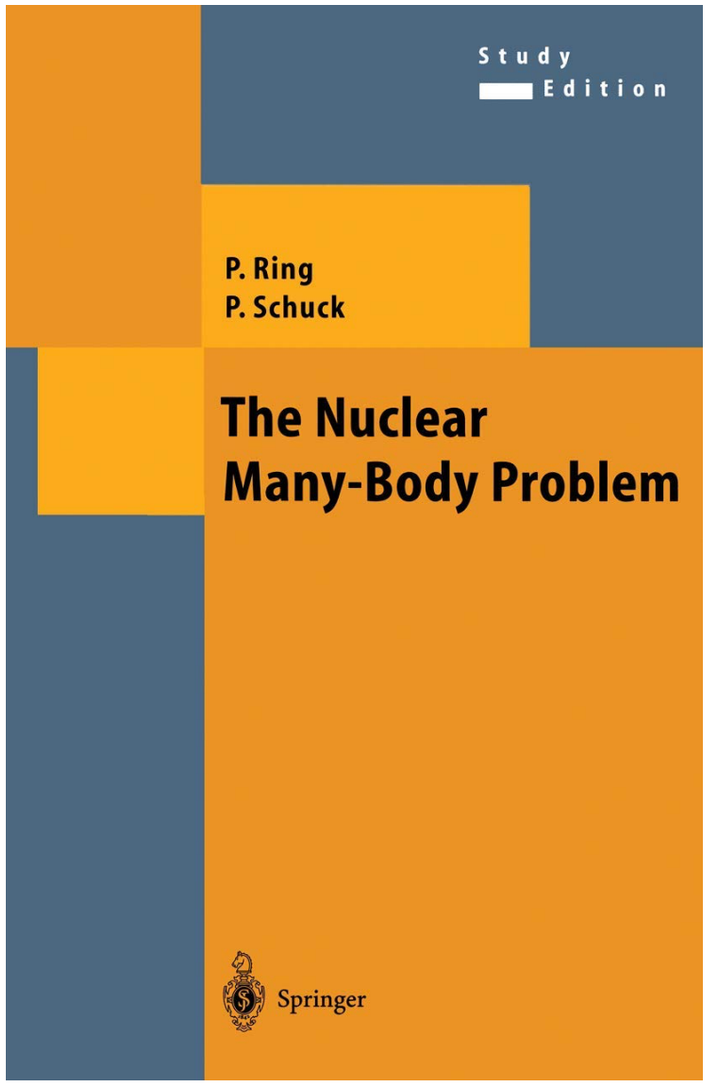

Introduction

Let us assume that *we know* the nuclear interaction. Exact nuclear wave functions and energies cannot be obtained in general because of:

a) the exploding dimensionality of the many-body Hilbert space

b) the huge amount of two-, three- (eventually, *N*-) body matrix elements that are impossible to store

Most widely used *solutions* to attack these problems:

- **Valence-space (Shell Model) calculations** with phenomenological (or normal-ordered, SRG evolved) two-body Hamiltonians
- **Approximate methods (variational)** with phenomenological interactions (or energy density functionals)

Introduction

Let us assume that *we know* the nuclear interaction. Exact nuclear wave functions and energies cannot be obtained in general because of:

a) the exploding dimensionality of the many-body Hilbert space

b) the huge amount of two-, three- (eventually, *N*-) body matrix elements that are impossible to store

Most widely used *solutions* to attack these problems:

- **Valence-space (Shell Model) calculations** with phenomenological (or normal-ordered, SRG evolved) two-body Hamiltonians

- **Approximate methods (variational)** with phenomenological interactions (or energy density functionals)

Introduction

- Effective nucleon-nucleon interaction: Gogny force (D1S/D1M)

$$V(1,2) = \sum_{i=1}^{2} e^{-(\vec{r}_1-\vec{r}_2)^2/\mu_i^2} \left(W_i + B_i P^\sigma - H_i P^\tau - M_i P^\sigma P^\tau\right)$$
$$+iW_0(\sigma_1+\sigma_2)\vec{k}\times\delta(\vec{r}_1-\vec{r}_2)\vec{k} + V_{\text{Coulomb}}(\vec{r}_1,\vec{r}_2)$$

2-body potential

$$+t_3(1+x_0P^\sigma)\delta(\vec{r}_1-\vec{r}_2)\rho^\alpha\left((\vec{r}_1+\vec{r}_2)/2\right)$$

Density dependent term

- Other alternatives: Skyrme, relativistic Lagrangians, BCPM, ...

Outline

Outline

PGCM with axial quadrupole+octupole

- Initial intrinsic states: PN-VAP

$$E[\Phi] = \langle\Phi|\hat{H}_{2b}|\Phi\rangle + \varepsilon_{DD}^{N,Z}(\Phi) - \lambda_N\langle\Phi|\hat{N}|\Phi\rangle - \lambda_Z\langle\Phi|\hat{Z}|\Phi\rangle - \lambda_{q_{20}}\langle\Phi|\hat{Q}_{20}|\Phi\rangle - \lambda_{q_{30}}\langle\Phi|\hat{Q}_{30}|\Phi\rangle$$

- Intermediate Parity, Particle Number and Angular Momentum Projected states

axial quadrupole term!! octupole term!!

$$|I;NZ;\Pi;\beta_2,\beta_3\rangle = \frac{2I+1}{2}\int_0^\pi d_{00}^{I*}(\beta)e^{-i\beta\hat{J}_y}\hat{P}^N\hat{P}^Z\hat{P}^\Pi|\Phi\rangle d\beta$$

- Final GCM states

$$|I;NZ;\Pi;\sigma\rangle = \sum_{\beta_2\beta_3} f_{\beta_2\beta_3}^{I;NZ;\Pi;\sigma}|I;NZ;\Pi;\beta_2,\beta_3\rangle$$

$$\sum_{\beta_2'\beta_3'}\left(\mathcal{H}_{\beta_2\beta_3,\beta_2'\beta_3'}^{I;NZ;\Pi} - E^{I;NZ;\Pi;\sigma}\mathcal{N}_{\beta_2\beta_3,\beta_2'\beta_3'}^{I;NZ;\Pi}\right) f_{\beta_2'\beta_3'}^{I;NZ;\Pi;\sigma} = 0$$

$$\mathcal{N}_{\beta_2\beta_3,\beta_2'\beta_3'}^{I;NZ;\Pi} = \langle I;NZ;\Pi;\beta_2,\beta_3|I;NZ;\Pi;\beta_2',\beta_3'\rangle$$

$$\mathcal{H}_{\beta_2\beta_3,\beta_2'\beta_3'}^{I;NZ;\Pi} = \langle I;NZ;\Pi;\beta_2,\beta_3|\hat{H}_{2b}|I;NZ;\Pi;\beta_2',\beta_3'\rangle + \varepsilon_{DD}^{I;NZ;\Pi}(\Phi(\beta_2,\beta_3),\Phi(\beta_2',\beta_3'))$$

HFB energy surface

Example: ^{144}Ba axial calculations

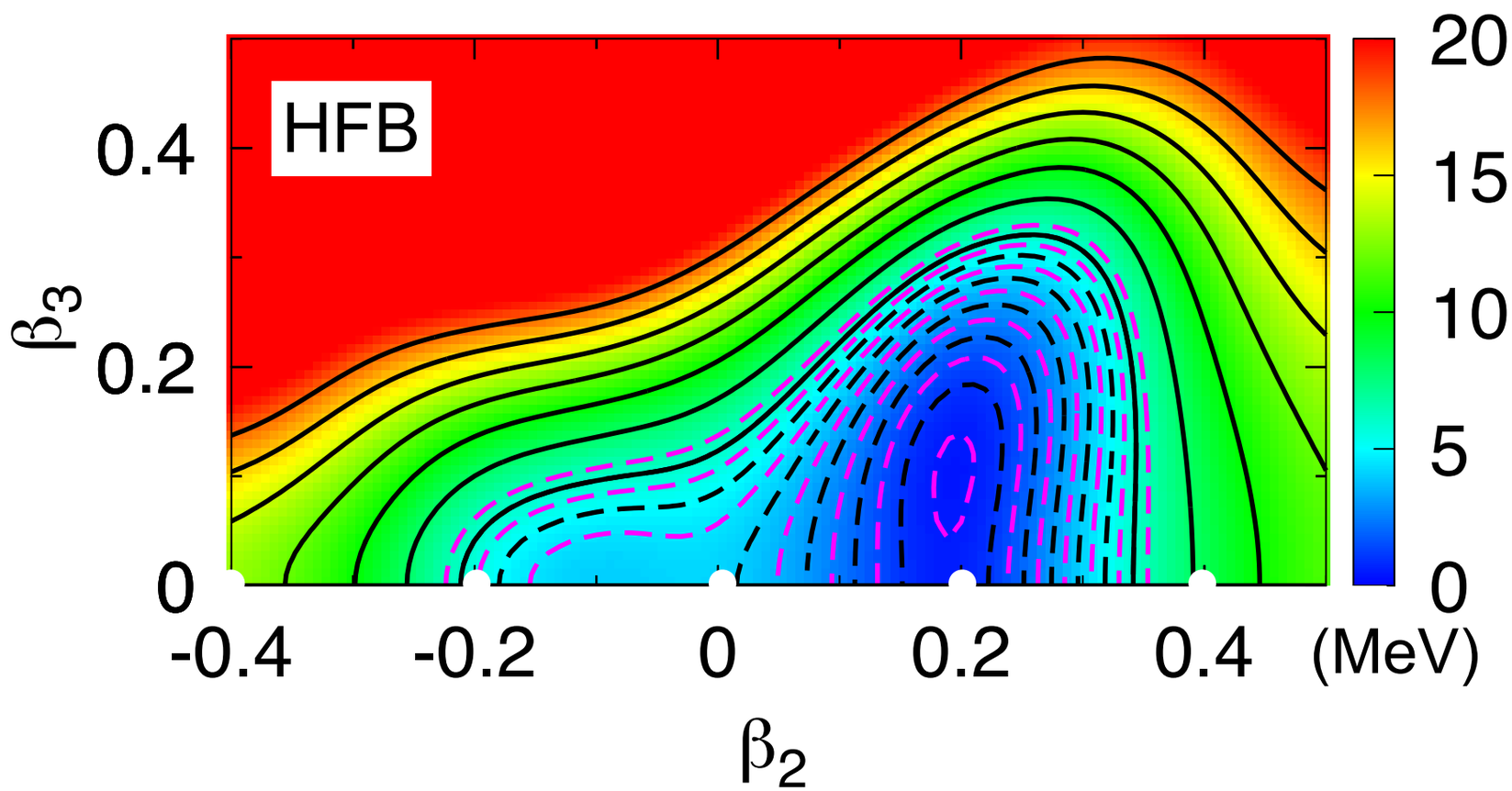

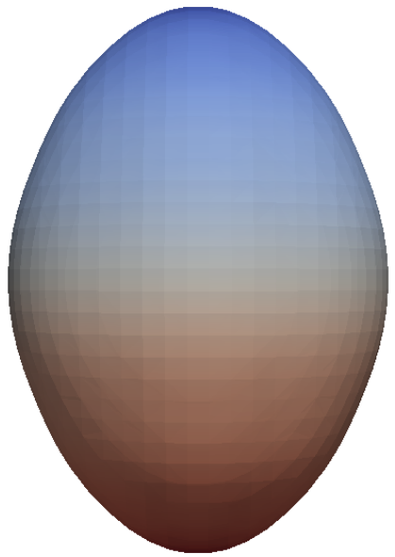

R. Bernard, L. M. Robledo, T. R. R., PRC (2016)

HFB energy surface

Example: ^{144}Ba axial calculations

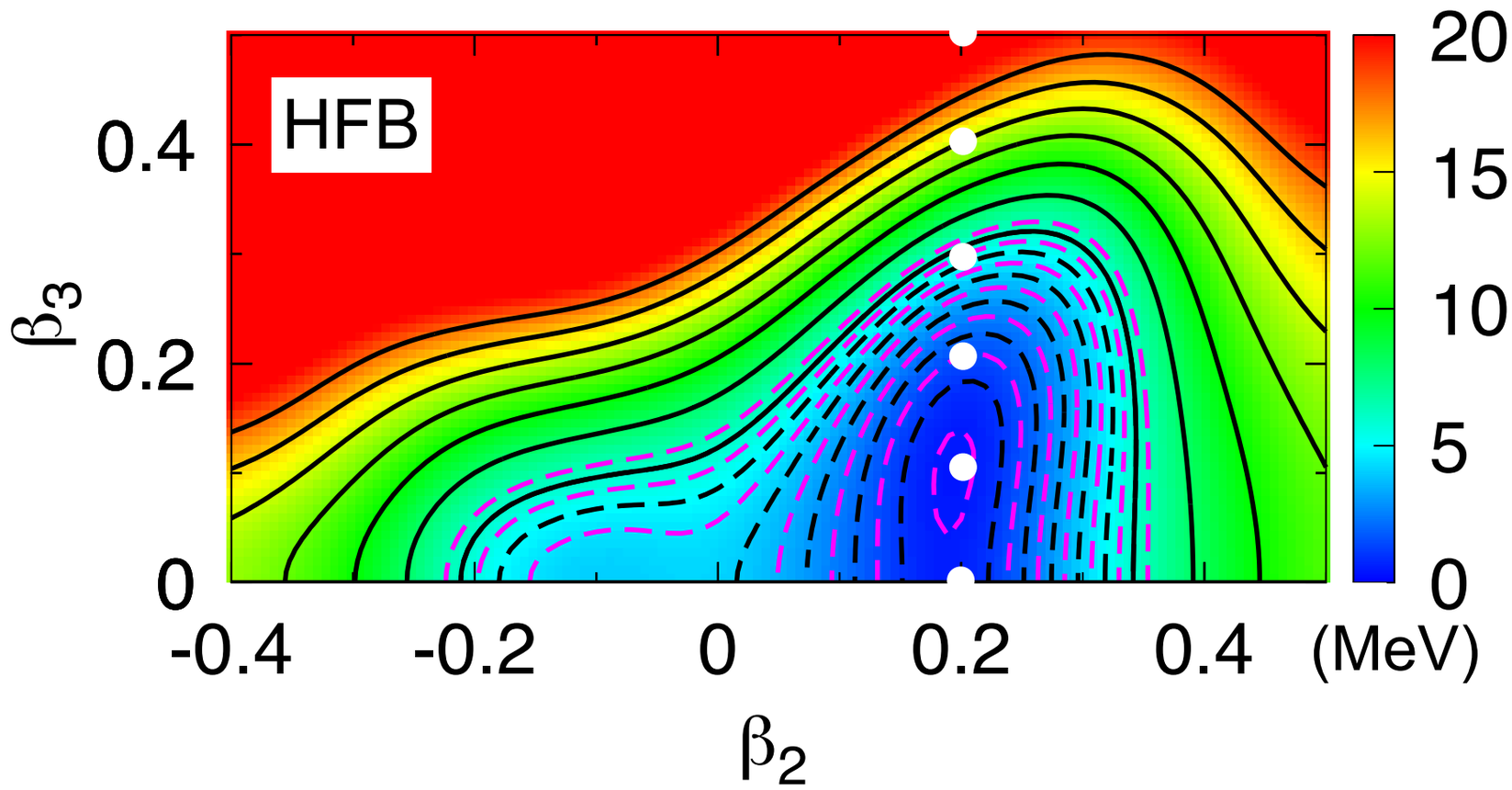

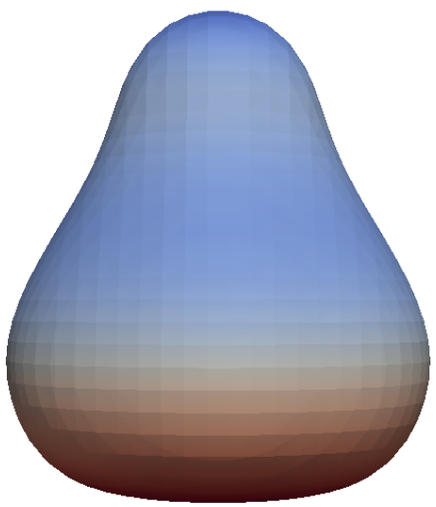

R. Bernard, L. M. Robledo, T. R. R., PRC (2016)

P+PN+AM projected energy surfaces

Example: ^{144}Ba axial calculations

Particle number, angular momentum and parity projected PES

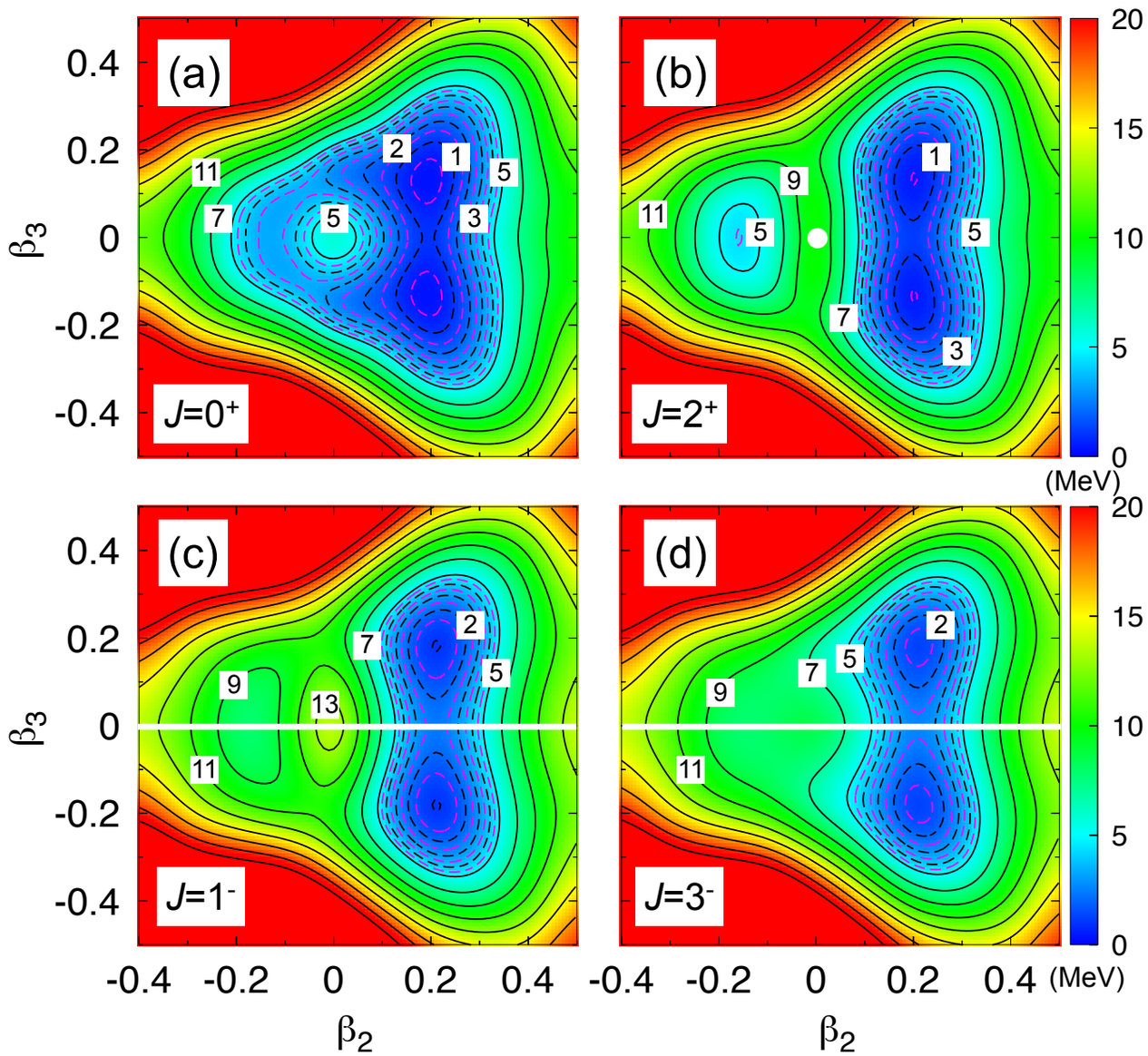

R. Bernard, L. M. Robledo, T. R. R., PRC (2016)

Collective wave functions

Example: ^{144}Ba axial calculations

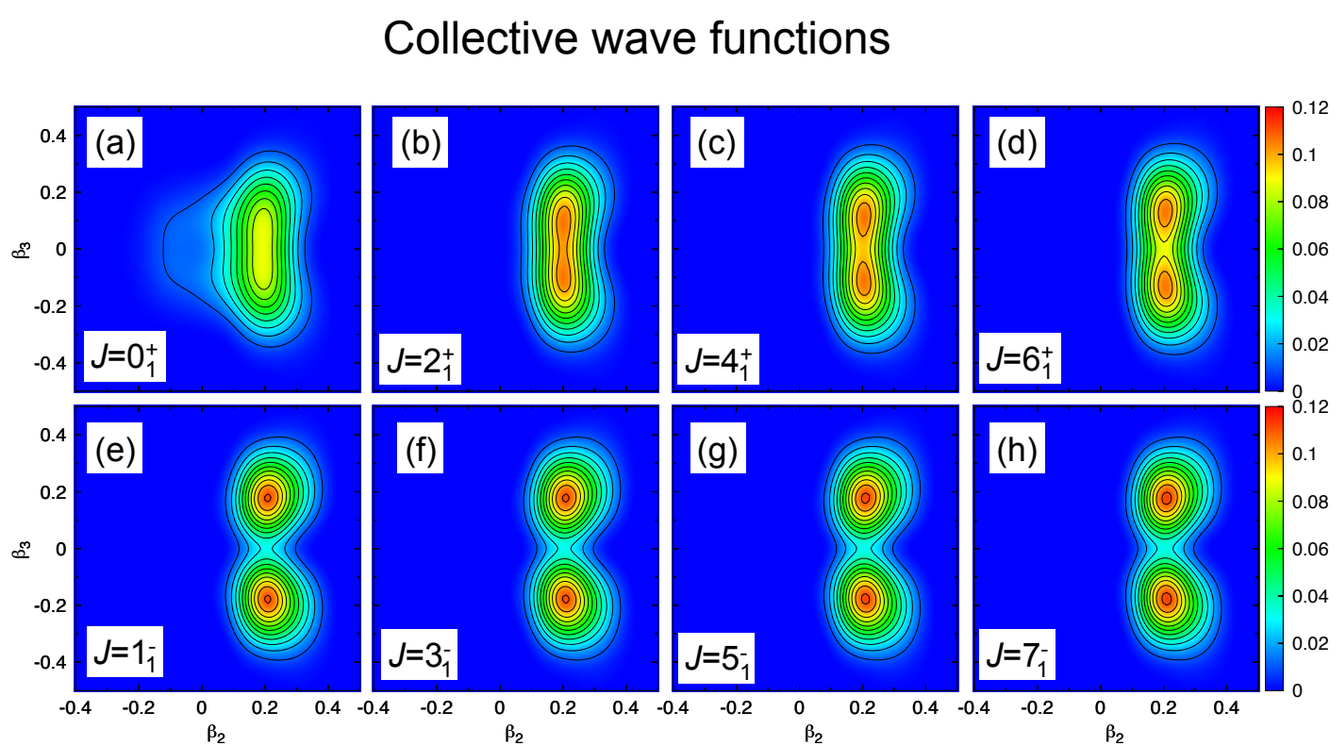

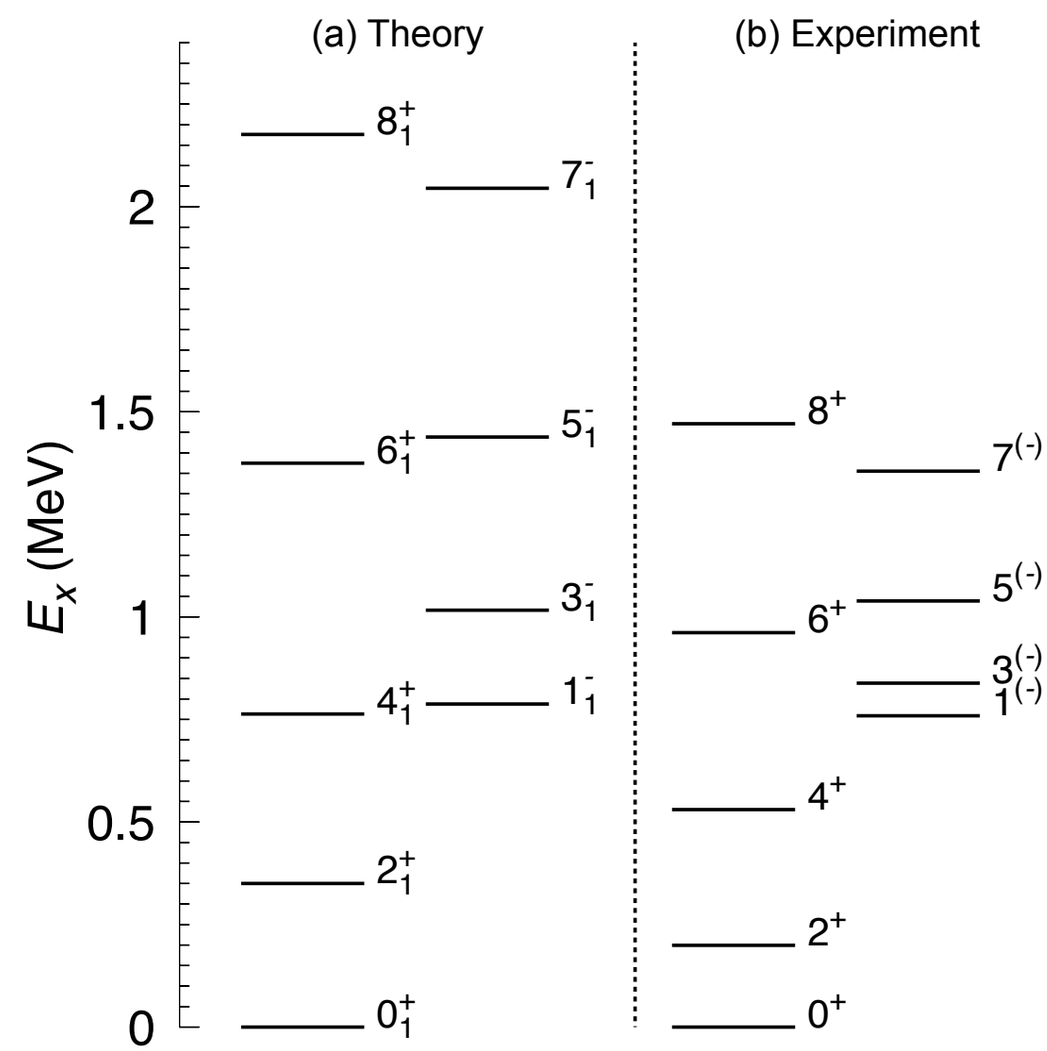

R. Bernard, L. M. Robledo, T. R. R., PRC (2016)

Results: Transition probabilities.

^{144}Ba

$J_i^\pi \to J_f^\pi$	$E\lambda$	GCM β_2	GCM β_3	GCM $\beta_2 - \beta_3$	Exp
$0^+ \to 2^+$	E2	1.148	1.121	1.023	1.042^{+17}_{-22}
$2^+ \to 4^+$	E2	1.865	1.803	1.845	1.860^{+86}_{-81}
$4^+ \to 6^+$	E2	2.371	2.287	2.360	1.78^{+12}_{-10}
$6^+ \to 8^+$	E2	2.800	2.696	2.793	2.04^{+35}_{-23}
$0^+ \to 1^-$	E1	0.007	0.006	0.008	
$1^- \to 2^+$	E1	0.005	0.009	0.006	
$0^+ \to 3^-$	E3	0.450	0.477	0.460	0.65^{+17}_{-23}
$1^- \to 4^+$	E3	0.599	0.635	0.695	
$2^+ \to 5^-$	E3	0.708	0.745	0.810	< 1.2
$3^- \to 6^+$	E3	0.804	0.865	0.810	
$4^+ \to 7^-$	E3	0.887	0.945	1.031	< 1.6

TABLE I. Absolute values of the transition matrix elements $|\langle J_i^\pi || E\lambda || J_f^\pi \rangle|$ (in $eb^{\lambda/2}$) for several transitions of interest. The experimental values are taken from [29].

R. Bernard, L. M. Robledo, T. R. R., PRC 93, 054316 (2016)

^{146}Ba

TABLE I. The experimental $|\langle I_f^\pi \| \hat{M}_\lambda \| I_i^\pi \rangle|$ matrix elements ($e \cdot b^{\lambda/2}$) based on the GOSIA fit along with new symmetry-conserving configuration-mixing calculations (see text and Ref. [23] for details).

$I_i^\pi \to I_f^\pi$	$E\lambda$	Experimental	SCCM
$0^+ \to 1^-$	$E1$	$0.000223\binom{10}{-8}$ [a]	0.00474
$1^- \to 3^-$	$E2$	1.2(5)	1.6
$0^+ \to 2^+$	$E2$	1.17(2) [a]	1.14
$2^+ \to 4^+$	$E2$	1.97(14)	1.90
$4^+ \to 6^+$	$E2$	$2.35\binom{+20}{-24}$	2.43
$6^+ \to 8^+$	$E2$	$2.17\binom{+65}{-33}$	2.90
$0^+ \to 3^-$	$E3$	$0.65\binom{+14}{-20}$	0.54
$2^+ \to 5^-$	$E3$	$1.01\binom{+61}{-20}$	0.87
$4^+ \to 7^-$	$E3$	$1.25\binom{+85}{-34}$	1.11
$6^+ \to 9^-$	$E3$	$1.5\binom{+8}{-12}$	

[a] Primarily determined by previous lifetime and/or branching ratio data [10].

B. Bucher et al., PRL 118, 152504 (2017).

HFB energy surfaces

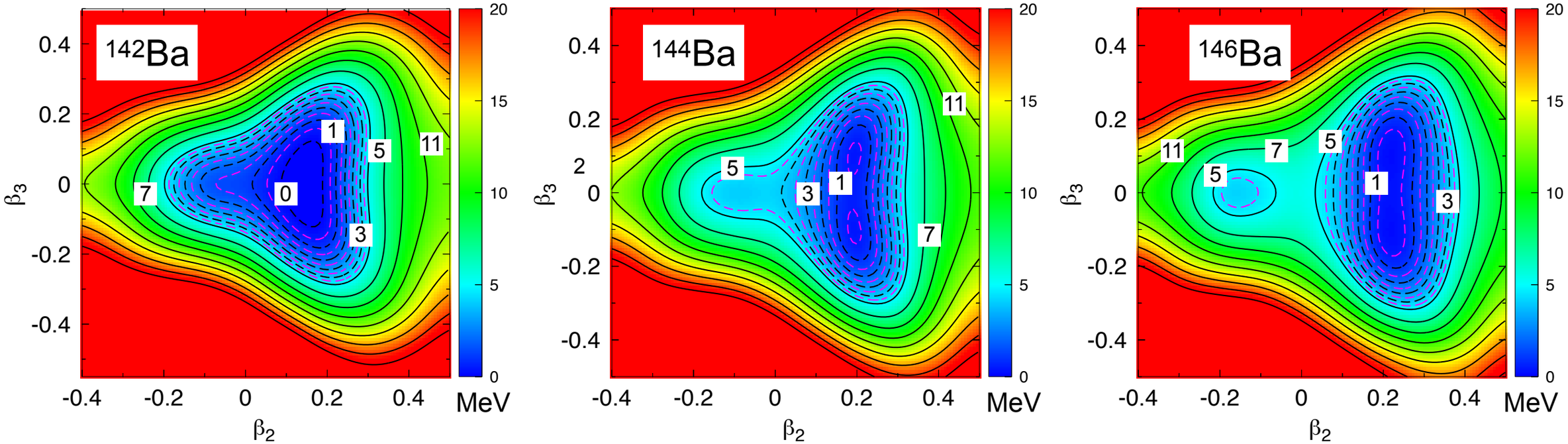

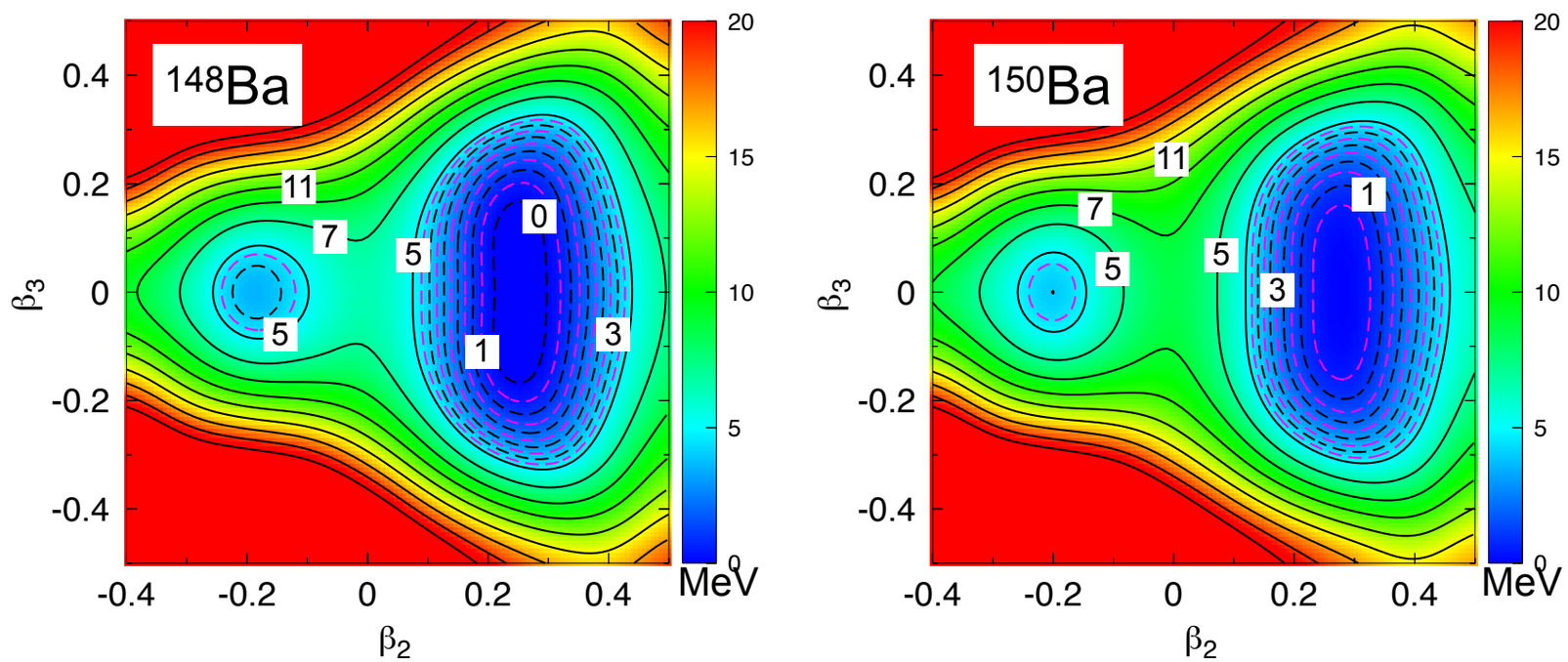

Collective wave functions

^{142}Ba

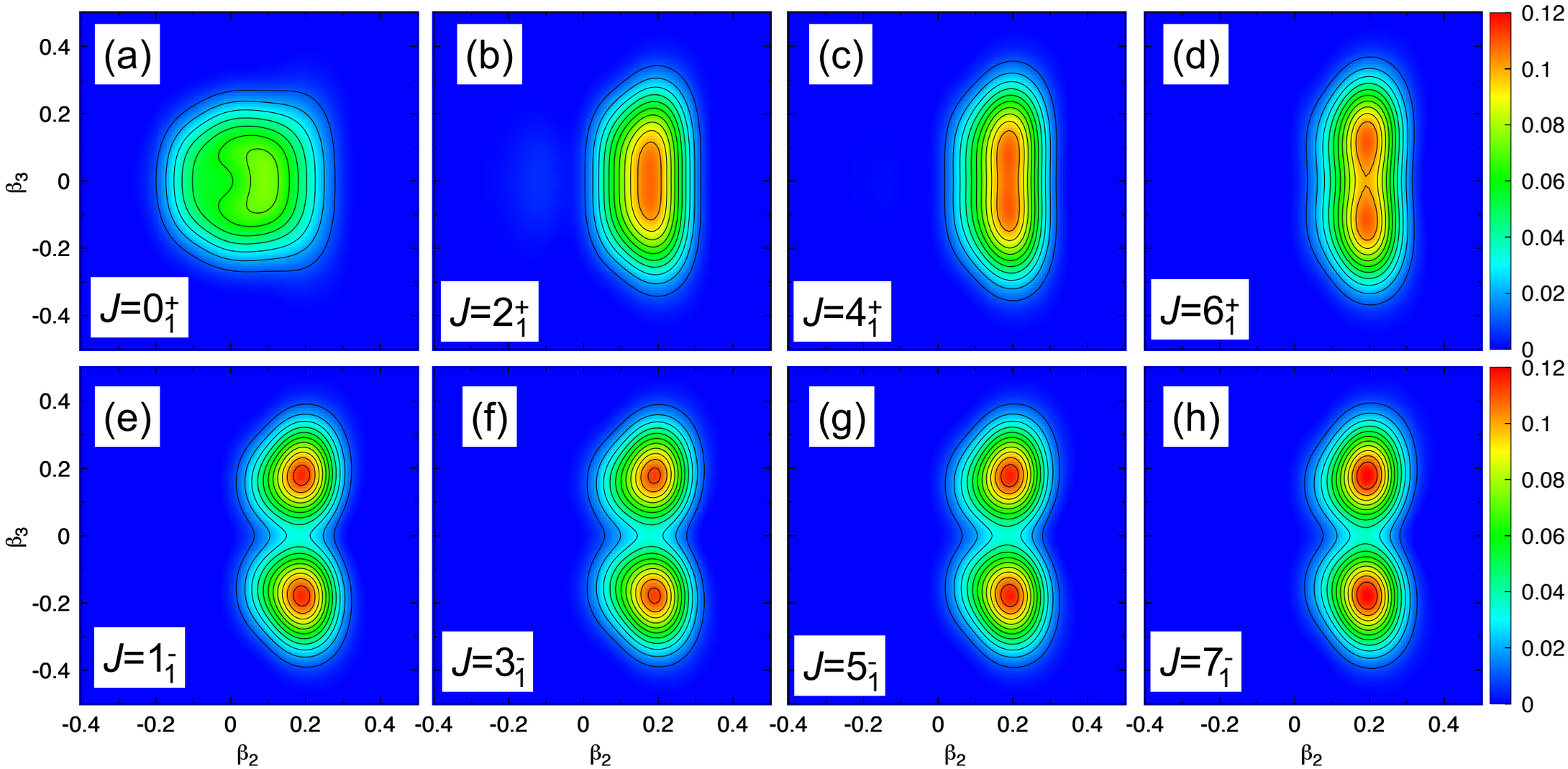

Collective wave functions

^{144}Ba

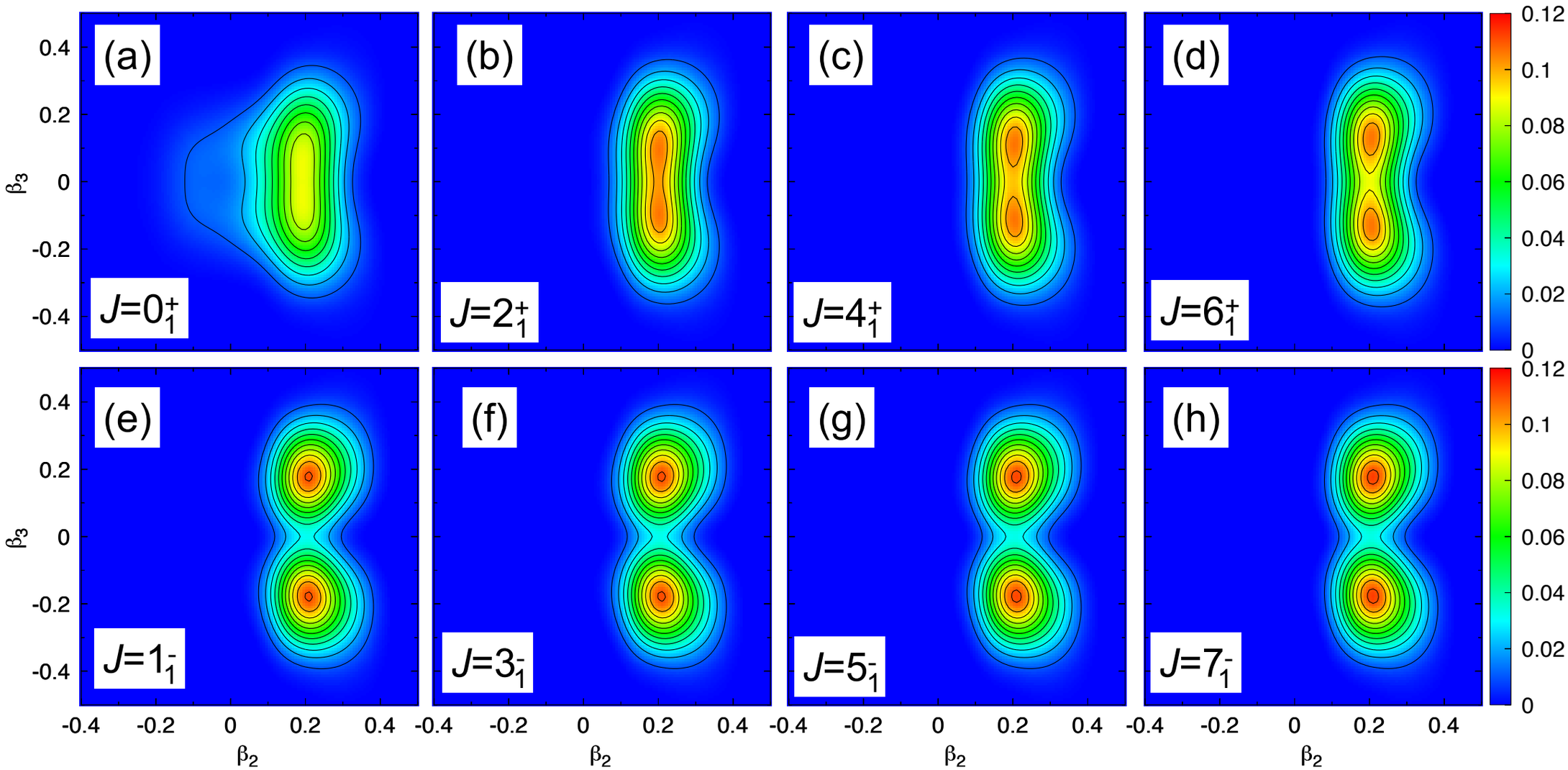

Collective wave functions

^{146}Ba

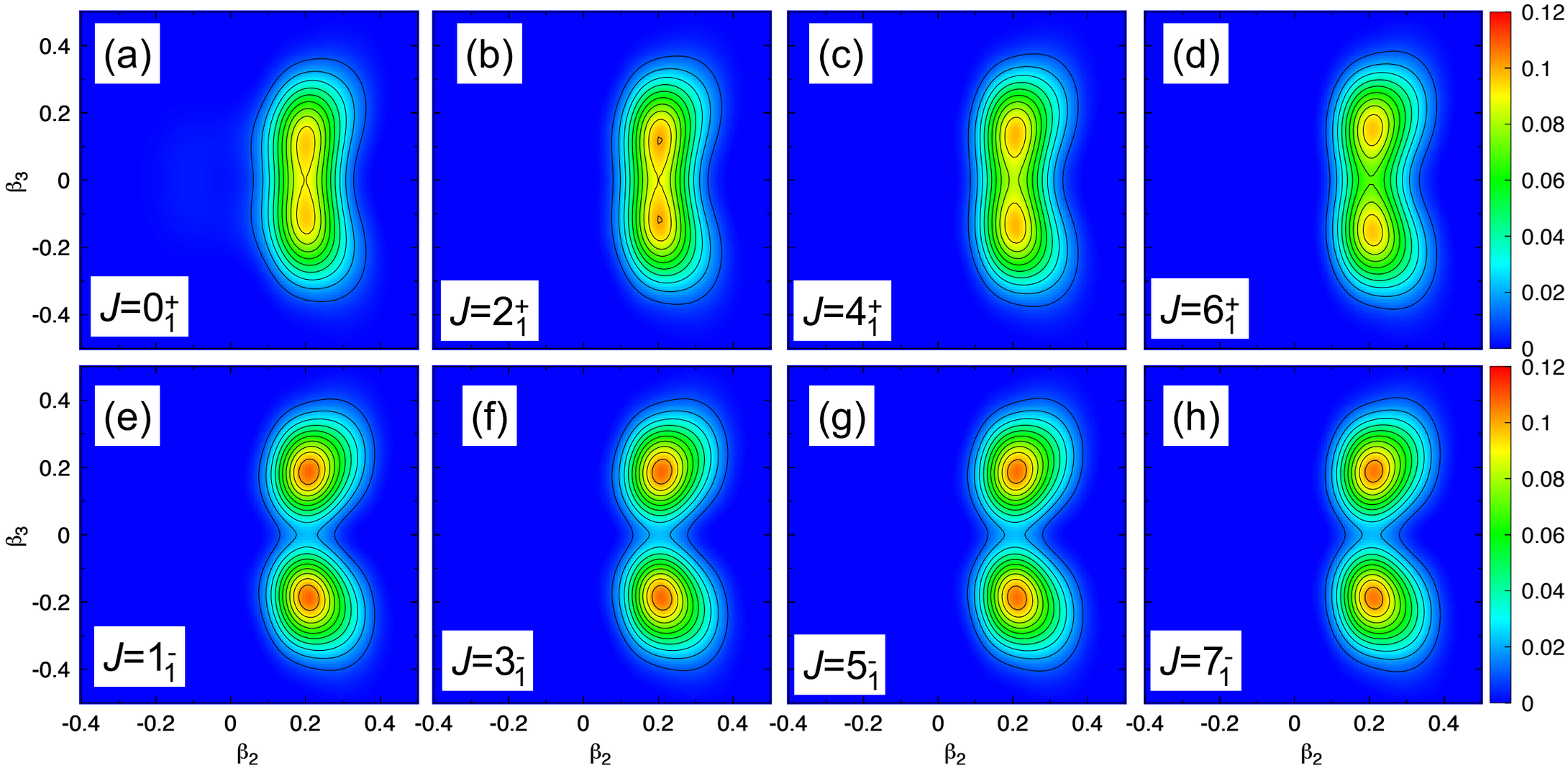

Collective wave functions

^{148}Ba

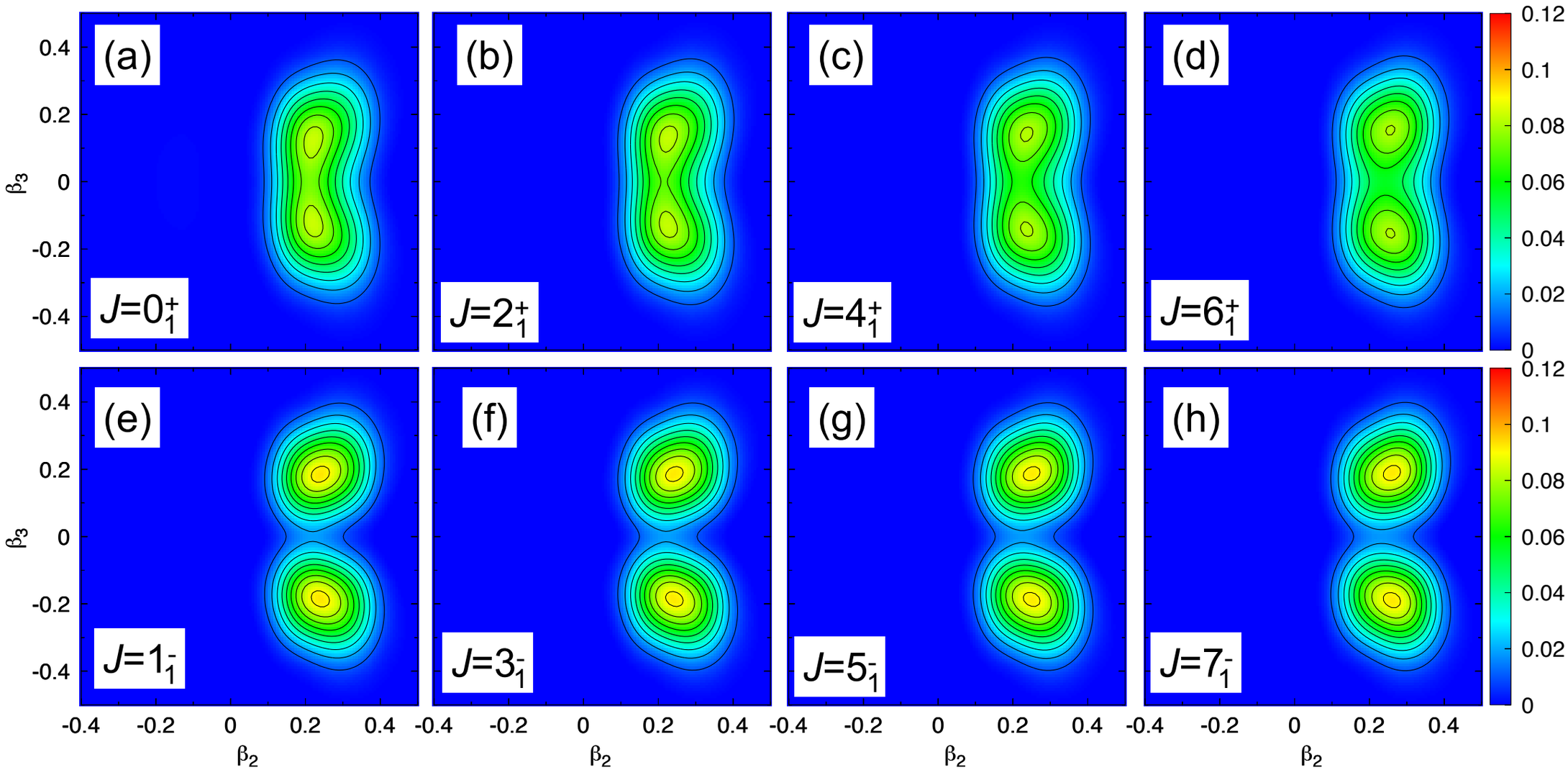

Collective wave functions

^{150}Ba

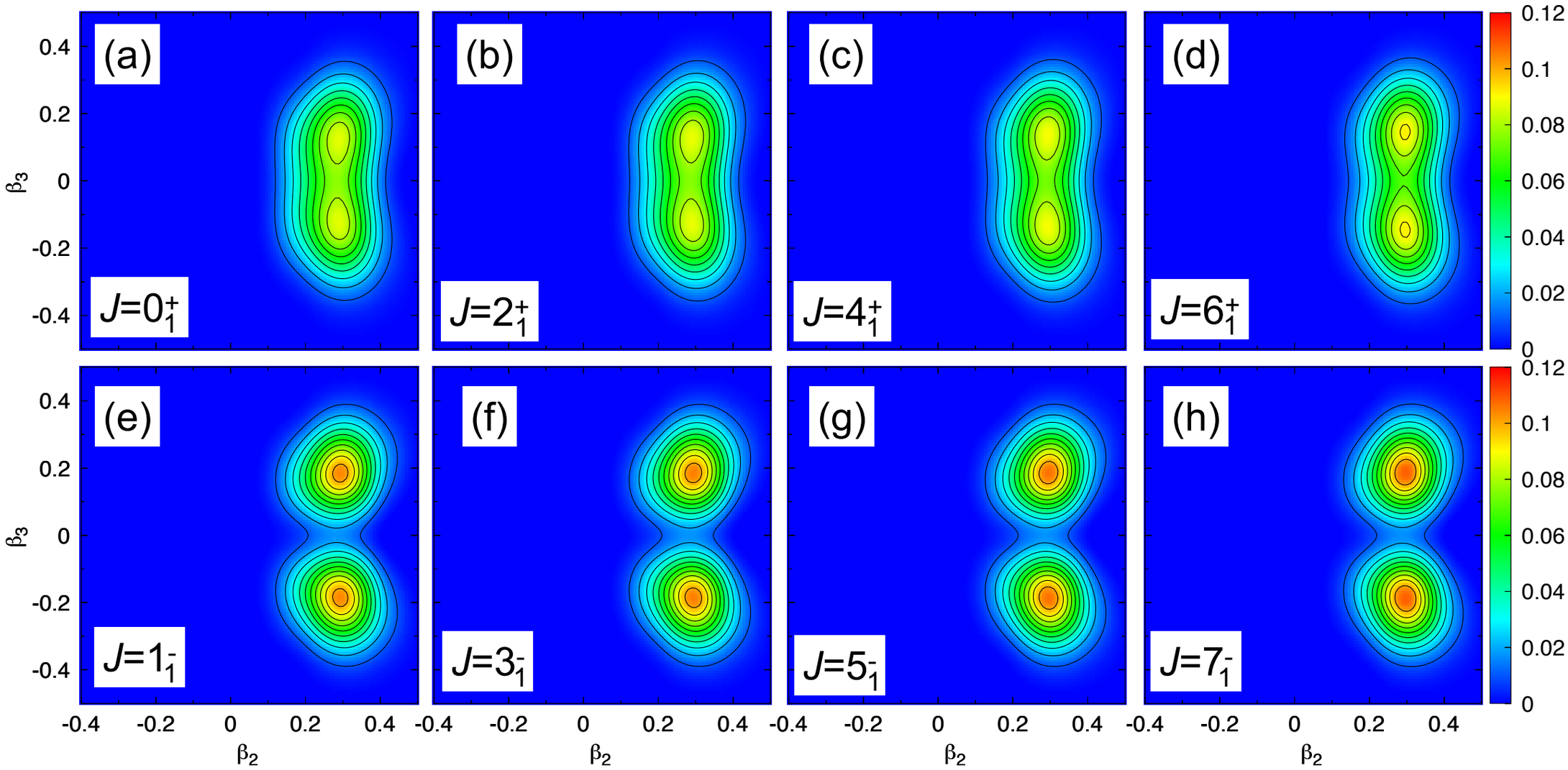

PGCM with axial quadrupole+octupole

- ➡ Good qualitative reproduction of the trends in the excitation energies for positive and negative parity bands
- ➡ Increase of collectivity when increasing the number of neutrons
- ➡ Sharper transition from spherical to deformed nuclei in theory than in the experiments

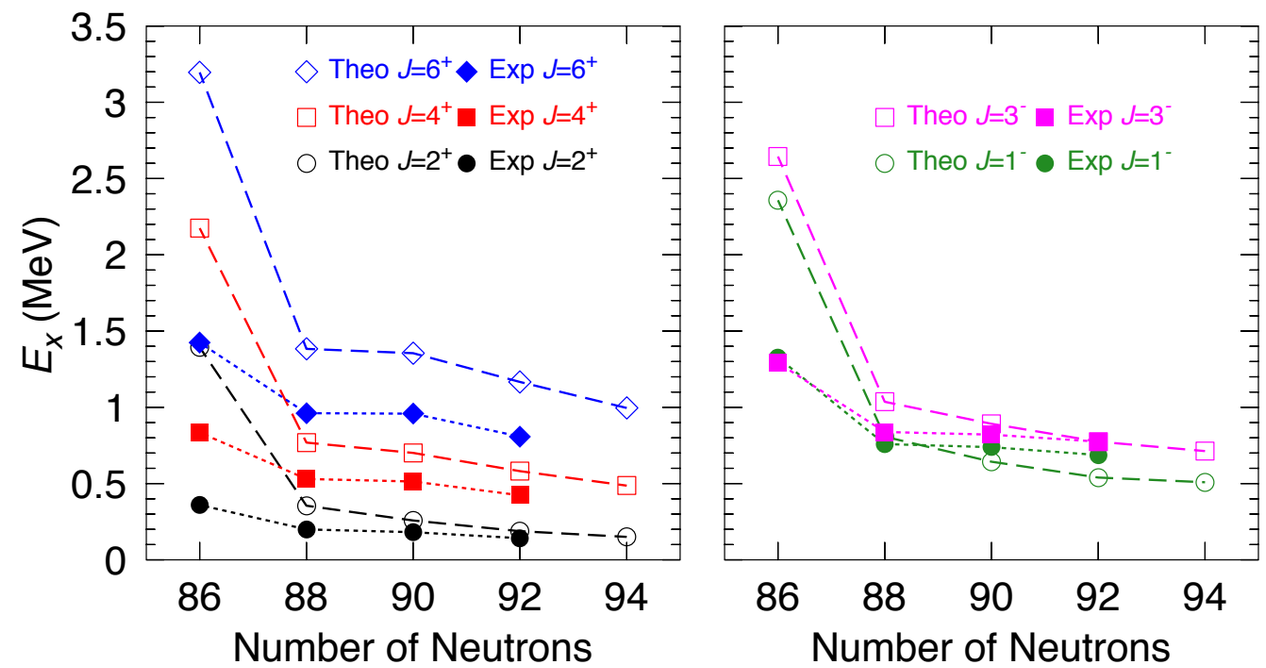

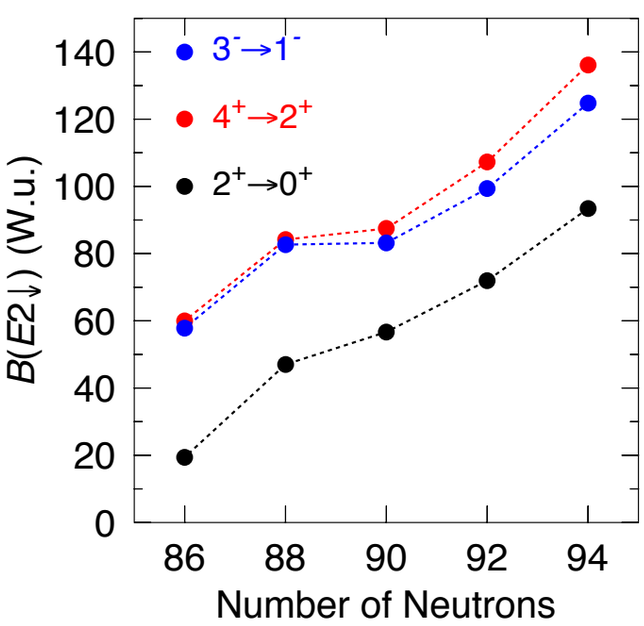

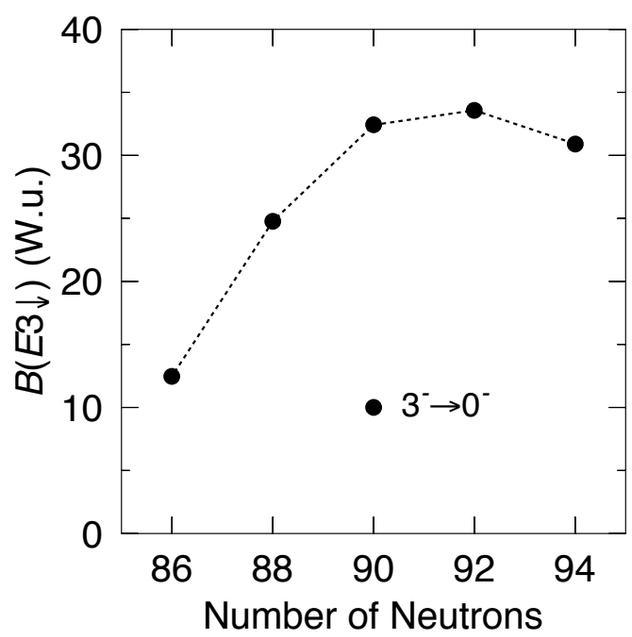

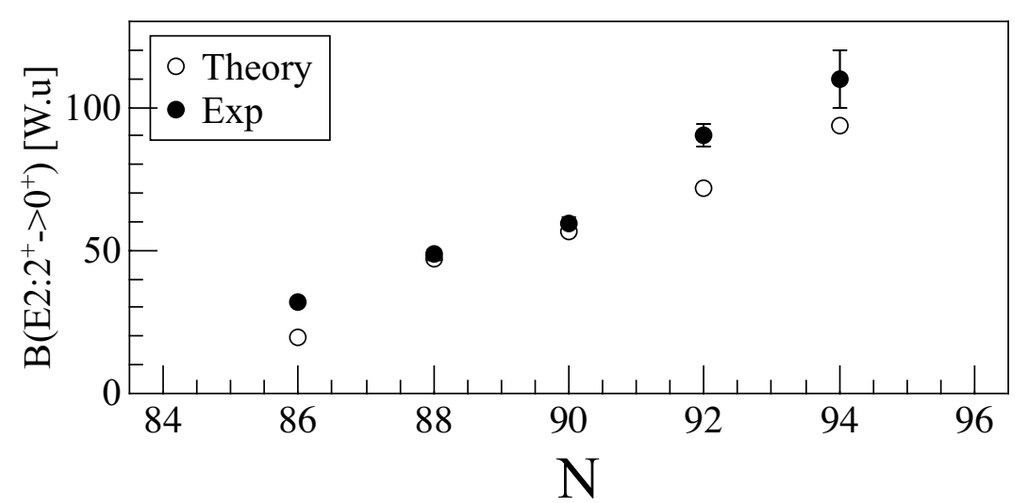

R. Lica et al., Phys. Rev. C (2018)

Outline

PGCM with triaxial quadrupole

- Initial intrinsic states: PN-VAP M. Anguiano, J. L. Egido, and L. M. Robledo, Nucl. Phys. A 696, 467 (2001).

$$E^{N,Z}[\Phi] = \frac{\langle\Phi|\hat{H}_{2b}\hat{P}^N\hat{P}^Z|\Phi\rangle}{\langle\Phi|\hat{P}^N\hat{P}^Z|\Phi\rangle} + \varepsilon_{DD}^{N,Z}(\Phi) - \lambda_{q_{20}}\langle\Phi|\hat{Q}_{20}|\Phi\rangle - \lambda_{q_{22}}\langle\Phi|\hat{Q}_{22}|\Phi\rangle$$

- Intermediate Particle Number and Angular Momentum Projected states

$$|IMK;NZ;\beta\gamma\rangle = \frac{2I+1}{8\pi^2}\int \mathcal{D}^{I*}_{MK}(\Omega)\hat{R}(\Omega)\hat{P}^N\hat{P}^Z|\Phi(\beta,\gamma)\rangle d\Omega$$

- Final GCM states

$$|IM;NZ\sigma\rangle = \sum_{K\beta\gamma} f^{I;NZ,\sigma}_{K\beta\gamma}|IMK;NZ;\beta\gamma\rangle$$

$$\sum_{K'\beta'\gamma'}\left(\mathcal{H}^{I;NZ}_{K\beta\gamma K'\beta'\gamma'} - E^{I;NZ;\sigma}\mathcal{N}^{I;NZ}_{K\beta\gamma K'\beta'\gamma'}\right) f^{I;NZ;\sigma}_{K'\beta'\gamma'} = 0$$

$$\begin{aligned}
\mathcal{N}^{I;NZ}_{K\beta\gamma K'\beta'\gamma'} &\equiv \langle IMK;NZ;\beta\gamma|IMK';NZ;\beta'\gamma'\rangle \\
\mathcal{H}^{I;NZ}_{K\beta\gamma K'\beta'\gamma'} &\equiv \langle IMK;NZ;\beta\gamma|\hat{H}_{2b}|IMK';NZ;\beta'\gamma'\rangle + \varepsilon_{DD}^{IKK';NZ}[\Phi(\beta,\gamma),\Phi'(\beta',\gamma')]
\end{aligned}$$

PN-VAP energy surfaces

Example: Multiple shape coexistence in ^{80}Zr

$$\delta E^{N,Z}\left[\bar{\Phi}(\beta,\gamma)\right]\Big|_{\bar{\Phi}=\Phi} = 0$$

$$E^{N,Z}[\Phi] = \frac{\langle\Phi|\hat{H}_{2b}\hat{P}^N\hat{P}^Z|\Phi\rangle}{\langle\Phi|\hat{P}^N\hat{P}^Z|\Phi\rangle} + \varepsilon_{DD}^{N,Z}(\Phi) - \lambda_{q_{20}}\langle\Phi|\hat{Q}_{20}|\Phi\rangle - \lambda_{q_{22}}\langle\Phi|\hat{Q}_{22}|\Phi\rangle$$

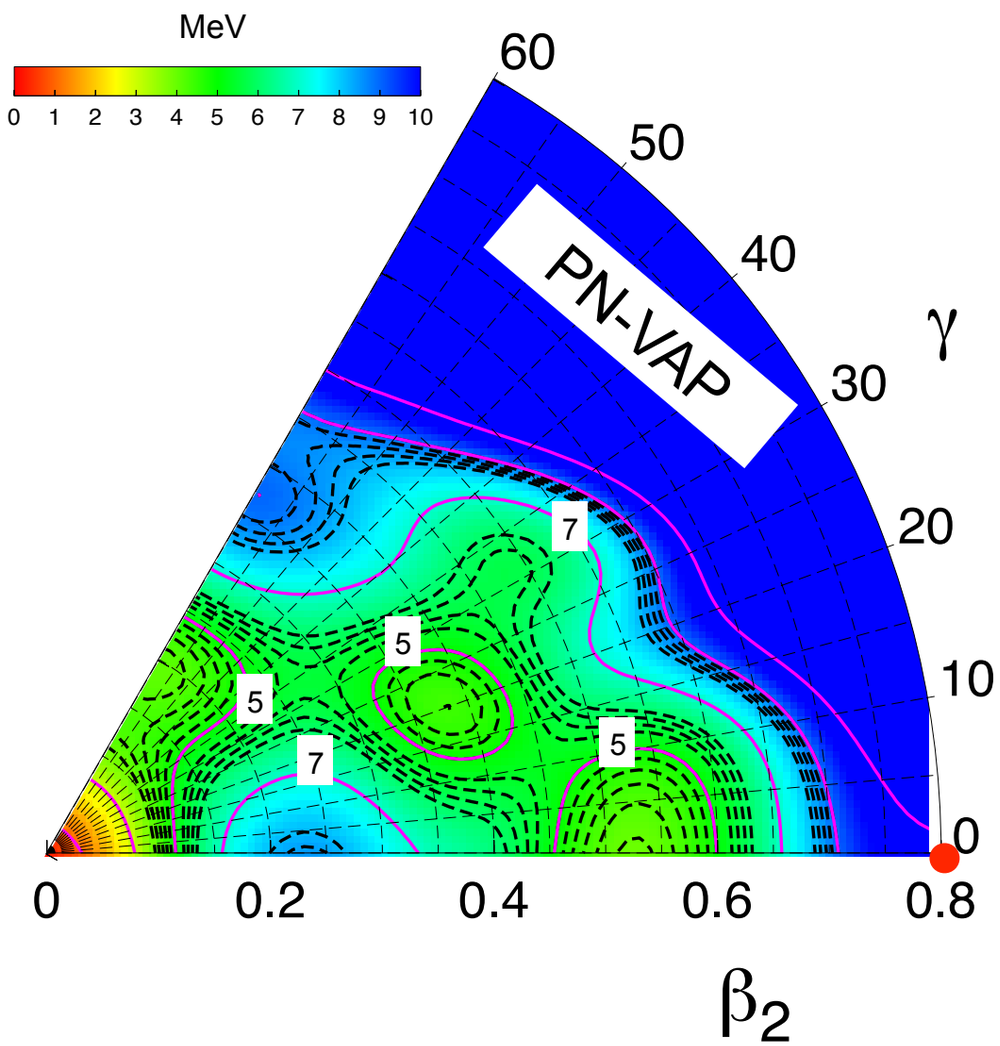

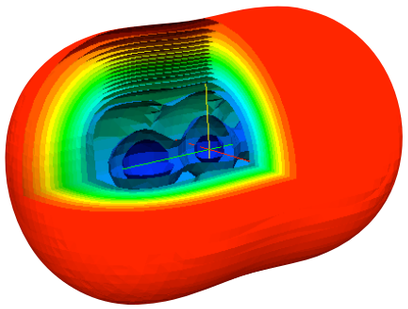

PN-VAP energy surfaces

Example: Multiple shape coexistence in ^{80}Zr

$$\delta E^{N,Z}\left[\bar{\Phi}(\beta,\gamma)\right]\Big|_{\bar{\Phi}=\Phi} = 0$$

$$E^{N,Z}[\Phi] = \frac{\langle\Phi|\hat{H}_{2b}\hat{P}^N\hat{P}^Z|\Phi\rangle}{\langle\Phi|\hat{P}^N\hat{P}^Z|\Phi\rangle} + \varepsilon_{DD}^{N,Z}(\Phi) - \lambda_{q_{20}}\langle\Phi|\hat{Q}_{20}|\Phi\rangle - \lambda_{q_{22}}\langle\Phi|\hat{Q}_{22}|\Phi\rangle$$

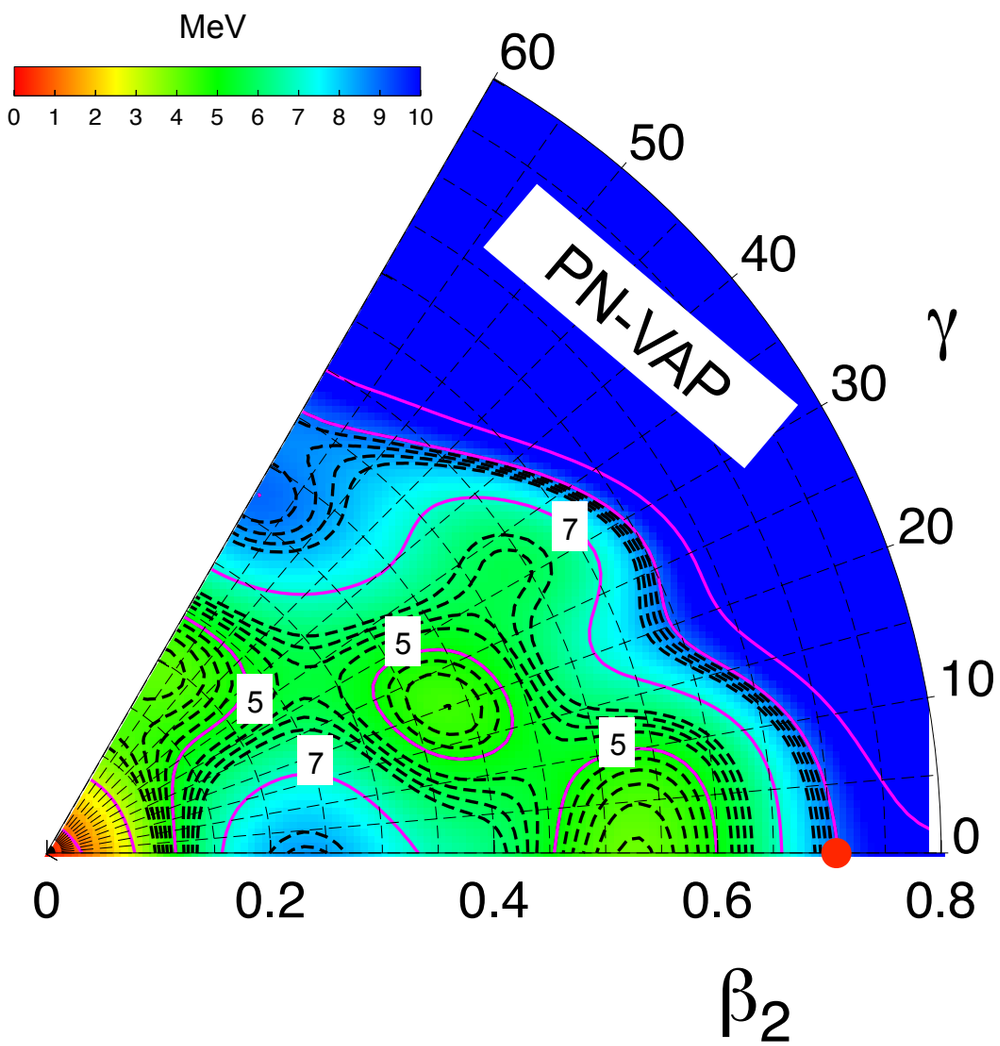

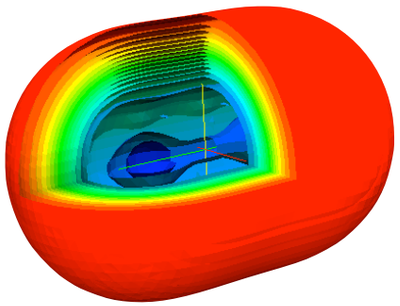

PN-VAP energy surfaces

Example: Multiple shape coexistence in ^{80}Zr

$$\delta E^{N,Z}\left[\bar{\Phi}(\beta,\gamma)\right]\Big|_{\bar{\Phi}=\Phi} = 0$$

$$E^{N,Z}[\Phi] = \frac{\langle\Phi|\hat{H}_{2b}\hat{P}^N\hat{P}^Z|\Phi\rangle}{\langle\Phi|\hat{P}^N\hat{P}^Z|\Phi\rangle} + \varepsilon_{DD}^{N,Z}(\Phi) - \lambda_{q_{20}}\langle\Phi|\hat{Q}_{20}|\Phi\rangle - \lambda_{q_{22}}\langle\Phi|\hat{Q}_{22}|\Phi\rangle$$

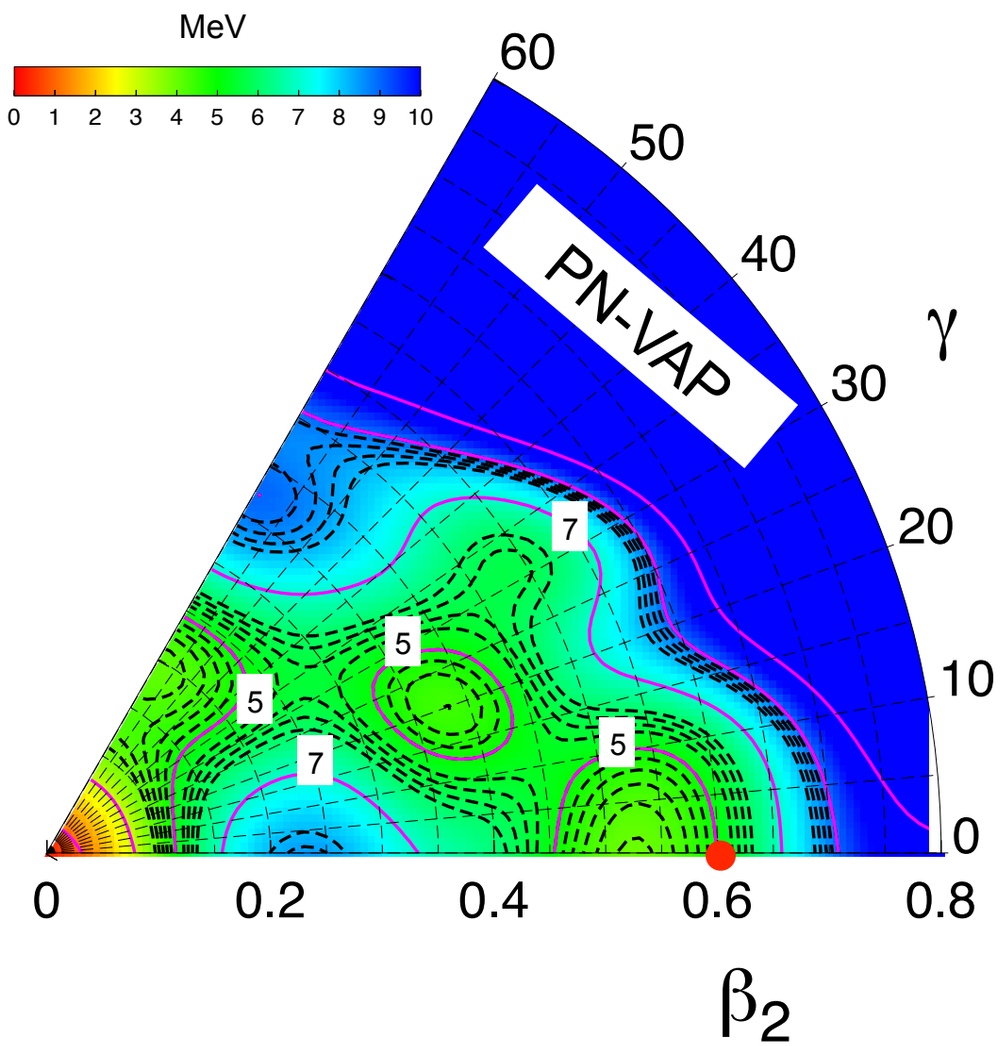

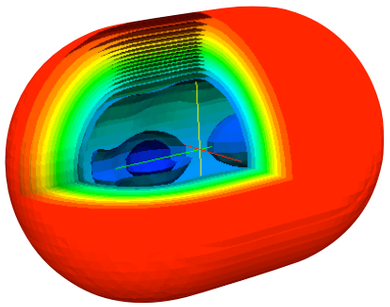

PN-VAP energy surfaces

Example: Multiple shape coexistence in ^{80}Zr

$$\delta E^{N,Z}\left[\bar{\Phi}(\beta,\gamma)\right]\Big|_{\bar{\Phi}=\Phi} = 0$$

$$E^{N,Z}[\Phi] = \frac{\langle\Phi|\hat{H}_{2b}\hat{P}^N\hat{P}^Z|\Phi\rangle}{\langle\Phi|\hat{P}^N\hat{P}^Z|\Phi\rangle} + \varepsilon_{DD}^{N,Z}(\Phi) - \lambda_{q_{20}}\langle\Phi|\hat{Q}_{20}|\Phi\rangle - \lambda_{q_{22}}\langle\Phi|\hat{Q}_{22}|\Phi\rangle$$

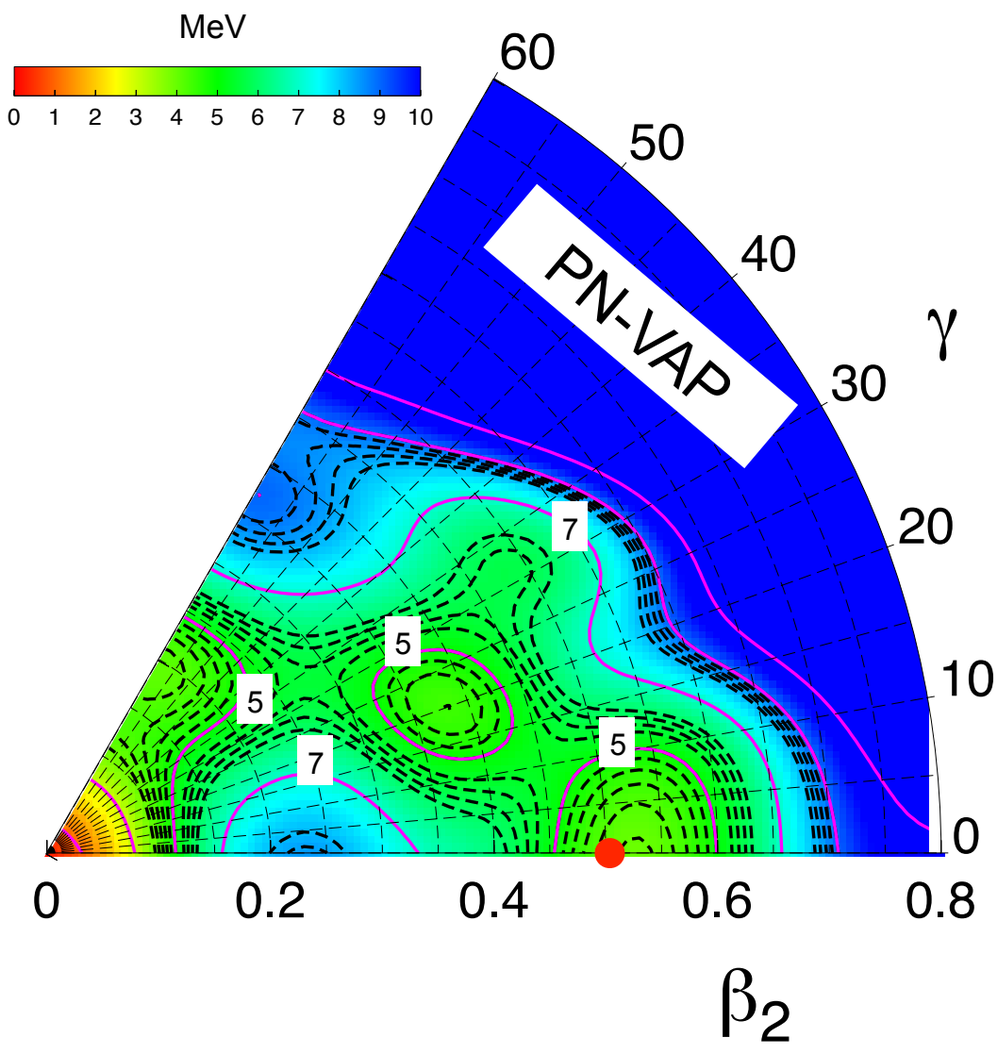

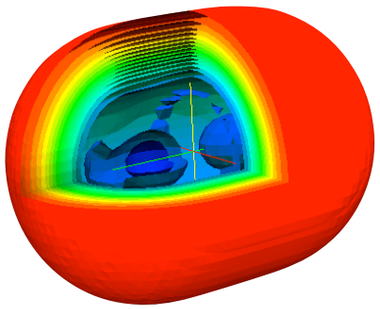

PN-VAP energy surfaces

Example: Multiple shape coexistence in ^{80}Zr

$$\delta E^{N,Z}\left[\bar{\Phi}(\beta,\gamma)\right]\Big|_{\bar{\Phi}=\Phi} = 0$$

$$E^{N,Z}[\Phi] = \frac{\langle\Phi|\hat{H}_{2b}\hat{P}^N\hat{P}^Z|\Phi\rangle}{\langle\Phi|\hat{P}^N\hat{P}^Z|\Phi\rangle} + \varepsilon_{DD}^{N,Z}(\Phi) - \lambda_{q_{20}}\langle\Phi|\hat{Q}_{20}|\Phi\rangle - \lambda_{q_{22}}\langle\Phi|\hat{Q}_{22}|\Phi\rangle$$

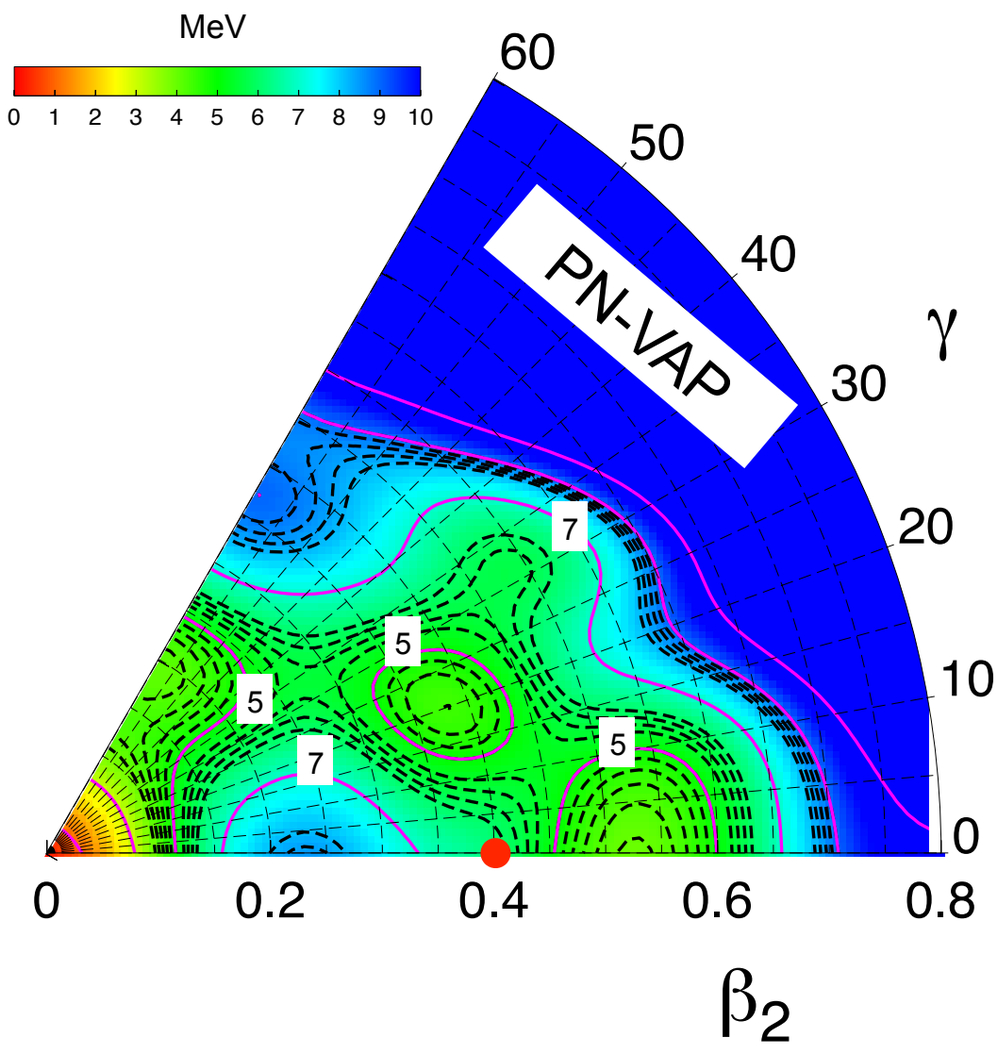

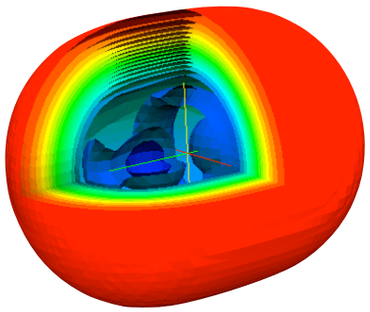

PN-VAP energy surfaces

Example: Multiple shape coexistence in ^{80}Zr

$$\delta E^{N,Z}\left[\bar{\Phi}(\beta,\gamma)\right]\Big|_{\bar{\Phi}=\Phi} = 0$$

$$E^{N,Z}[\Phi] = \frac{\langle\Phi|\hat{H}_{2b}\hat{P}^N\hat{P}^Z|\Phi\rangle}{\langle\Phi|\hat{P}^N\hat{P}^Z|\Phi\rangle} + \varepsilon_{DD}^{N,Z}(\Phi) - \lambda_{q_{20}}\langle\Phi|\hat{Q}_{20}|\Phi\rangle - \lambda_{q_{22}}\langle\Phi|\hat{Q}_{22}|\Phi\rangle$$

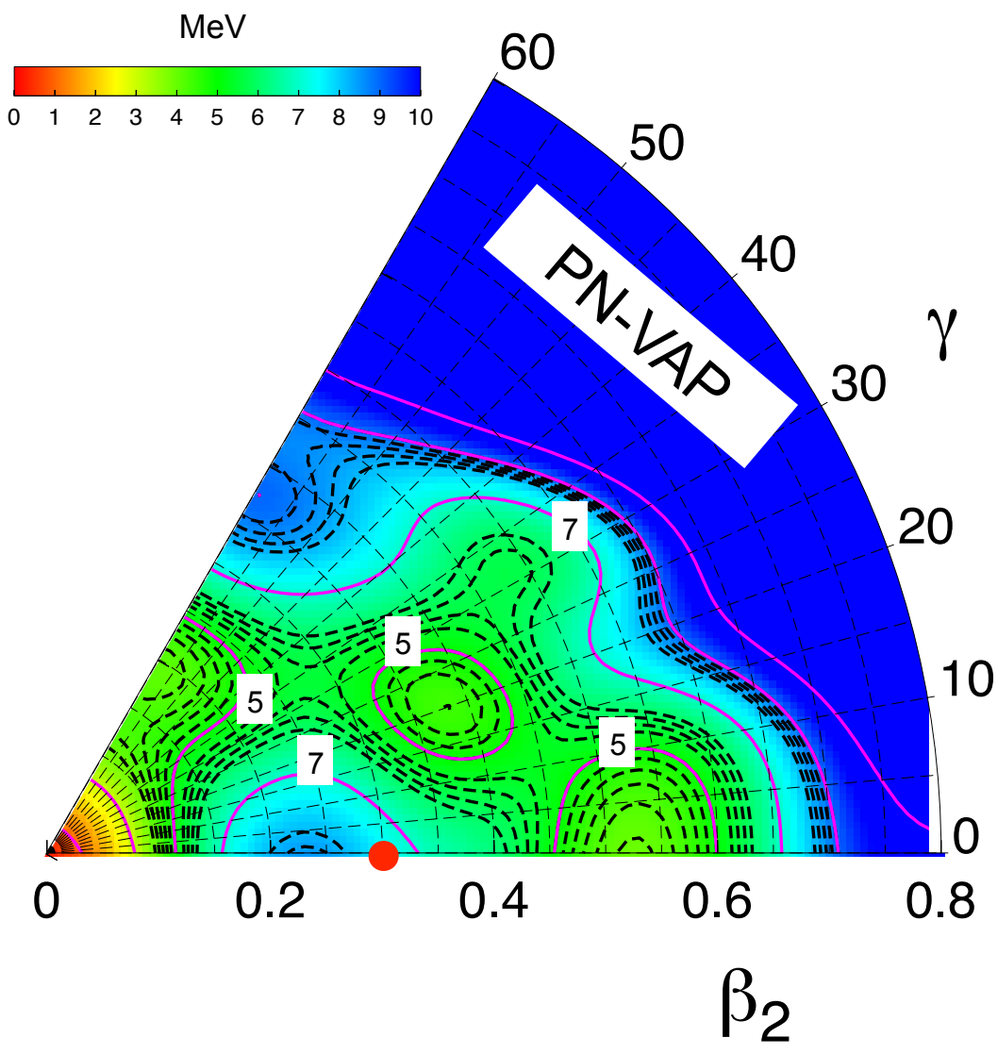

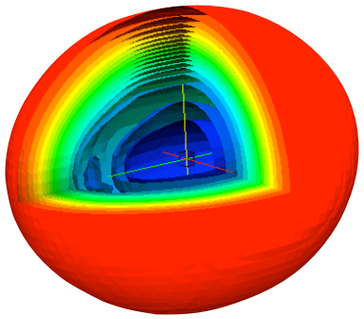

PN-VAP energy surfaces

Example: Multiple shape coexistence in ^{80}Zr

$$\delta E^{N,Z}\left[\bar{\Phi}(\beta,\gamma)\right]\Big|_{\bar{\Phi}=\Phi} = 0$$

$$E^{N,Z}[\Phi] = \frac{\langle\Phi|\hat{H}_{2b}\hat{P}^N\hat{P}^Z|\Phi\rangle}{\langle\Phi|\hat{P}^N\hat{P}^Z|\Phi\rangle} + \varepsilon_{DD}^{N,Z}(\Phi) - \lambda_{q_{20}}\langle\Phi|\hat{Q}_{20}|\Phi\rangle - \lambda_{q_{22}}\langle\Phi|\hat{Q}_{22}|\Phi\rangle$$

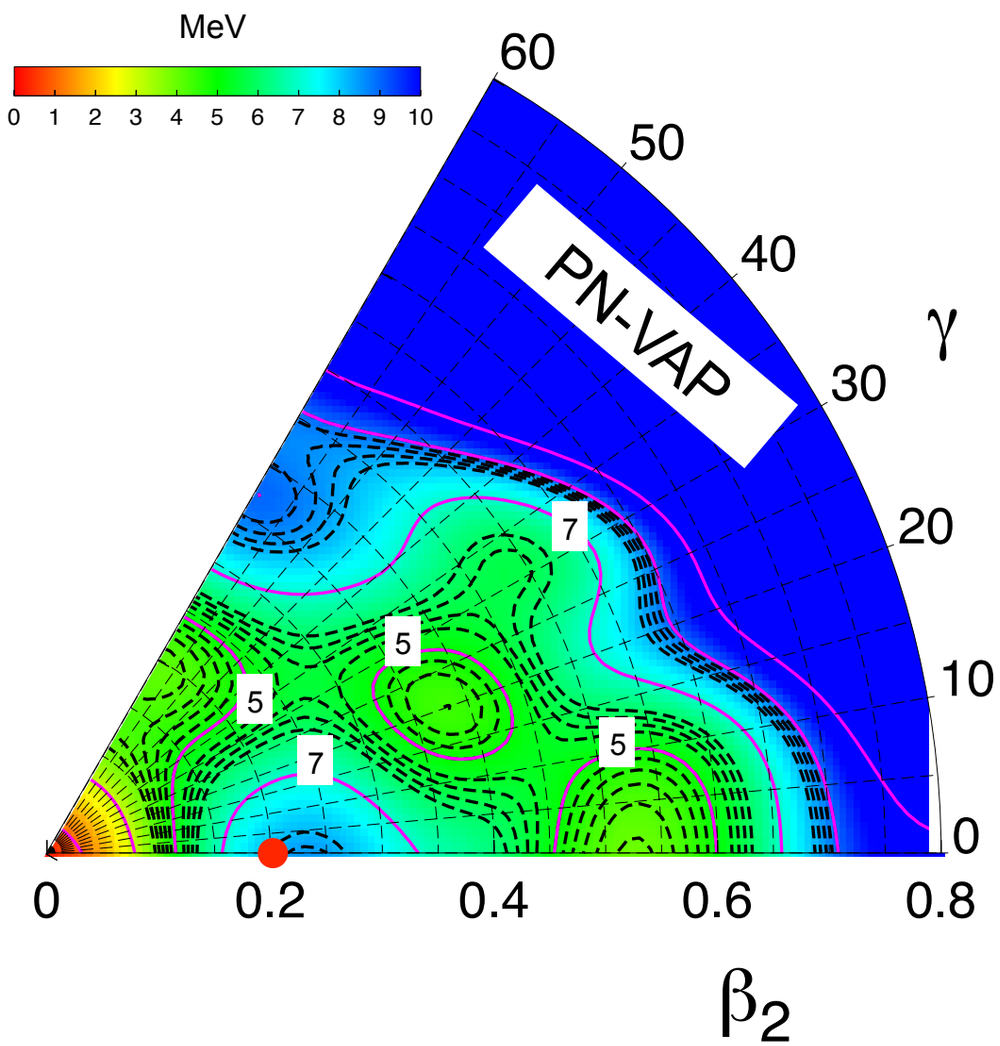

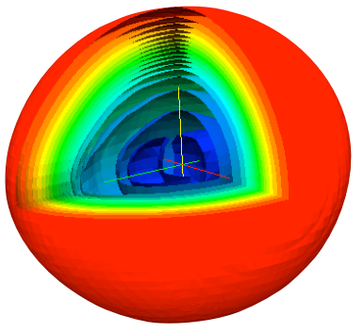

PN-VAP energy surfaces

Example: Multiple shape coexistence in ^{80}Zr

$$\delta E^{N,Z}\left[\bar{\Phi}(\beta,\gamma)\right]\Big|_{\bar{\Phi}=\Phi} = 0$$

$$E^{N,Z}[\Phi] = \frac{\langle\Phi|\hat{H}_{2b}\hat{P}^N\hat{P}^Z|\Phi\rangle}{\langle\Phi|\hat{P}^N\hat{P}^Z|\Phi\rangle} + \varepsilon_{DD}^{N,Z}(\Phi) - \lambda_{q_{20}}\langle\Phi|\hat{Q}_{20}|\Phi\rangle - \lambda_{q_{22}}\langle\Phi|\hat{Q}_{22}|\Phi\rangle$$

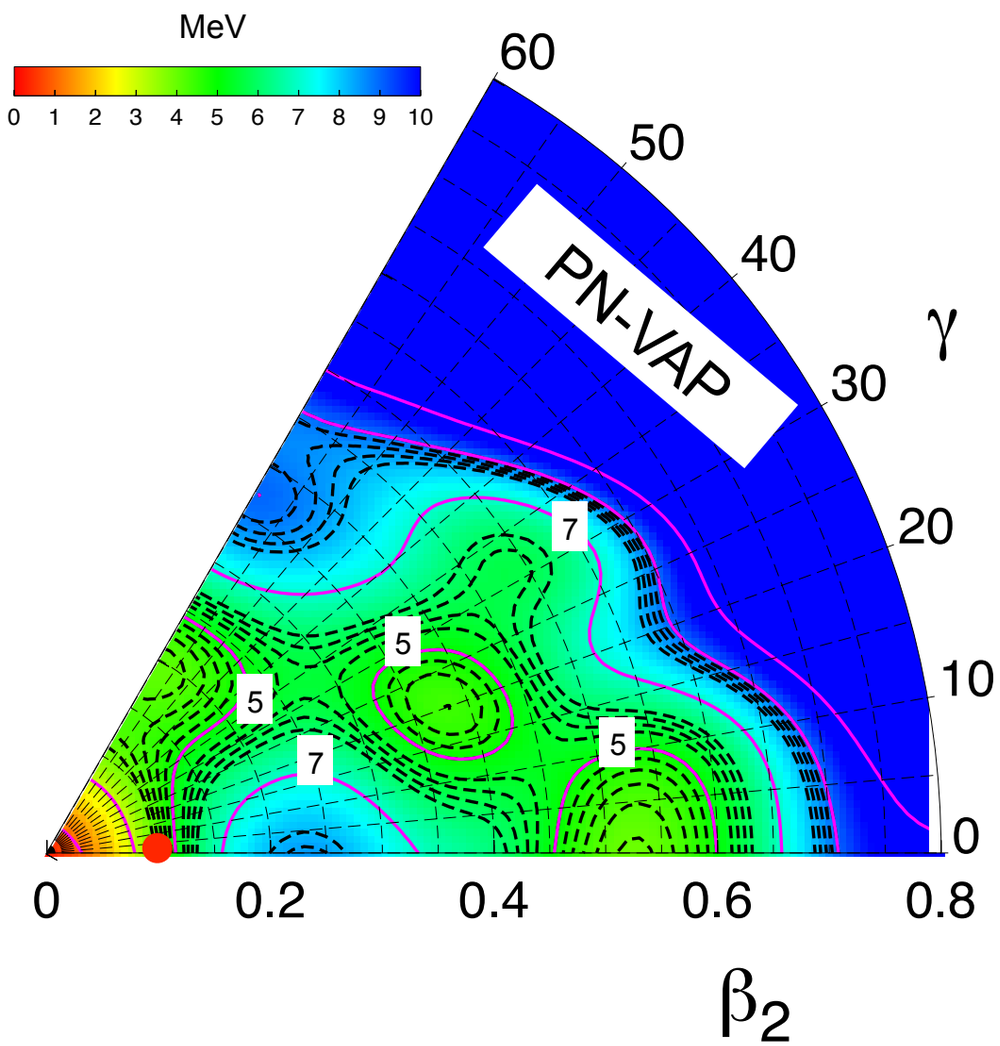

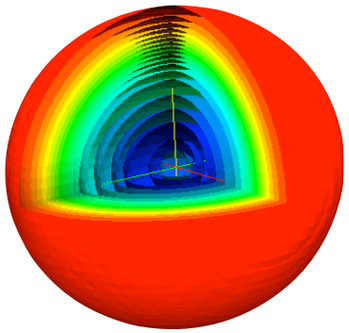

PN-VAP energy surfaces

Example: Multiple shape coexistence in ^{80}Zr

$$\delta E^{N,Z}\left[\bar{\Phi}(\beta,\gamma)\right]\Big|_{\bar{\Phi}=\Phi} = 0$$

$$E^{N,Z}[\Phi] = \frac{\langle\Phi|\hat{H}_{2b}\hat{P}^N\hat{P}^Z|\Phi\rangle}{\langle\Phi|\hat{P}^N\hat{P}^Z|\Phi\rangle} + \varepsilon_{DD}^{N,Z}(\Phi) - \lambda_{q_{20}}\langle\Phi|\hat{Q}_{20}|\Phi\rangle - \lambda_{q_{22}}\langle\Phi|\hat{Q}_{22}|\Phi\rangle$$

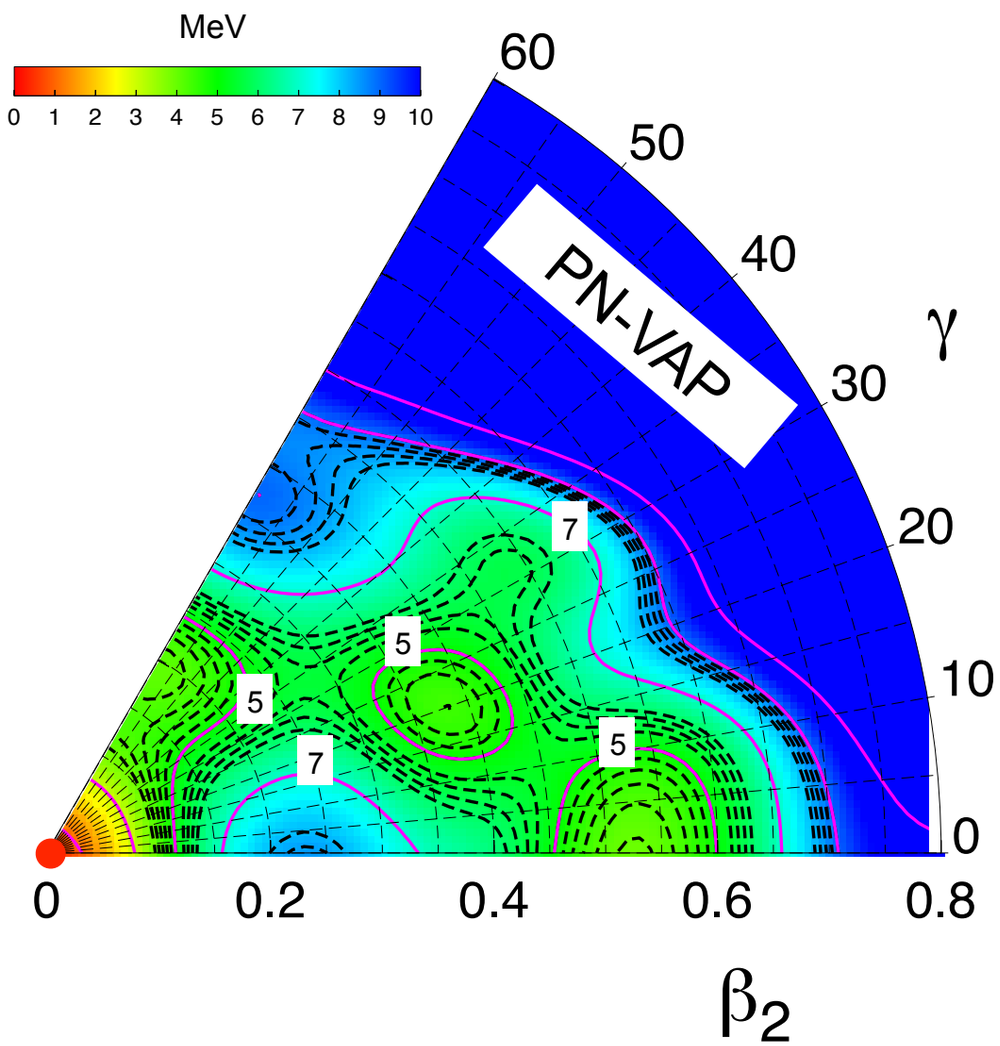

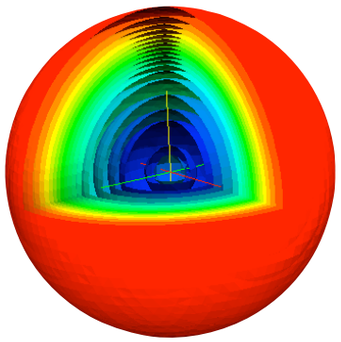

PN-VAP energy surfaces

Example: Multiple shape coexistence in ^{80}Zr

$$\delta E^{N,Z}\left[\bar{\Phi}(\beta,\gamma)\right]\Big|_{\bar{\Phi}=\Phi} = 0$$

$$E^{N,Z}[\Phi] = \frac{\langle\Phi|\hat{H}_{2b}\hat{P}^N\hat{P}^Z|\Phi\rangle}{\langle\Phi|\hat{P}^N\hat{P}^Z|\Phi\rangle} + \varepsilon_{DD}^{N,Z}(\Phi) - \lambda_{q_{20}}\langle\Phi|\hat{Q}_{20}|\Phi\rangle - \lambda_{q_{22}}\langle\Phi|\hat{Q}_{22}|\Phi\rangle$$

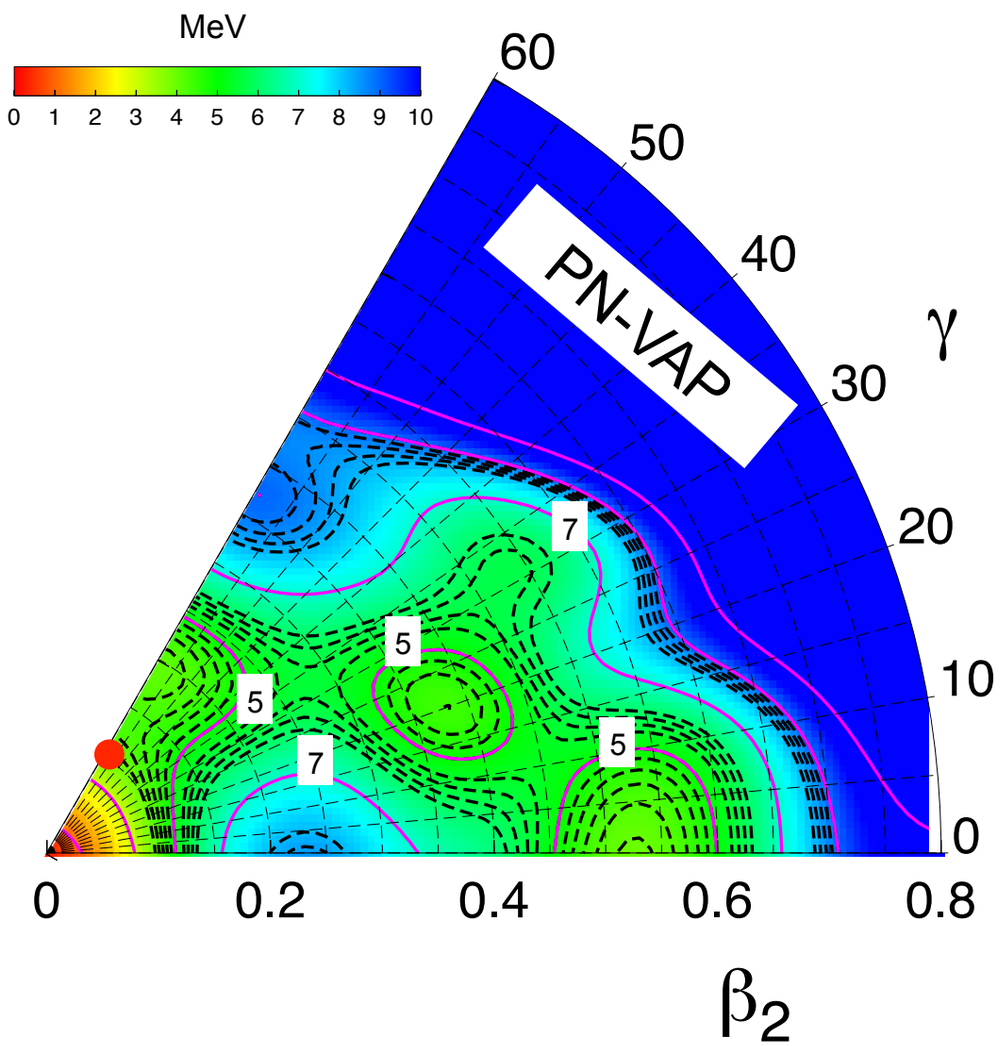

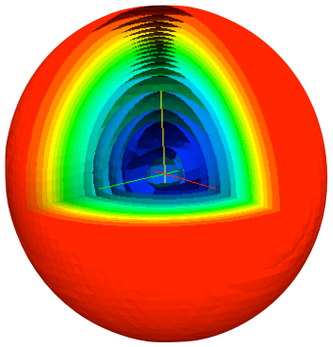

PN-VAP energy surfaces

Example: Multiple shape coexistence in ^{80}Zr

$$\delta E^{N,Z}\left[\bar{\Phi}(\beta,\gamma)\right]\Big|_{\bar{\Phi}=\Phi} = 0$$

$$E^{N,Z}[\Phi] = \frac{\langle\Phi|\hat{H}_{2b}\hat{P}^N\hat{P}^Z|\Phi\rangle}{\langle\Phi|\hat{P}^N\hat{P}^Z|\Phi\rangle} + \varepsilon_{DD}^{N,Z}(\Phi) - \lambda_{q_{20}}\langle\Phi|\hat{Q}_{20}|\Phi\rangle - \lambda_{q_{22}}\langle\Phi|\hat{Q}_{22}|\Phi\rangle$$

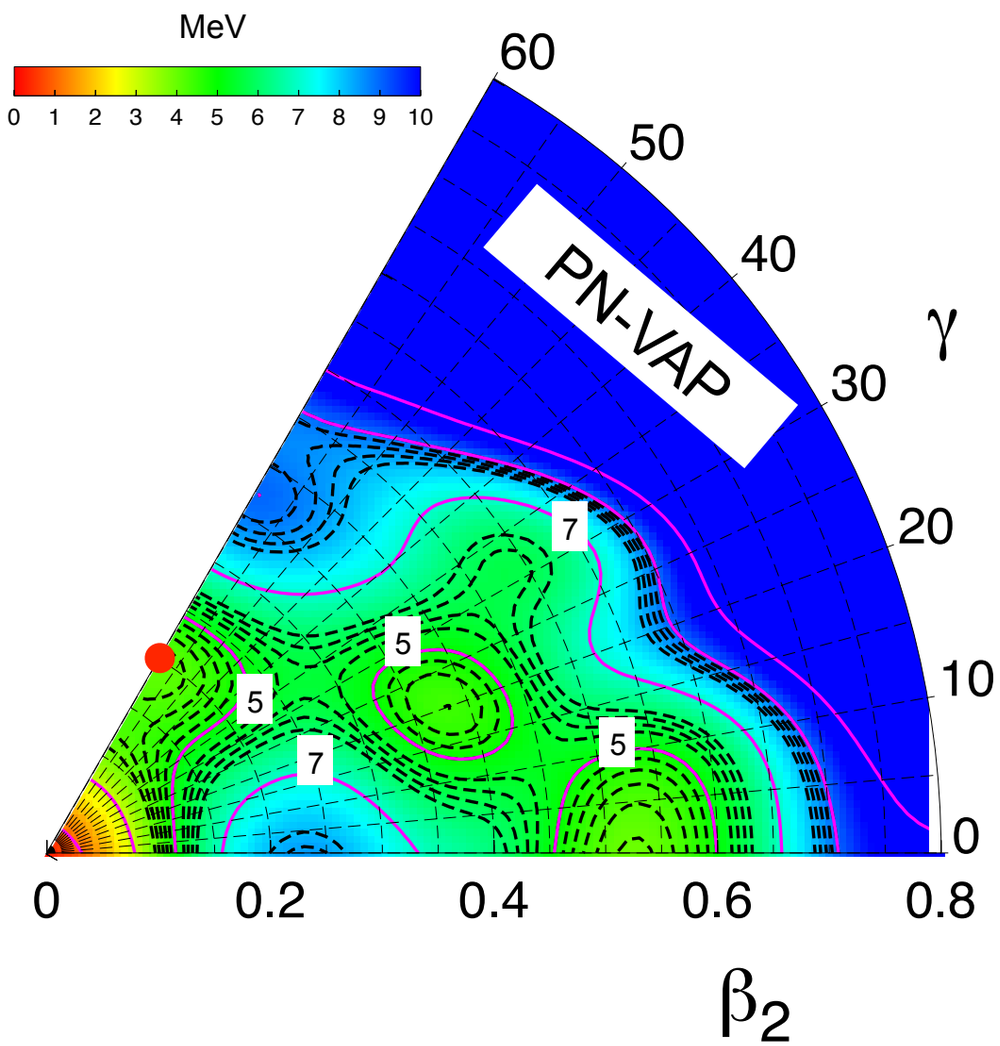

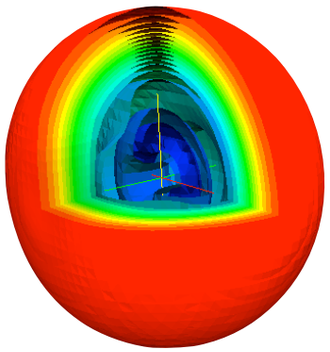

PN-VAP energy surfaces

Example: Multiple shape coexistence in ^{80}Zr

$$\delta E^{N,Z}\left[\bar{\Phi}(\beta,\gamma)\right]\Big|_{\bar{\Phi}=\Phi} = 0$$

$$E^{N,Z}[\Phi] = \frac{\langle\Phi|\hat{H}_{2b}\hat{P}^N\hat{P}^Z|\Phi\rangle}{\langle\Phi|\hat{P}^N\hat{P}^Z|\Phi\rangle} + \varepsilon_{DD}^{N,Z}(\Phi) - \lambda_{q_{20}}\langle\Phi|\hat{Q}_{20}|\Phi\rangle - \lambda_{q_{22}}\langle\Phi|\hat{Q}_{22}|\Phi\rangle$$

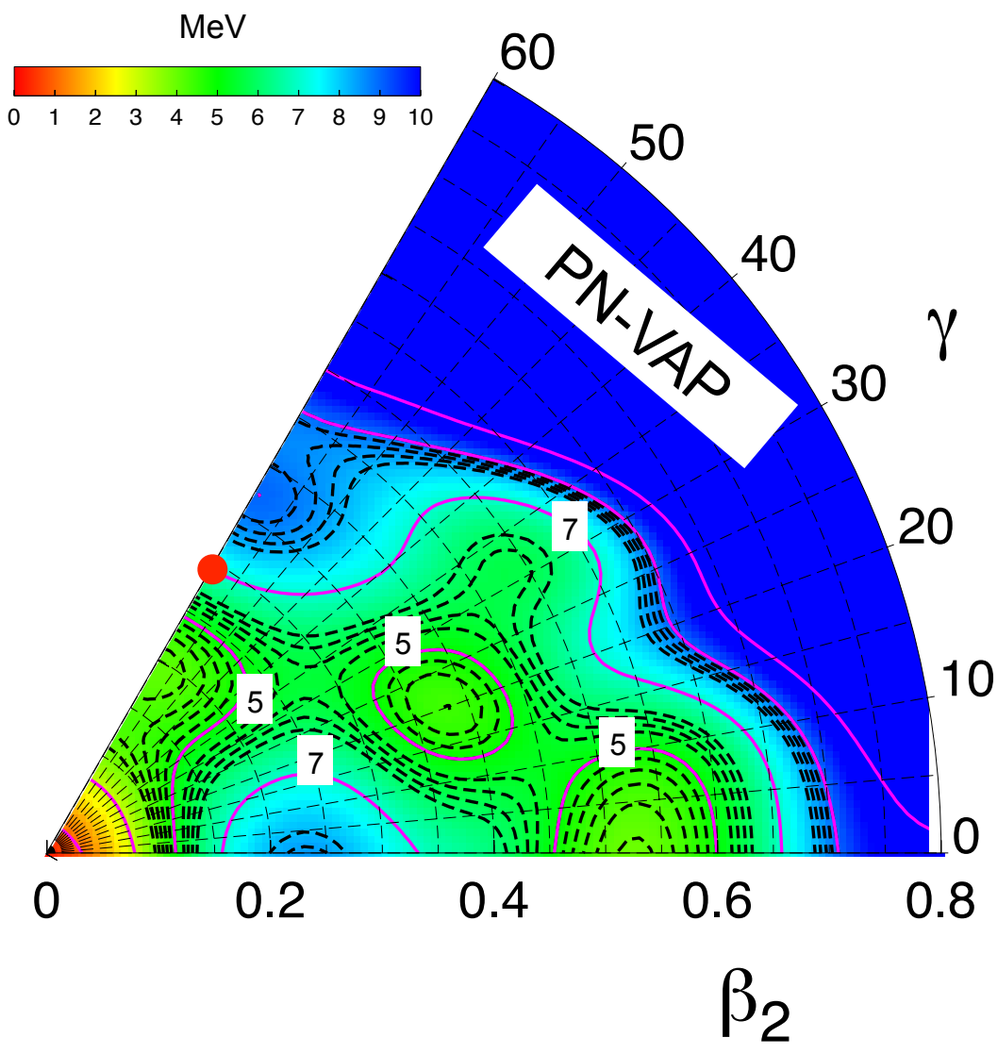

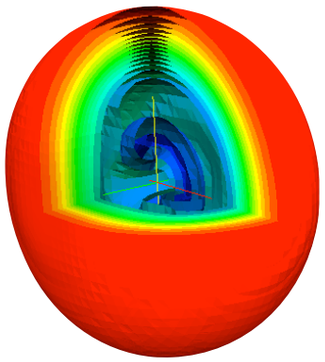

PN-VAP energy surfaces

Example: Multiple shape coexistence in ^{80}Zr

$$\delta E^{N,Z}\left[\bar{\Phi}(\beta,\gamma)\right]\Big|_{\bar{\Phi}=\Phi} = 0$$

$$E^{N,Z}[\Phi] = \frac{\langle\Phi|\hat{H}_{2b}\hat{P}^N\hat{P}^Z|\Phi\rangle}{\langle\Phi|\hat{P}^N\hat{P}^Z|\Phi\rangle} + \varepsilon_{DD}^{N,Z}(\Phi) - \lambda_{q_{20}}\langle\Phi|\hat{Q}_{20}|\Phi\rangle - \lambda_{q_{22}}\langle\Phi|\hat{Q}_{22}|\Phi\rangle$$

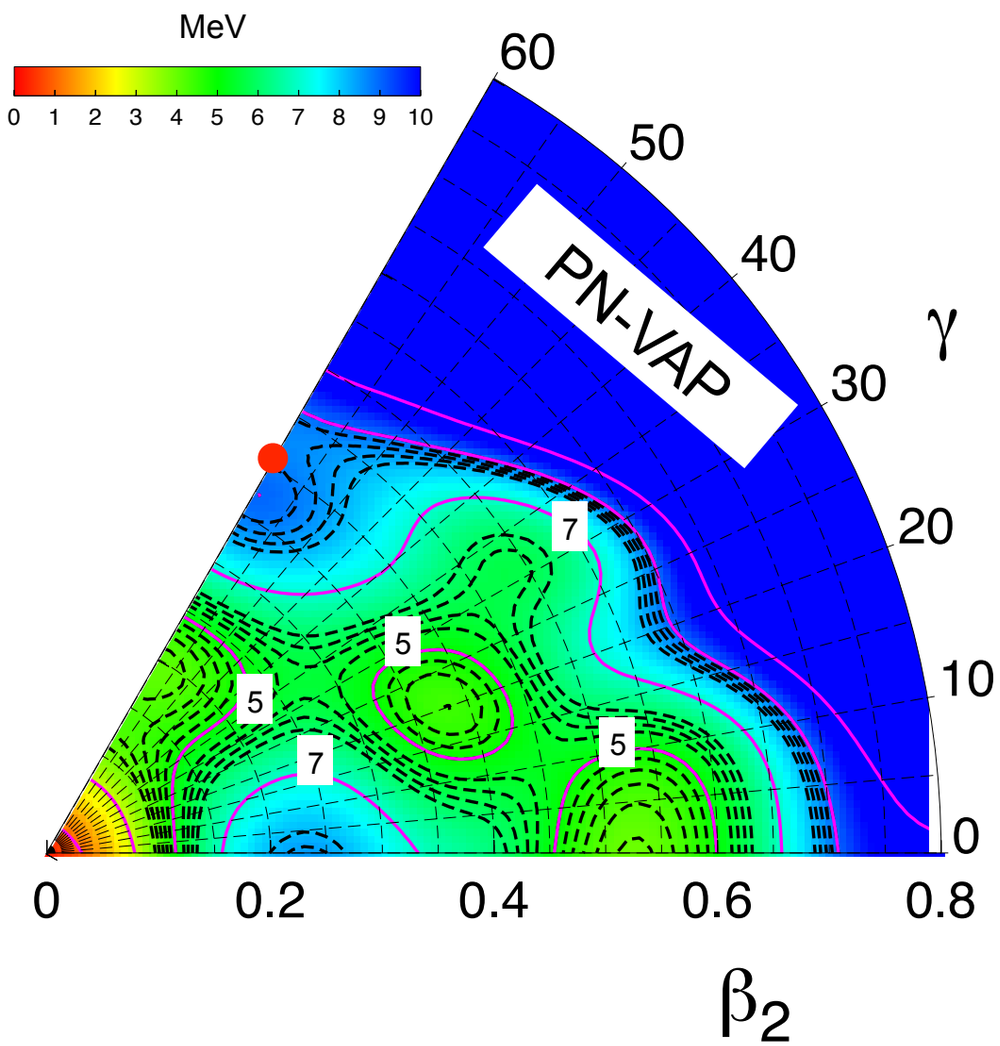

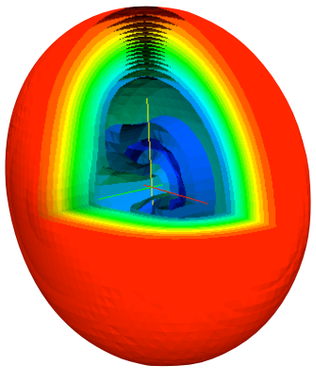

PN-VAP energy surfaces

Example: Multiple shape coexistence in ^{80}Zr

$$\delta E^{N,Z}\left[\bar{\Phi}(\beta,\gamma)\right]\Big|_{\bar{\Phi}=\Phi} = 0$$

$$E^{N,Z}[\Phi] = \frac{\langle\Phi|\hat{H}_{2b}\hat{P}^N\hat{P}^Z|\Phi\rangle}{\langle\Phi|\hat{P}^N\hat{P}^Z|\Phi\rangle} + \varepsilon_{DD}^{N,Z}(\Phi) - \lambda_{q_{20}}\langle\Phi|\hat{Q}_{20}|\Phi\rangle - \lambda_{q_{22}}\langle\Phi|\hat{Q}_{22}|\Phi\rangle$$

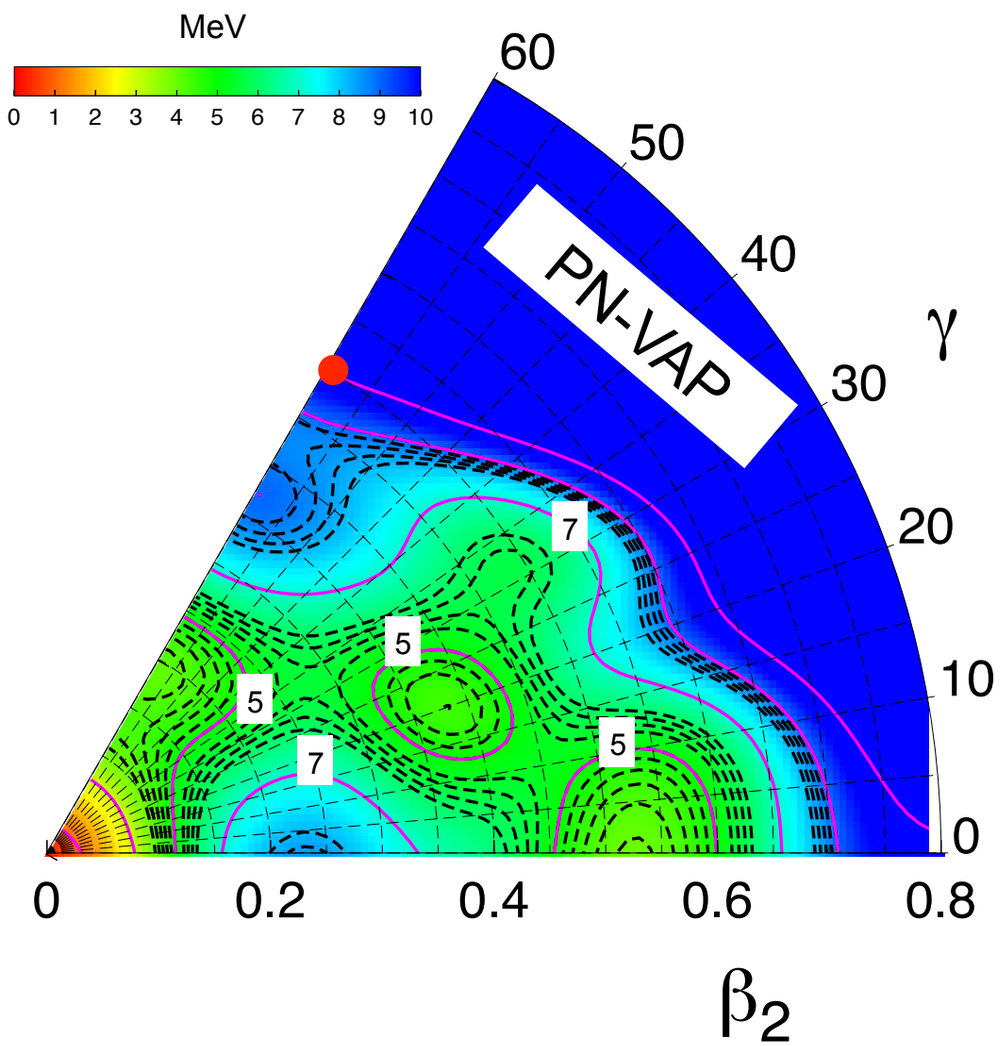

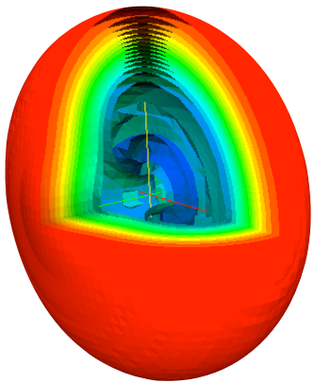

PN-VAP energy surfaces

Example: Multiple shape coexistence in ^{80}Zr

$$\delta E^{N,Z}\left[\bar{\Phi}(\beta,\gamma)\right]\Big|_{\bar{\Phi}=\Phi} = 0$$

$$E^{N,Z}[\Phi] = \frac{\langle\Phi|\hat{H}_{2b}\hat{P}^N\hat{P}^Z|\Phi\rangle}{\langle\Phi|\hat{P}^N\hat{P}^Z|\Phi\rangle} + \varepsilon_{DD}^{N,Z}(\Phi) - \lambda_{q_{20}}\langle\Phi|\hat{Q}_{20}|\Phi\rangle - \lambda_{q_{22}}\langle\Phi|\hat{Q}_{22}|\Phi\rangle$$

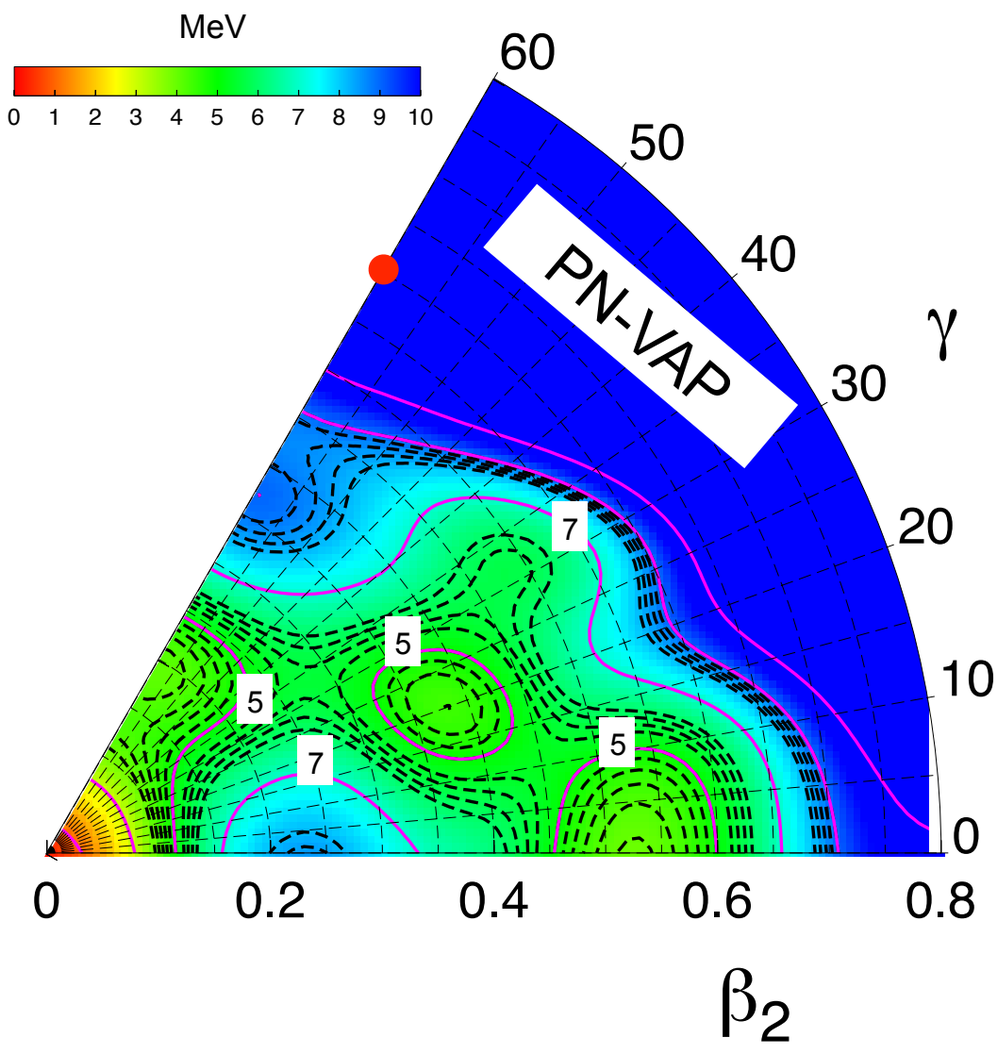

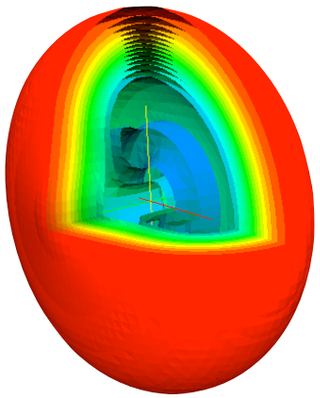

PN-VAP energy surfaces

Example: Multiple shape coexistence in ^{80}Zr

$$\delta E^{N,Z}\left[\bar{\Phi}(\beta,\gamma)\right]\Big|_{\bar{\Phi}=\Phi} = 0$$

$$E^{N,Z}[\Phi] = \frac{\langle\Phi|\hat{H}_{2b}\hat{P}^N\hat{P}^Z|\Phi\rangle}{\langle\Phi|\hat{P}^N\hat{P}^Z|\Phi\rangle} + \varepsilon_{DD}^{N,Z}(\Phi) - \lambda_{q_{20}}\langle\Phi|\hat{Q}_{20}|\Phi\rangle - \lambda_{q_{22}}\langle\Phi|\hat{Q}_{22}|\Phi\rangle$$

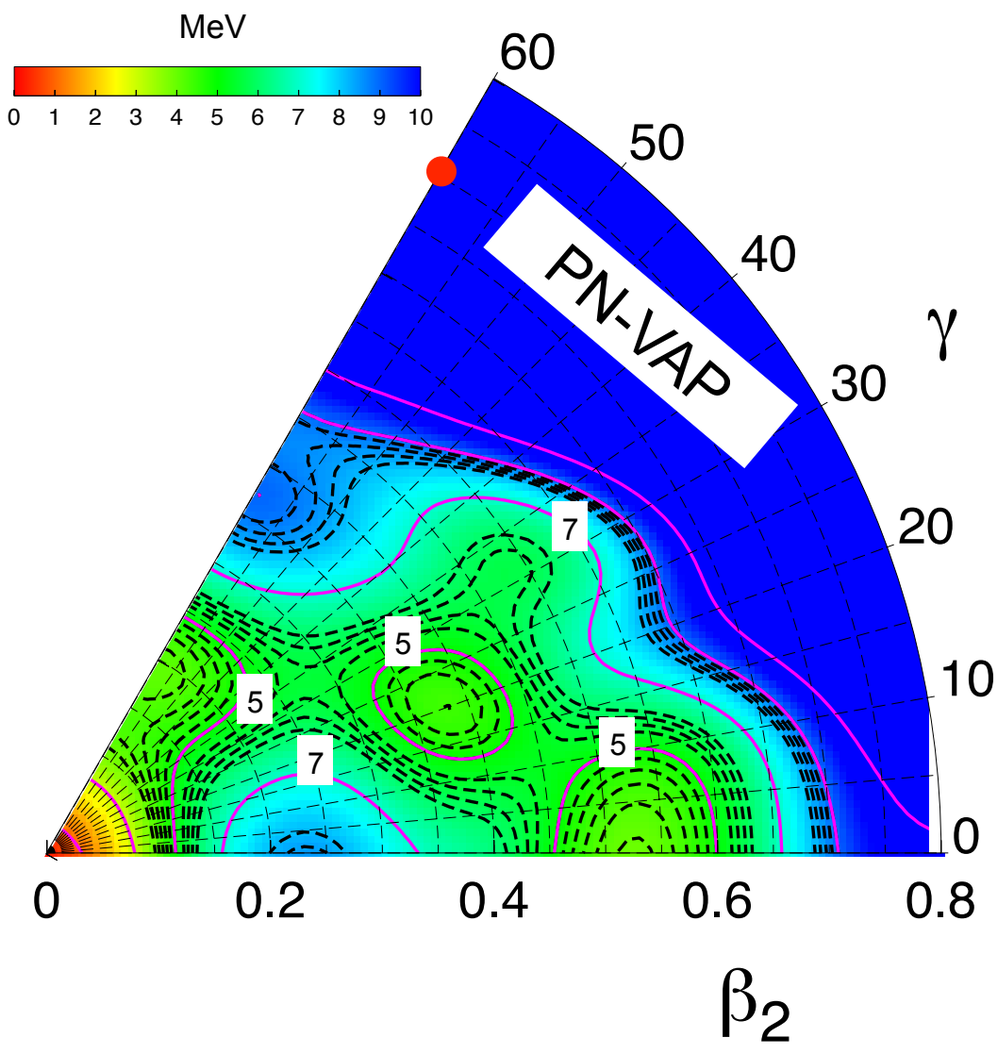

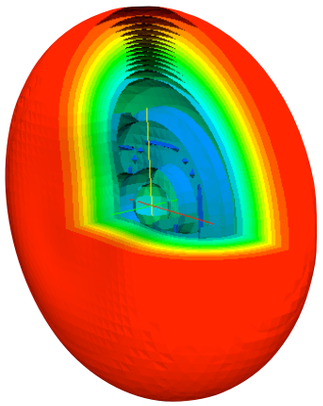

PN-VAP energy surfaces

Example: Multiple shape coexistence in ^{80}Zr

$$\delta E^{N,Z}\left[\bar{\Phi}(\beta,\gamma)\right]\Big|_{\bar{\Phi}=\Phi} = 0$$

$$E^{N,Z}[\Phi] = \frac{\langle\Phi|\hat{H}_{2b}\hat{P}^N\hat{P}^Z|\Phi\rangle}{\langle\Phi|\hat{P}^N\hat{P}^Z|\Phi\rangle} + \varepsilon_{DD}^{N,Z}(\Phi) - \lambda_{q_{20}}\langle\Phi|\hat{Q}_{20}|\Phi\rangle - \lambda_{q_{22}}\langle\Phi|\hat{Q}_{22}|\Phi\rangle$$

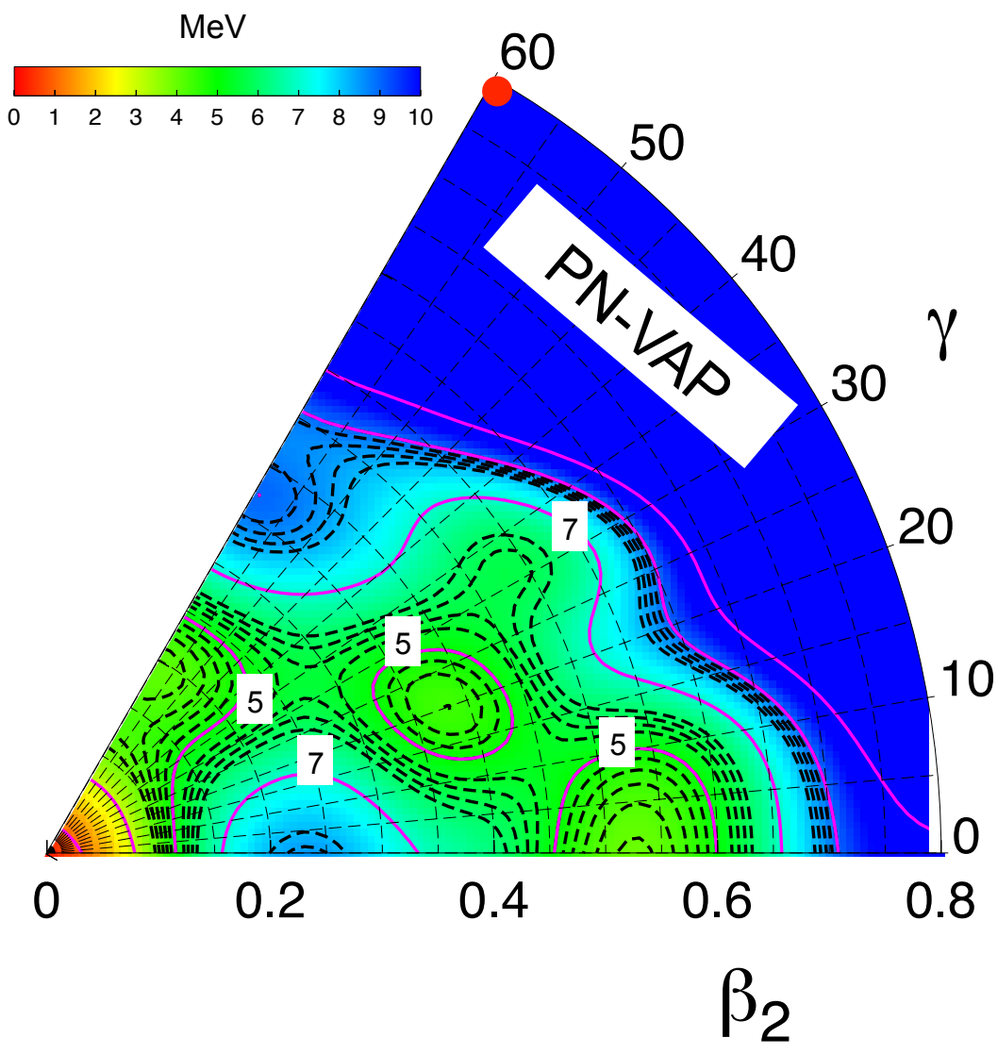

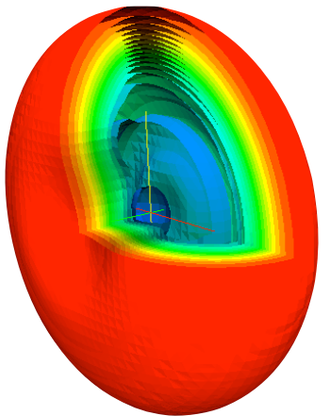

PN-VAP energy surfaces

Example: Multiple shape coexistence in ^{80}Zr

$$\delta E^{N,Z}\left[\bar{\Phi}(\beta,\gamma)\right]\Big|_{\bar{\Phi}=\Phi} = 0$$

$$E^{N,Z}[\Phi] = \frac{\langle\Phi|\hat{H}_{2b}\hat{P}^N\hat{P}^Z|\Phi\rangle}{\langle\Phi|\hat{P}^N\hat{P}^Z|\Phi\rangle} + \varepsilon_{DD}^{N,Z}(\Phi) - \lambda_{q_{20}}\langle\Phi|\hat{Q}_{20}|\Phi\rangle - \lambda_{q_{22}}\langle\Phi|\hat{Q}_{22}|\Phi\rangle$$

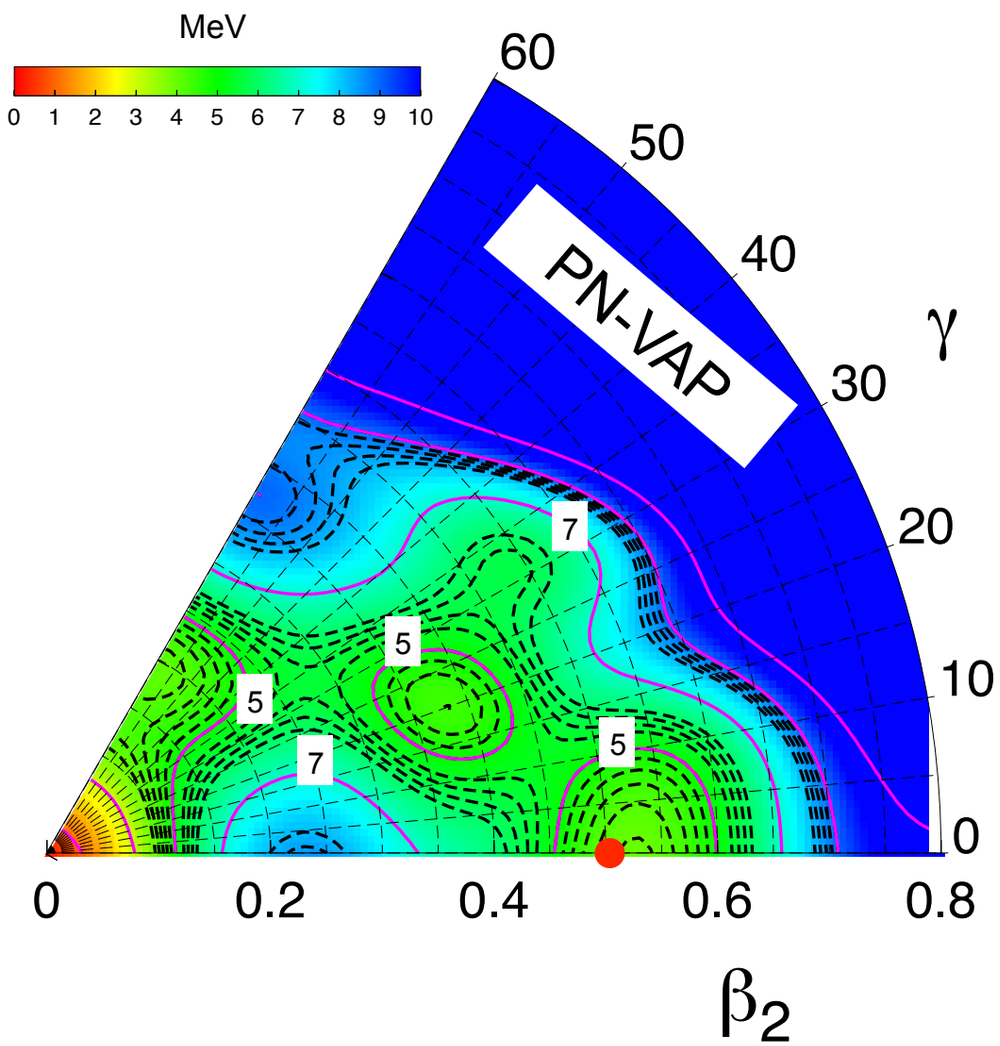

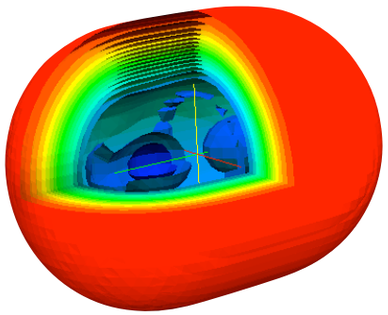

PN-VAP energy surfaces

Example: Multiple shape coexistence in ^{80}Zr

$$\delta E^{N,Z}\left[\bar{\Phi}(\beta,\gamma)\right]\Big|_{\bar{\Phi}=\Phi} = 0$$

$$E^{N,Z}[\Phi] = \frac{\langle\Phi|\hat{H}_{2b}\hat{P}^N\hat{P}^Z|\Phi\rangle}{\langle\Phi|\hat{P}^N\hat{P}^Z|\Phi\rangle} + \varepsilon_{DD}^{N,Z}(\Phi) - \lambda_{q_{20}}\langle\Phi|\hat{Q}_{20}|\Phi\rangle - \lambda_{q_{22}}\langle\Phi|\hat{Q}_{22}|\Phi\rangle$$

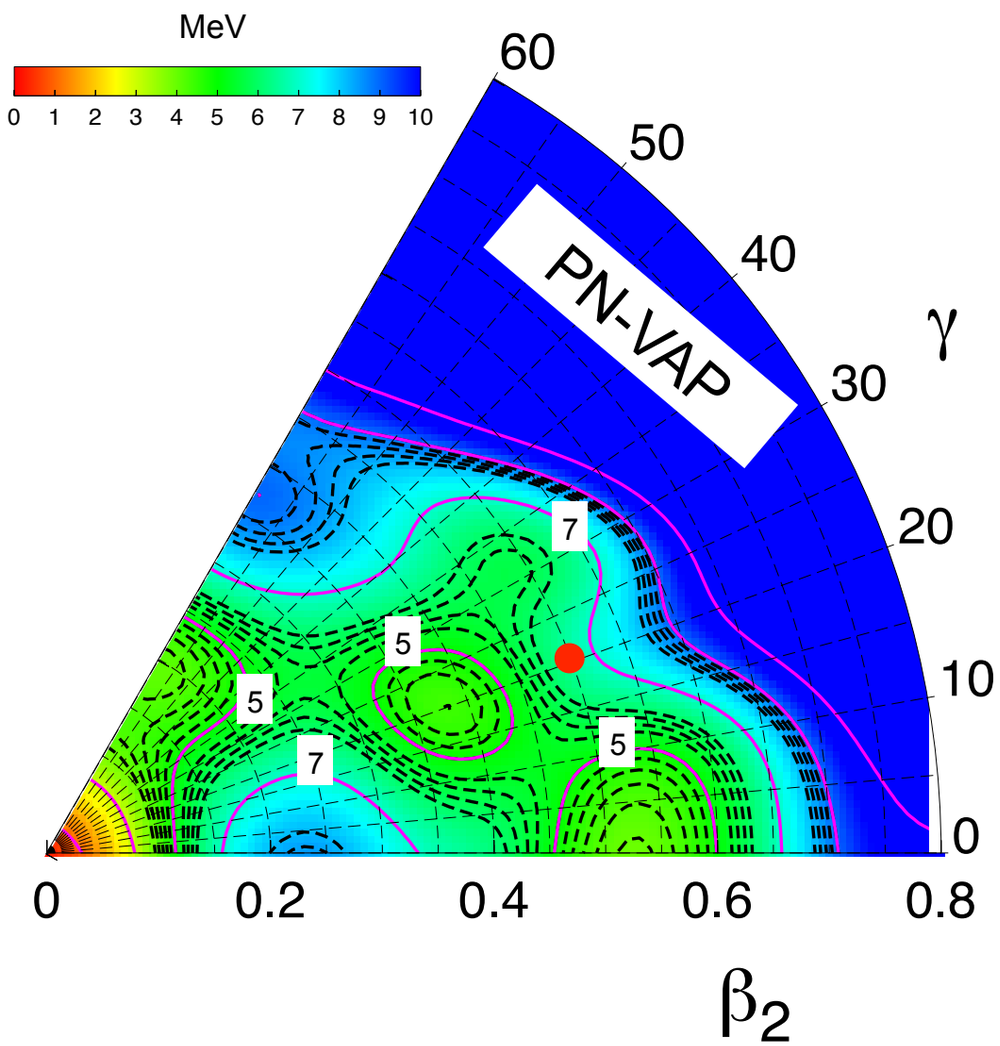

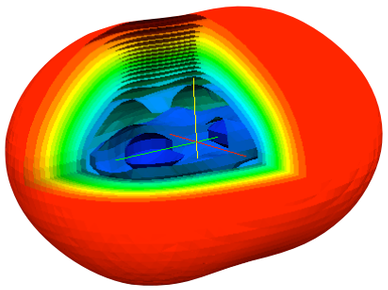

PN-VAP energy surfaces

Example: Multiple shape coexistence in ^{80}Zr

$$\delta E^{N,Z}\left[\bar{\Phi}(\beta,\gamma)\right]\Big|_{\bar{\Phi}=\Phi} = 0$$

$$E^{N,Z}[\Phi] = \frac{\langle\Phi|\hat{H}_{2b}\hat{P}^N\hat{P}^Z|\Phi\rangle}{\langle\Phi|\hat{P}^N\hat{P}^Z|\Phi\rangle} + \varepsilon_{DD}^{N,Z}(\Phi) - \lambda_{q_{20}}\langle\Phi|\hat{Q}_{20}|\Phi\rangle - \lambda_{q_{22}}\langle\Phi|\hat{Q}_{22}|\Phi\rangle$$

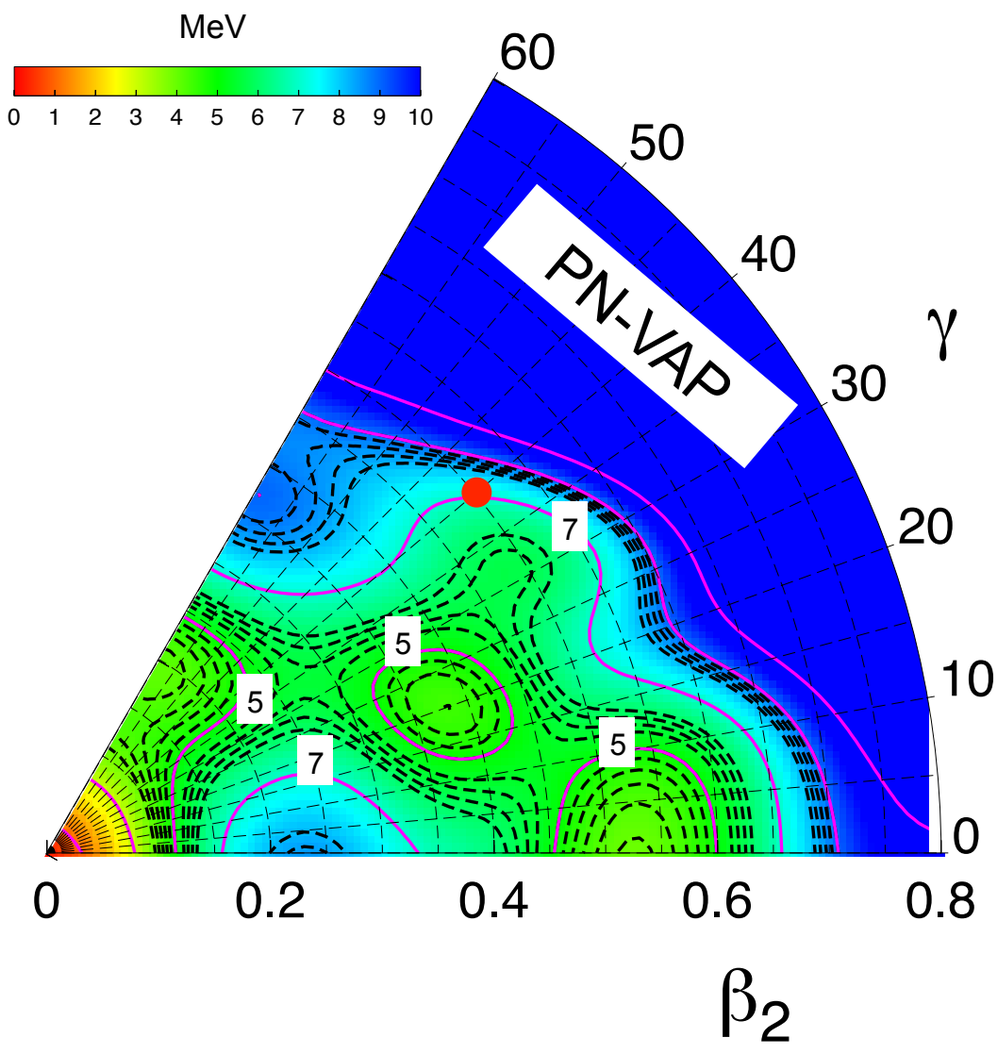

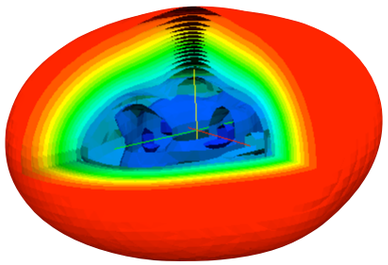

PN-VAP energy surfaces

Example: Multiple shape coexistence in ^{80}Zr

$$\delta E^{N,Z}\left[\bar{\Phi}(\beta,\gamma)\right]\Big|_{\bar{\Phi}=\Phi} = 0$$

$$E^{N,Z}[\Phi] = \frac{\langle\Phi|\hat{H}_{2b}\hat{P}^N\hat{P}^Z|\Phi\rangle}{\langle\Phi|\hat{P}^N\hat{P}^Z|\Phi\rangle} + \varepsilon_{DD}^{N,Z}(\Phi) - \lambda_{q_{20}}\langle\Phi|\hat{Q}_{20}|\Phi\rangle - \lambda_{q_{22}}\langle\Phi|\hat{Q}_{22}|\Phi\rangle$$

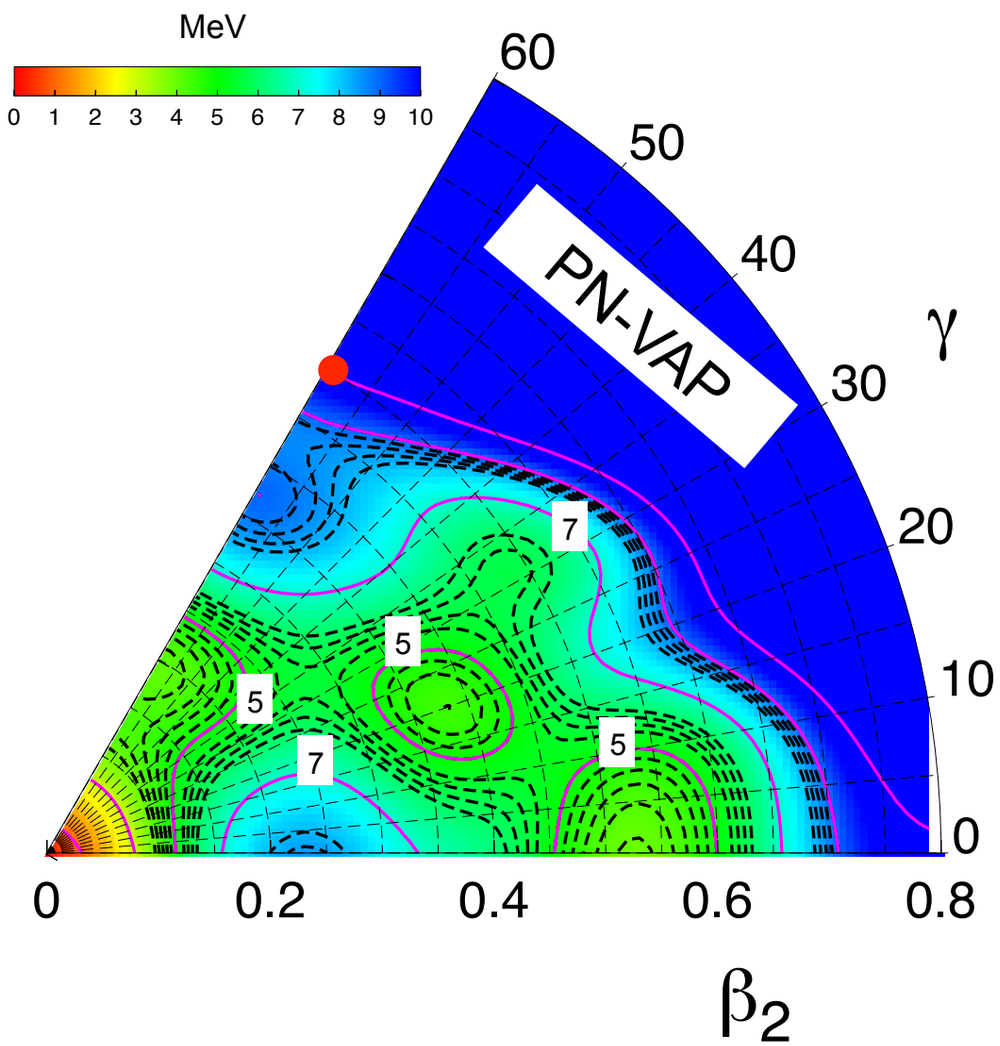

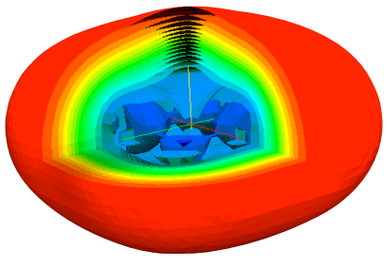

Example: Multiple shape coexistence in ^{80}Zr

$$\delta E^{N,Z}\left[\bar{\Phi}(\beta,\gamma)\right]\Big|_{\bar{\Phi}=\Phi} = 0$$

$$E^{N,Z}[\Phi] = \frac{\langle\Phi|\hat{H}_{2b}\hat{P}^N\hat{P}^Z|\Phi\rangle}{\langle\Phi|\hat{P}^N\hat{P}^Z|\Phi\rangle} + \varepsilon_{DD}^{N,Z}(\Phi) - \lambda_{q_{20}}\langle\Phi|\hat{Q}_{20}|\Phi\rangle - \lambda_{q_{22}}\langle\Phi|\hat{Q}_{22}|\Phi\rangle$$

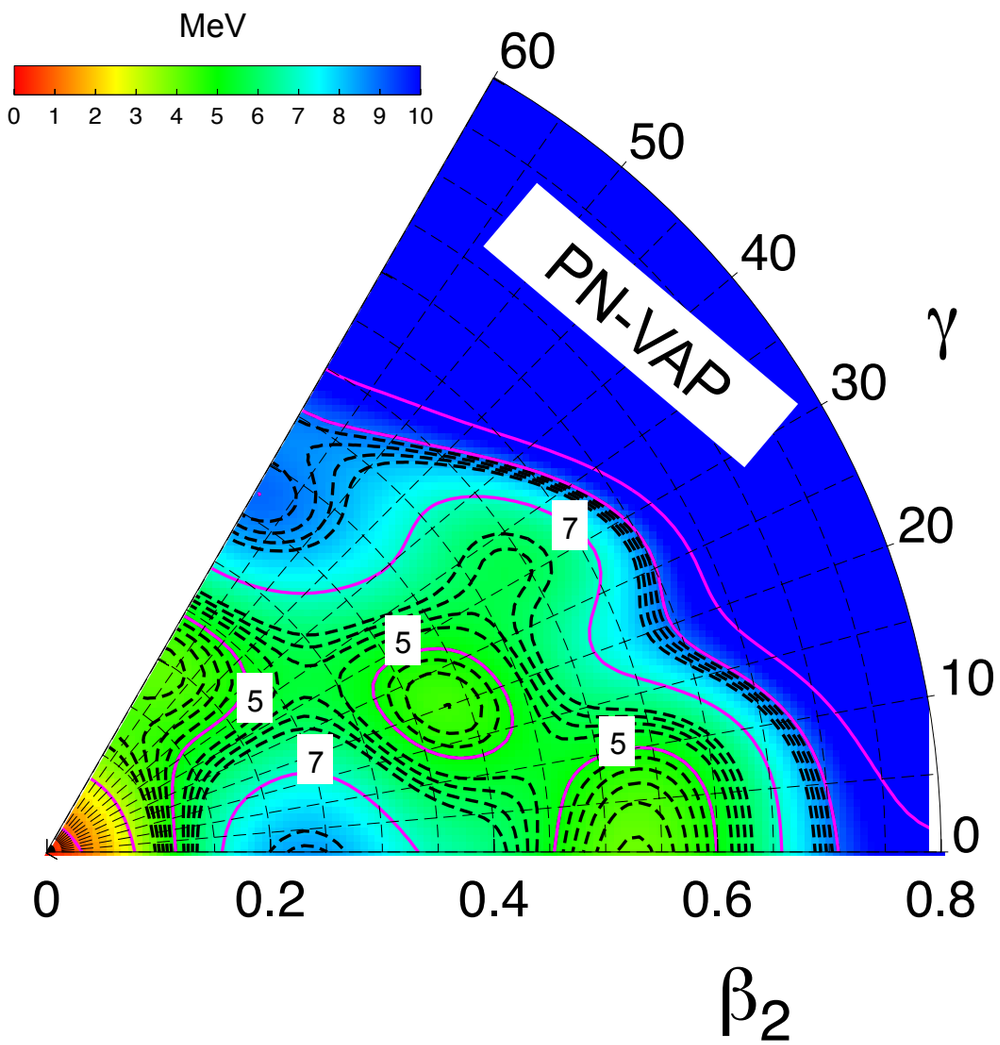

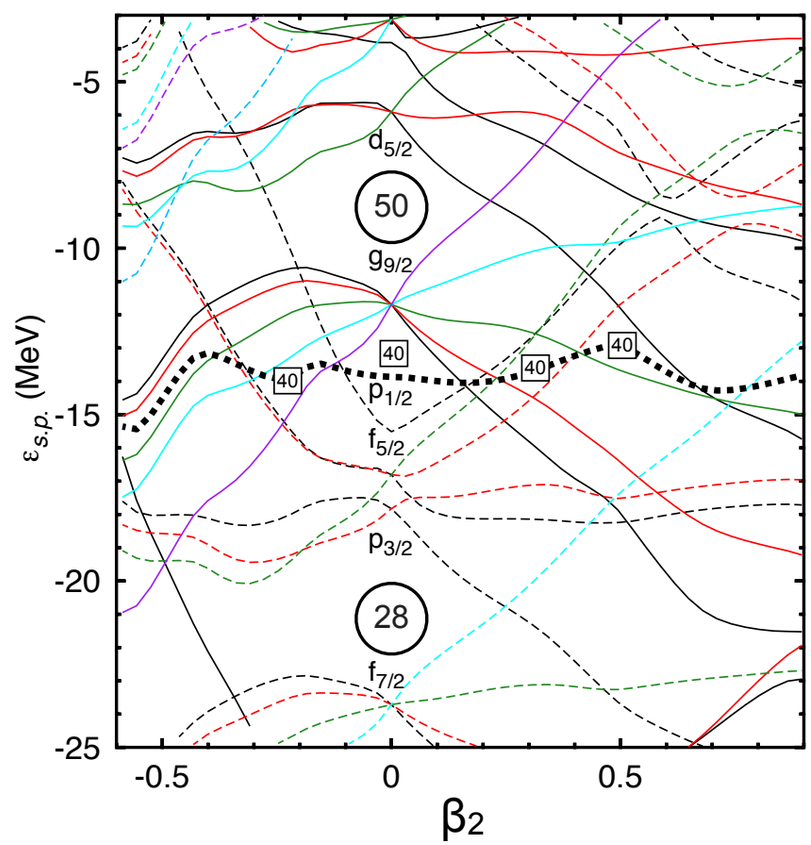

- Up to five minima in the potential energy surface.
- Absolute minimum corresponds to spherical configuration (N=40 spherical gap)
- Other minima related to the filling in and emptying of $g_{9/2}$, $p_{1/2}$, $f_{5/2}$ and $d_{5/2}$ orbits.

T. R. R., J. L. Egido, Phys. Lett. B 705, 255 (2011)

Example: Multiple shape coexistence in ^{80}Zr

$$|IMK;NZ;\beta\gamma\rangle = \frac{2I+1}{8\pi^2}\int \mathcal{D}^{I*}_{MK}(\Omega)\hat{R}(\Omega)\hat{P}^N\hat{P}^Z|\Phi(\beta,\gamma)\rangle d\Omega \qquad |IM;NZ;\beta\gamma\rangle = \sum_K g_K^{IM;NZ;\beta\gamma}|IMK;NZ;\beta\gamma\rangle$$

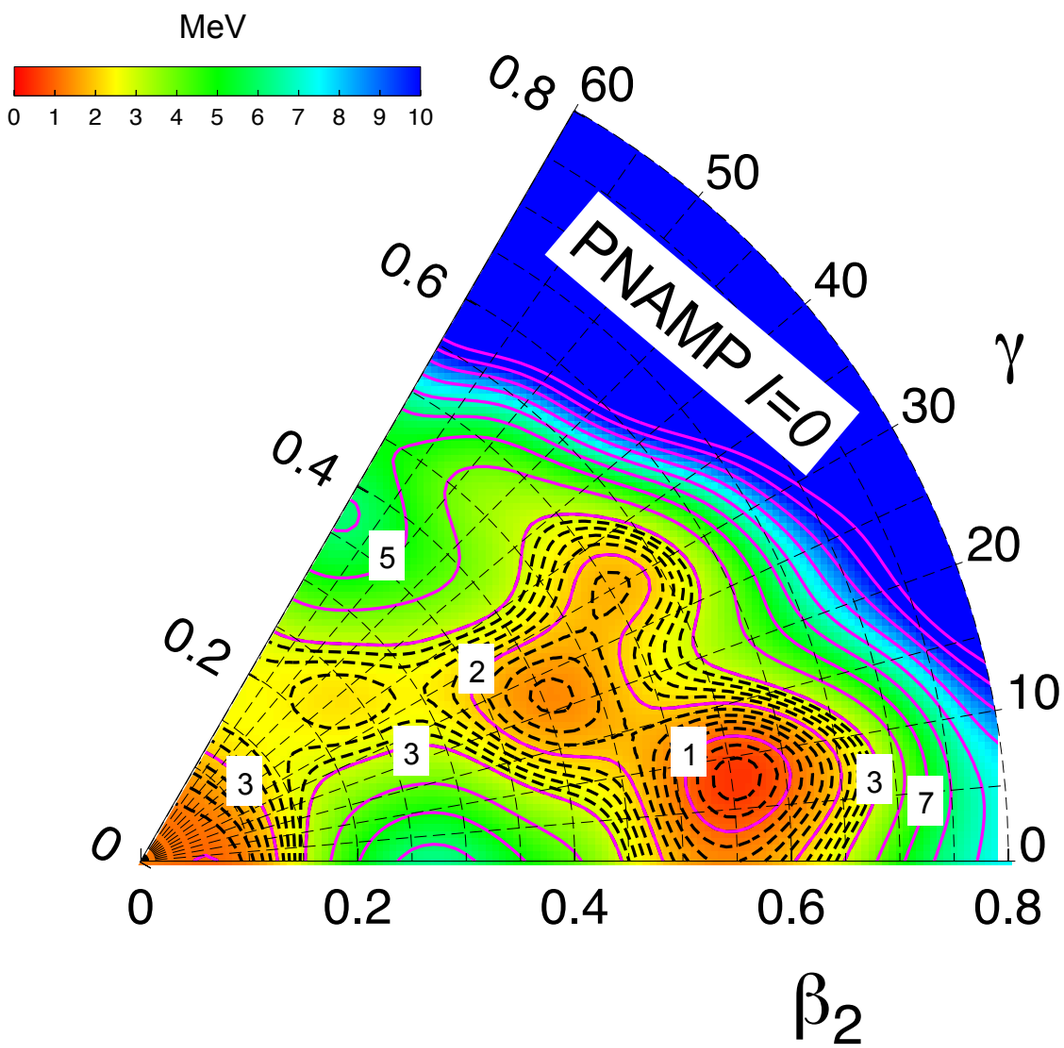

- Five minima are closer in energy whenever the rotational invariance is restored.
- Absolute minima corresponds to deformed configuration β_2~0.55
- Barriers between the minima are less than 1 MeV. **Mixing?**

T. R. R., J. L. Egido, Phys. Lett. B 705, 255 (2011)

Example: Multiple shape coexistence in ^{80}Zr

Relevance of angular momentum projection

(Similar feature as in ^{32}Mg, see R. Rodriguez-Guzmán et al., Nucl. Phys. A 709, 201 (2002))

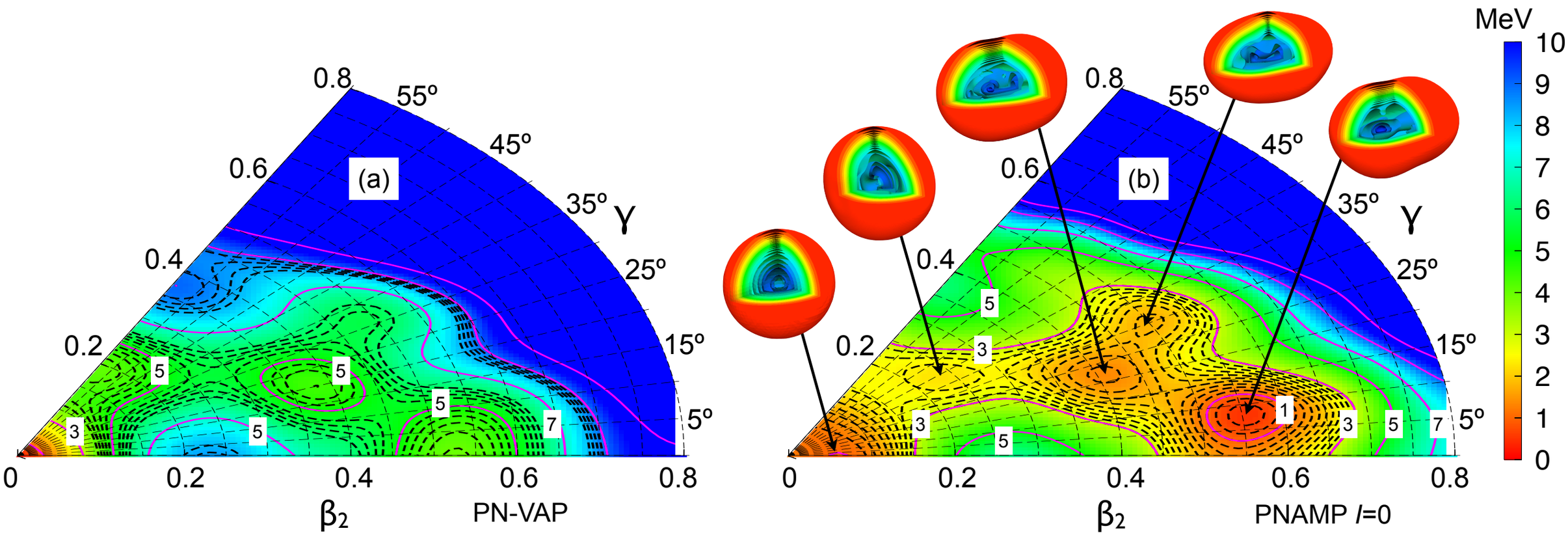

Multiple shape coexistence in ^{80}Zr

Configuration mixing within the framework of the **Generator Coordinate Method (GCM). *K* and deformation mixing**

$$|IM;NZ\sigma\rangle = \sum_{K\beta\gamma} f^{I;NZ,\sigma}_{K\beta\gamma} |IMK;NZ;\beta\gamma\rangle$$

$$\sum_{K'\beta'\gamma'} \left(\mathcal{H}^{I;NZ}_{K\beta\gamma K'\beta'\gamma'} - E^{I;NZ;\sigma} \mathcal{N}^{I;NZ}_{K\beta\gamma K'\beta'\gamma'} \right) f^{I;NZ;\sigma}_{K'\beta'\gamma'} = 0$$

-Several rotational bands and gamma bands partners associated to the different minima of the potential energy surfaces.

- Axial ground state rotational band in agreement with the experimental levels
(relevance of beyond-mean-field effects).

- Two triaxial rotational bands.

- Four excited 0^+ minima within a range of ~2.25 MeV ⇒ MULTISHAPE COEXISTENCE

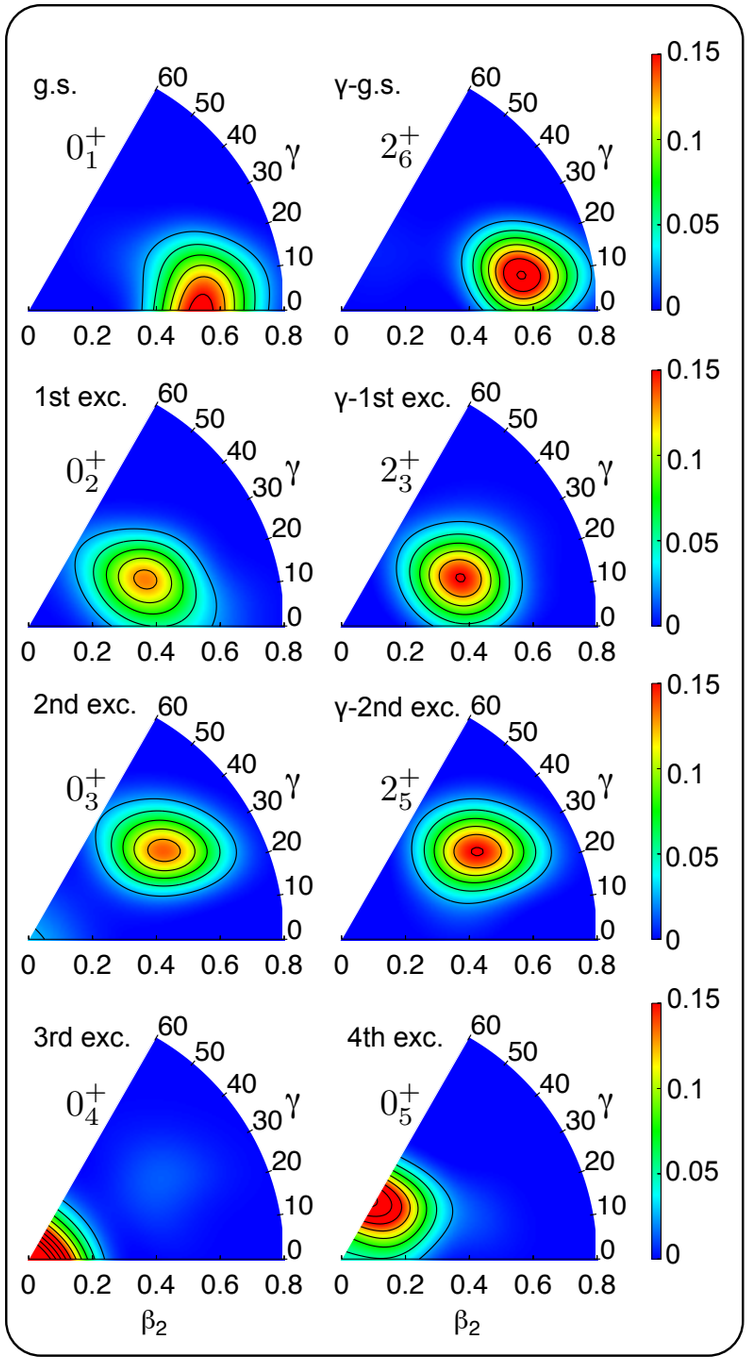

Multiple shape coexistence in ^{80}Zr

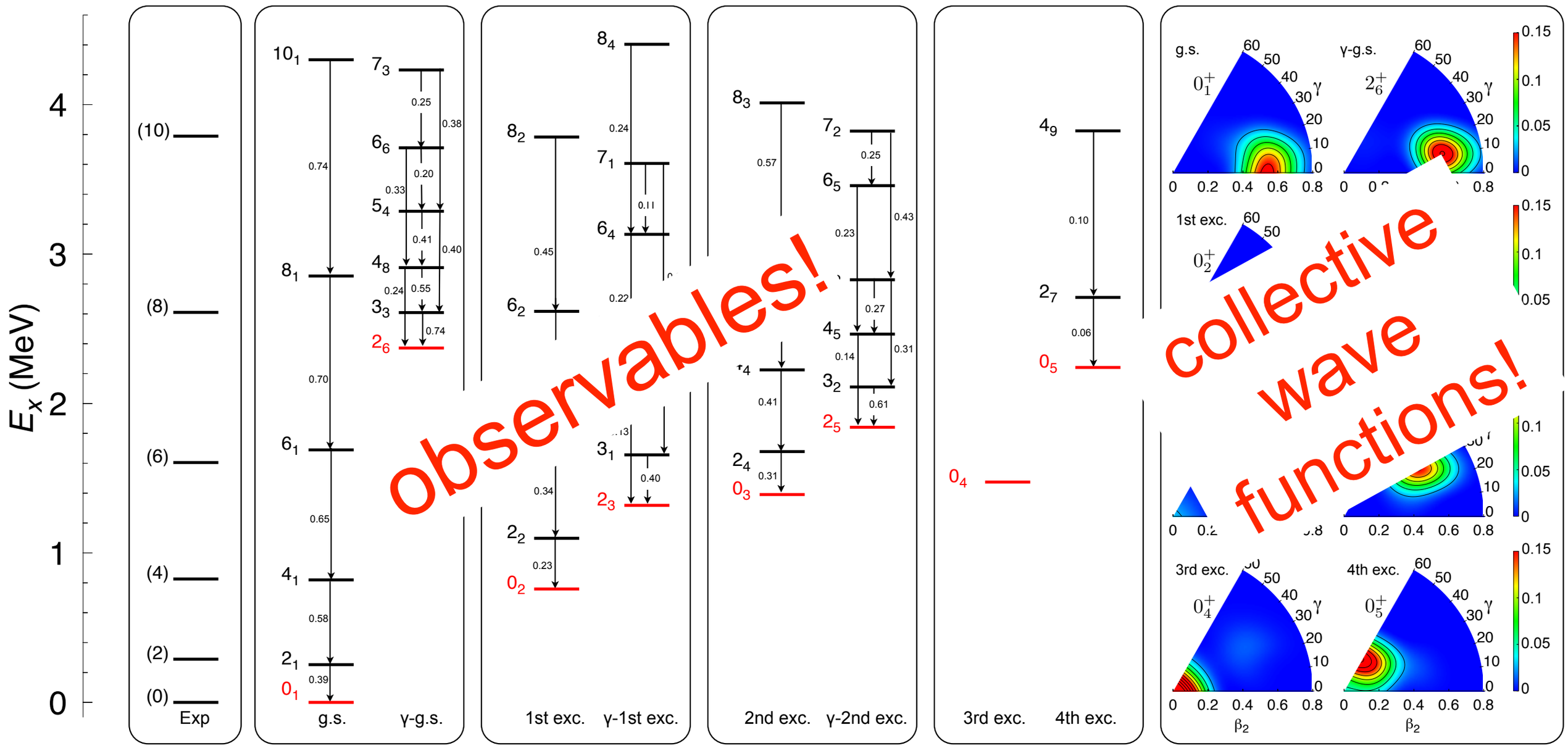

T. R. R., J. L. Egido, Phys. Lett. B 705, 255 (2011)

PN-VAP energy surfaces

Shape evolution in cadmium isotopes

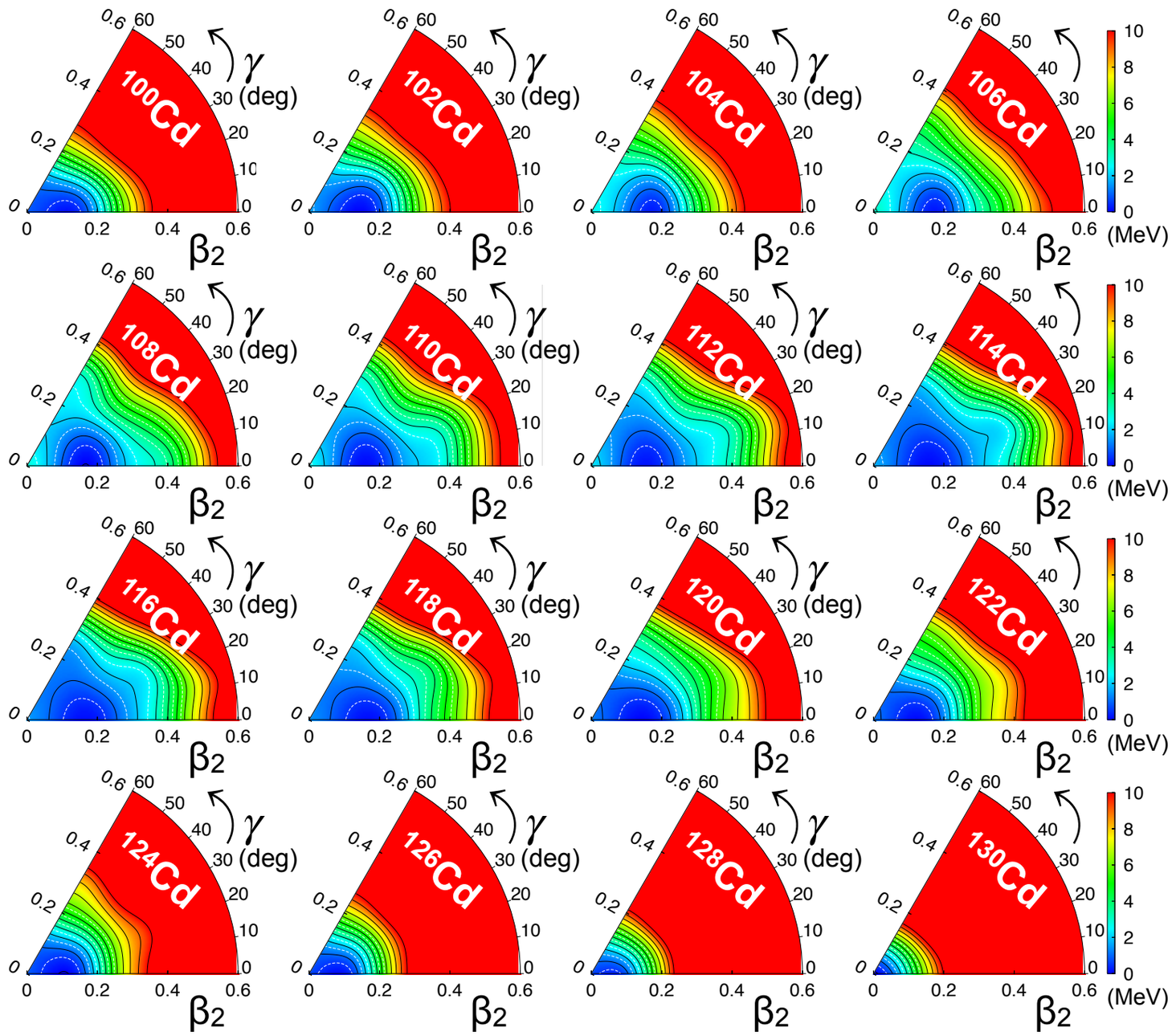

➡ Slightly prolate deformed minima are found along the whole isotopic chain.

➡ Deformation is larger (and almost constant) in the mid-shell and smaller when approaching to the magic neutron numbers (N = 50, 82).

➡ A depression at β_2~0.35, γ~20 is found in $^{110\text{-}118}$Cd.

M. Siciliano et al., Physical Review C 104, 034320 (2021)

Collective wave functions

- Shape evolution in cadmium isotopes

0_1^+

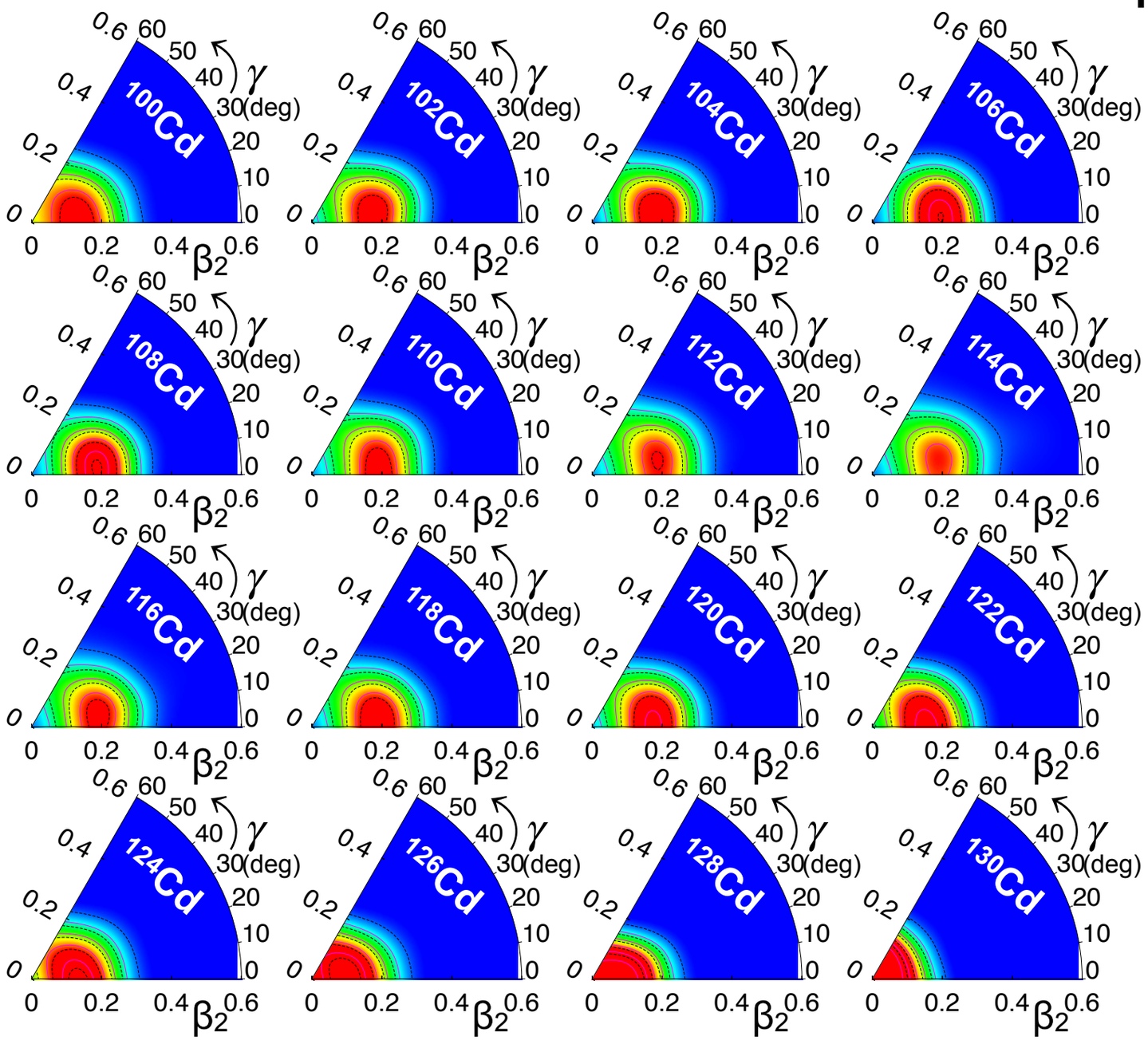

➡ Slightly prolate deformed ground state collective wave functions are found after performing PGCM.

➡ Deformation is larger (and almost constant) in the mid-shell and smaller when approaching to the magic neutron numbers (N = 50, 82).

M. Siciliano et al., Physical Review C 104, 034320 (2021)

Collective wave functions

- Shape evolution in cadmium isotopes

2_1^+

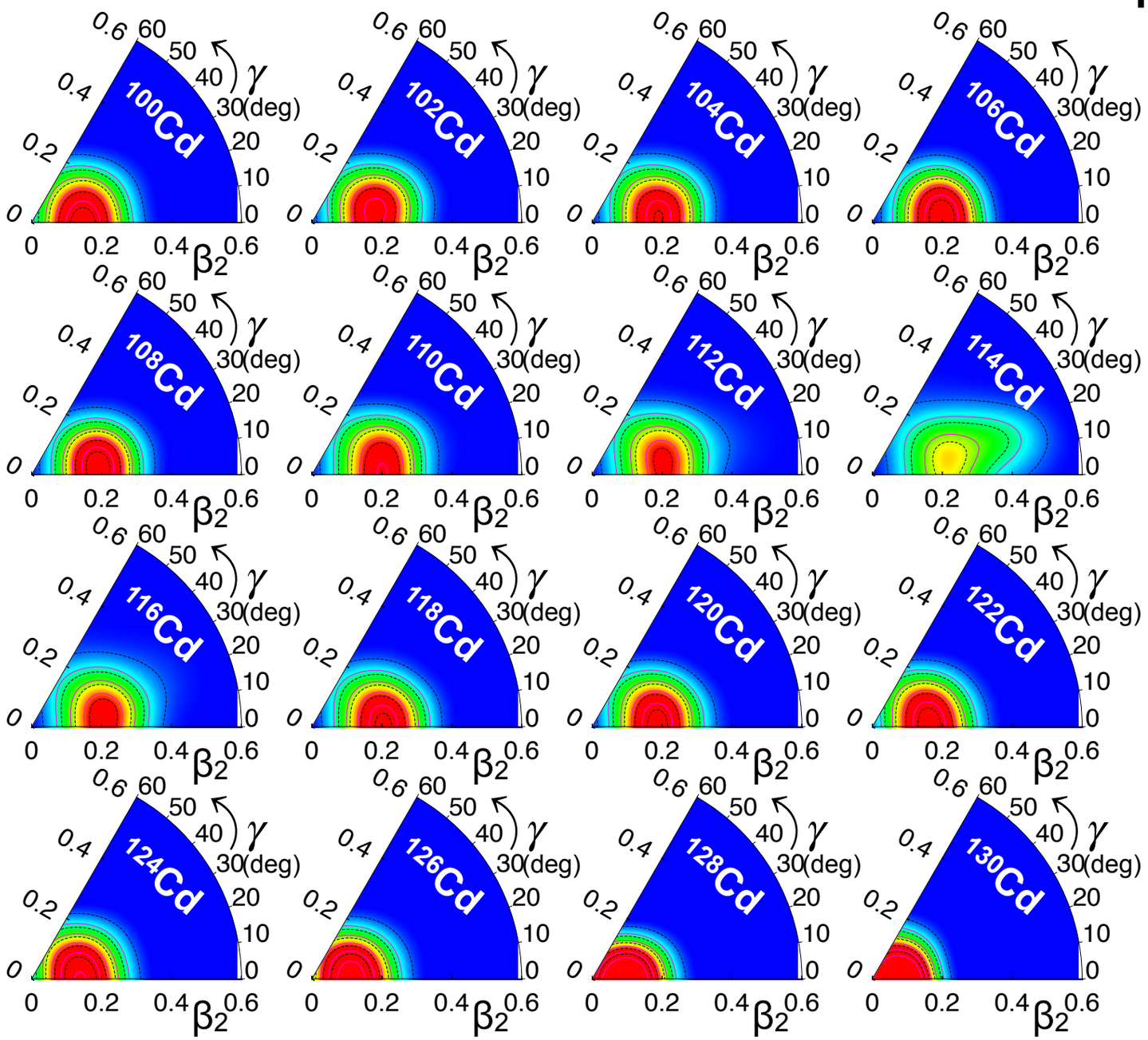

➡ Slightly prolate deformed 2_1^+ collective wave functions are found after performing PGCM.

➡ Similar to the 0_1^+ collective wave functions except for ^{114}Cd.

M. Siciliano et al., Physical Review C 104, 034320 (2021)

Collective wave functions

Shape evolution in cadmium isotopes

4_1^+

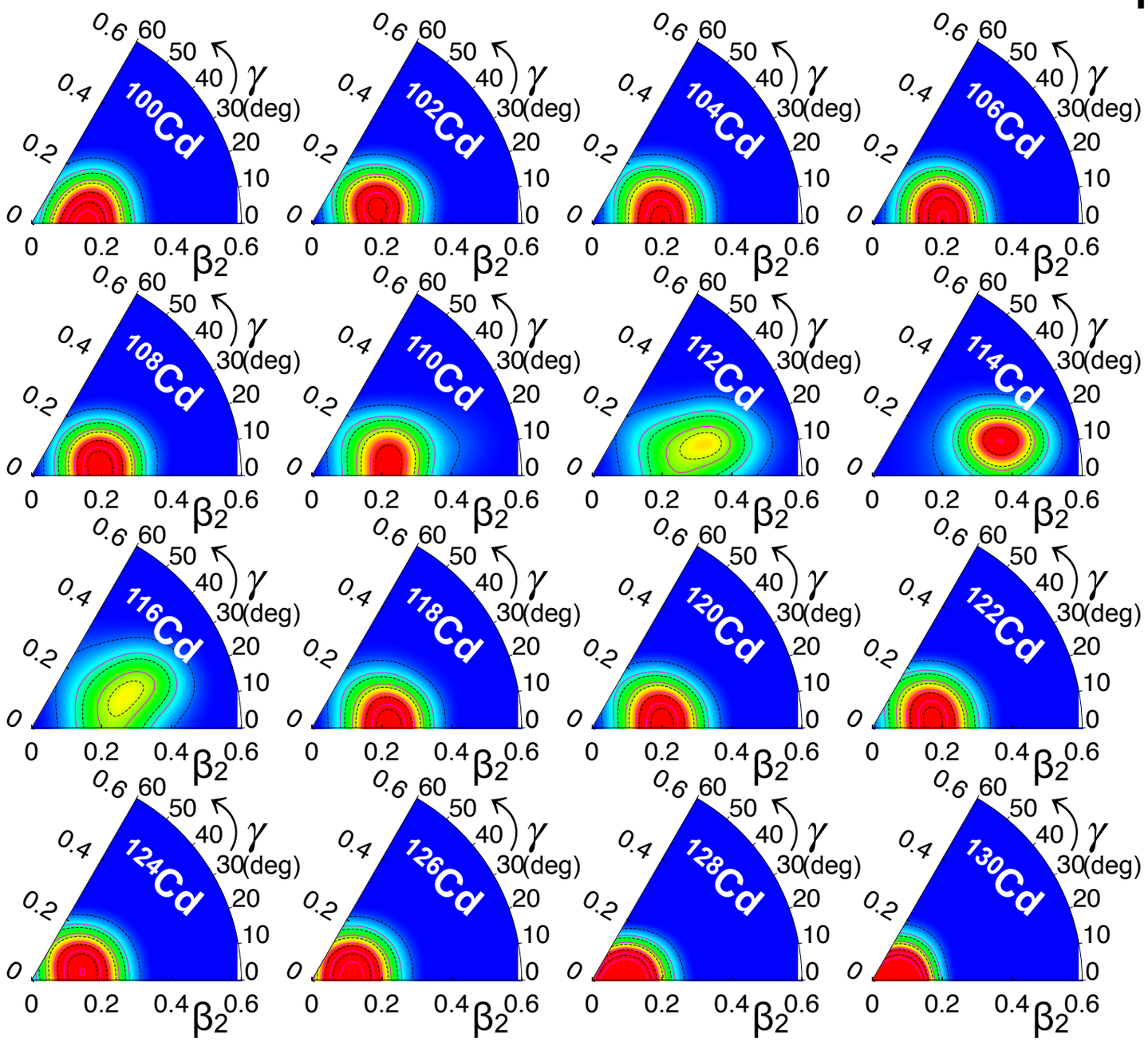

Shape evolution in cadmium isotopes

➡ Slightly prolate deformed 4_1^+ collective wave functions are found after performing PGCM except for $^{112\text{-}116}$Cd.

M. Siciliano et al., Physical Review C 104, 034320 (2021)

PGCM with triaxial quadrupole

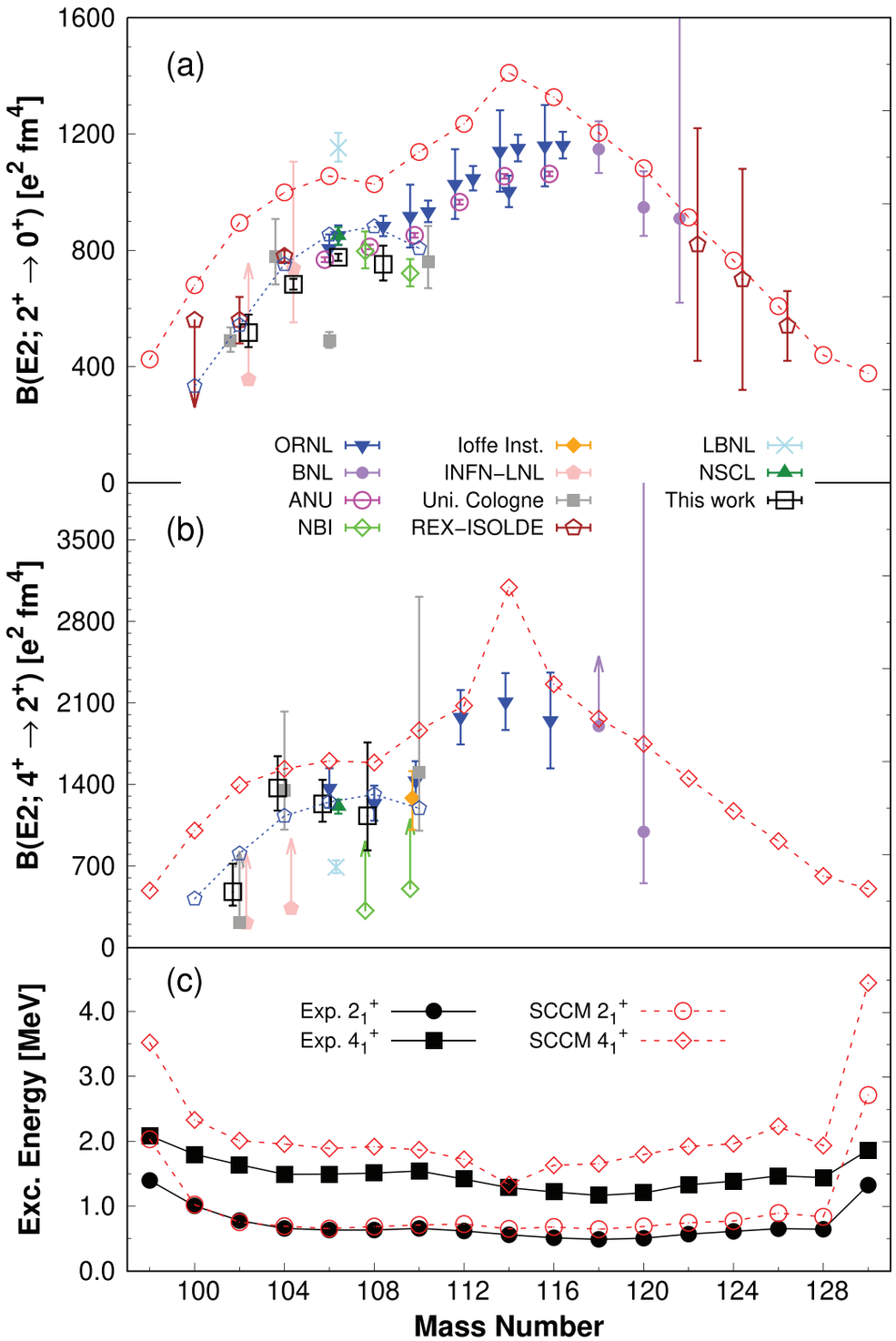

Shape evolution in cadmium isotopes

- ➡ Qualitative good agreement between theory and experiment for excitation energies and transition probabilities in the whole isotopic chain.
- ➡ 2^+, 4^+ excitation energies are stretched (lack of cranking components) although some 2^+ energies are on top of the experimental data, meaning that the deformation could be overestimated.
- ➡ B(E2) are systematically larger than the experimental data (deformation overestimated).
- ➡ $^{126\text{-}128}$Cd lowering of the 2^+ is well-reproduced contrary to most of the shell model calculations that predict a parabolic trend.
- ➡ Poor reproduction of excitation energies at the magic numbers (problems to describe pure spherical single-particle excitations)

M. Siciliano et al., Physical Review C 104, 034320 (2021)

PGCM with triaxial quadrupole

Experiment

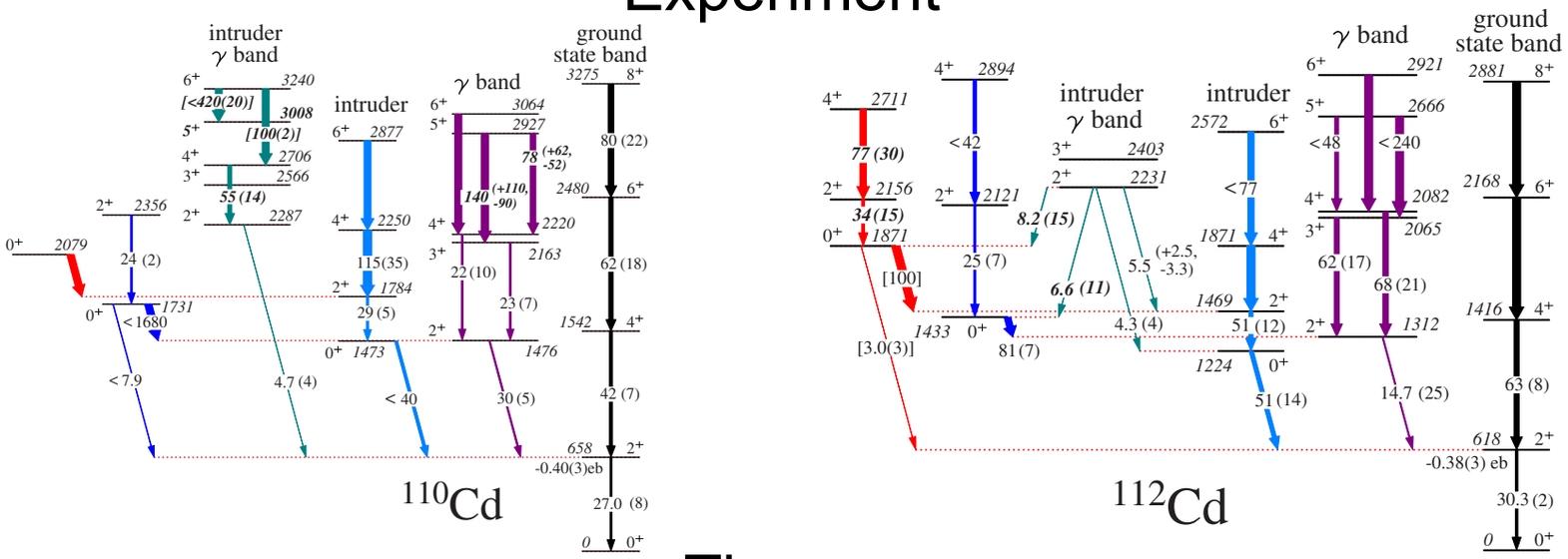

Theory

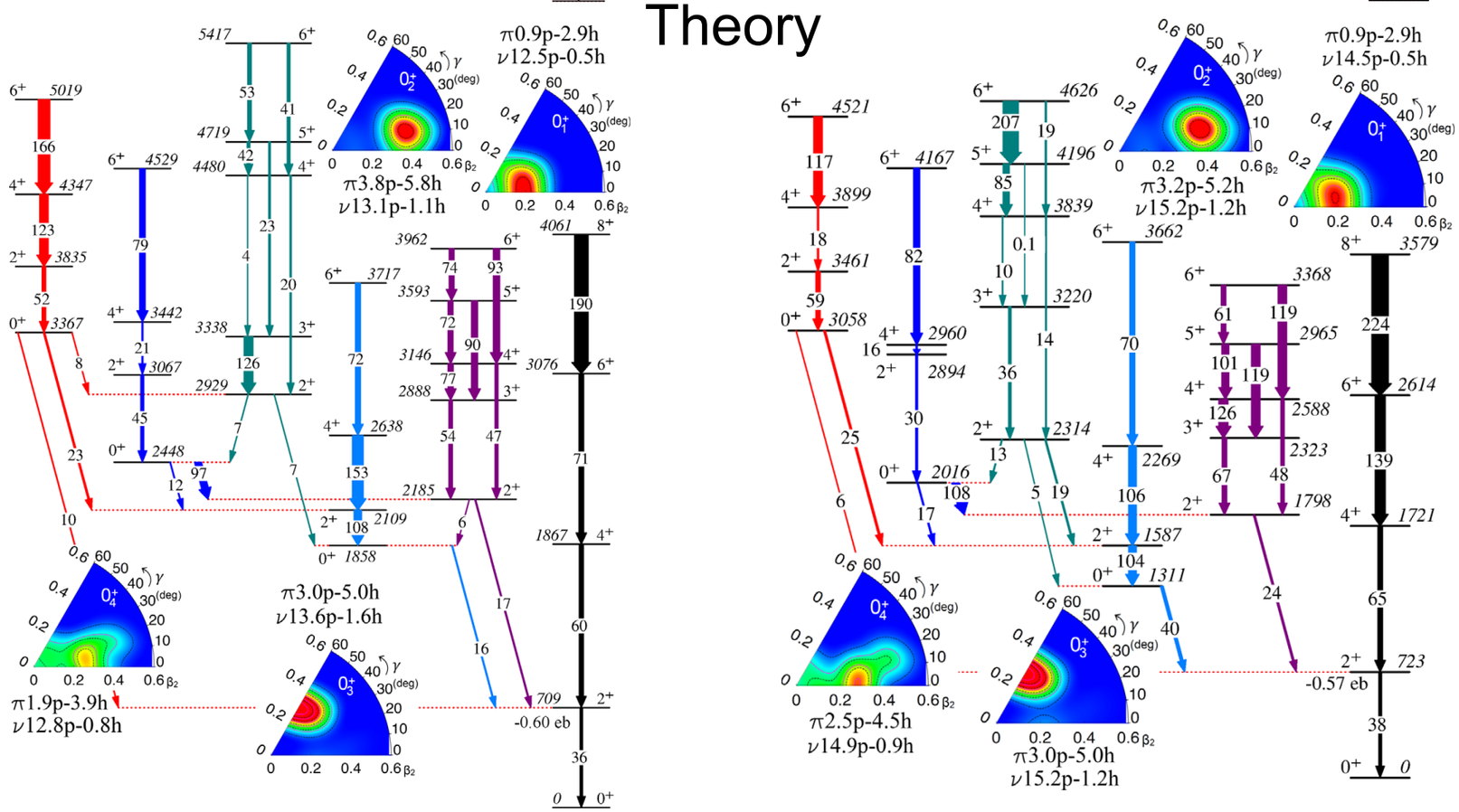

- Shape coexistence in stable cadmium isotopes

➡ Qualitative good agreement between theory and experiment for excitation energies and transition probabilities.

➡ Prolate slightly deformed ground state bands are predicted.

➡ Different bands correspond to different shapes.

➡ Different bands corresponds to different spherical shell occupancies

P. Garrett et al., Physical Review Letters 123, 142502 (2019)

Spherical HF occupation numbers

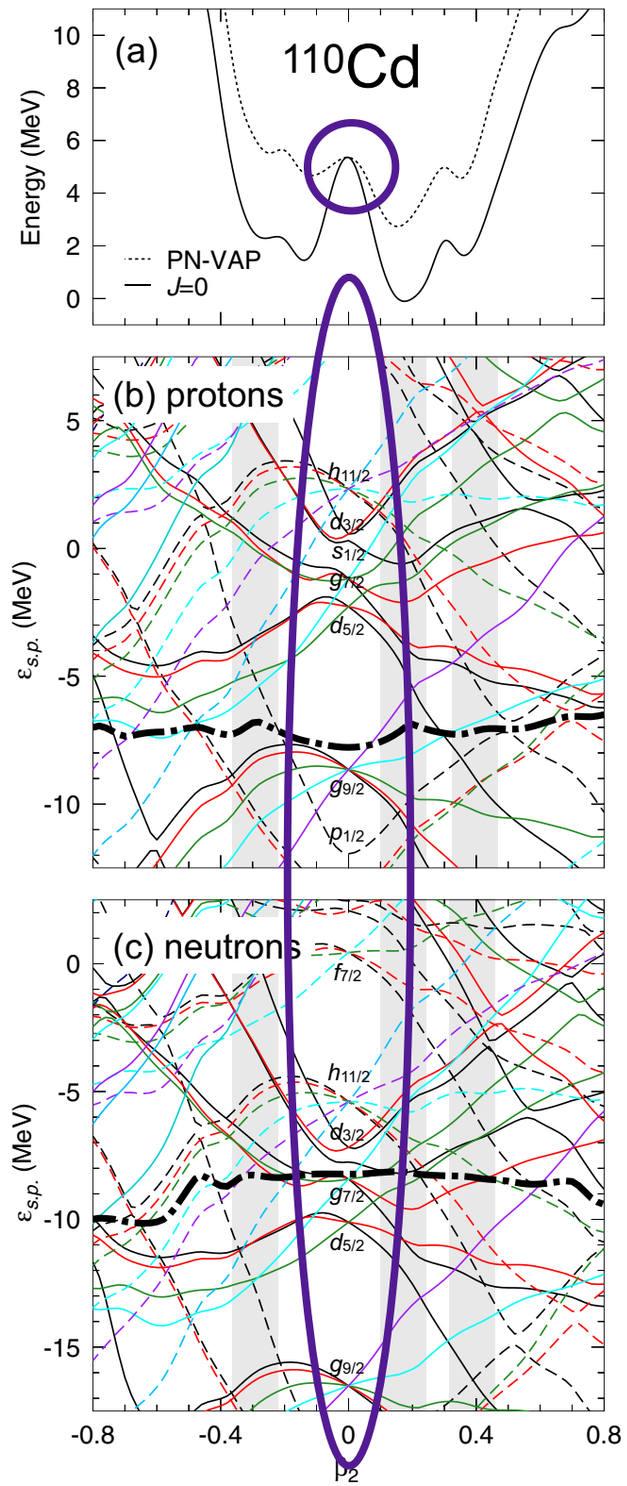

The spherical HFB wave function defines the spherical ("shell model like") orbits.

$$\hat{n}_\alpha = \sum_{m_\alpha} a^\dagger_{n_\alpha l_\alpha j_\alpha m_{j_\alpha}} a_{n_\alpha l_\alpha j_\alpha m_{j_\alpha}}$$

We can compute the number of particles occupying these spherical orbits in the full PGCM state

$$n_\alpha^{I;NZ;\sigma} = \langle I;NZ;\sigma|\hat{n}_\alpha|I;NZ;\sigma\rangle$$

Spherical HF occupation numbers

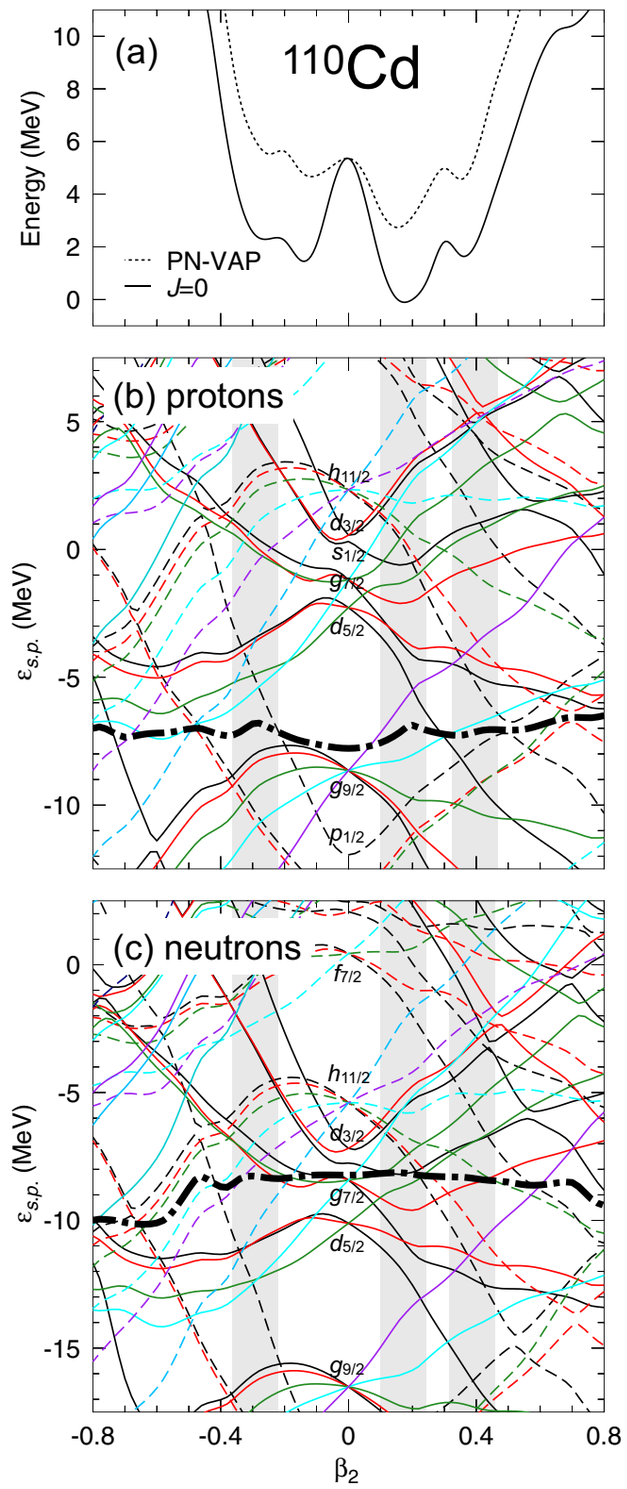

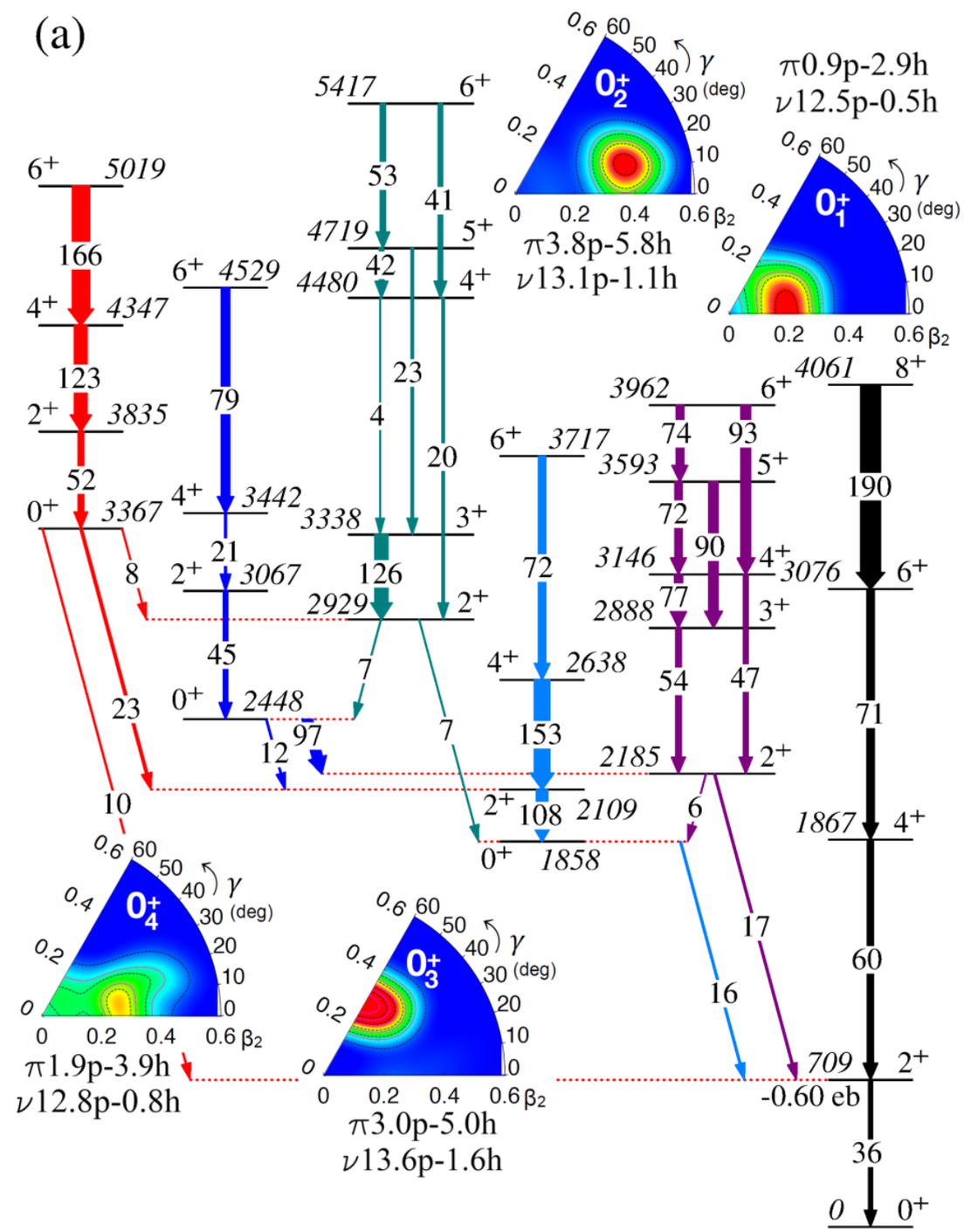

P. Garrett et al., Physical Review C 101, 044302 (2020)

PGCM with triaxial quadrupole

- Even-even palladium isotopes $^{96\text{-}118}$Pd

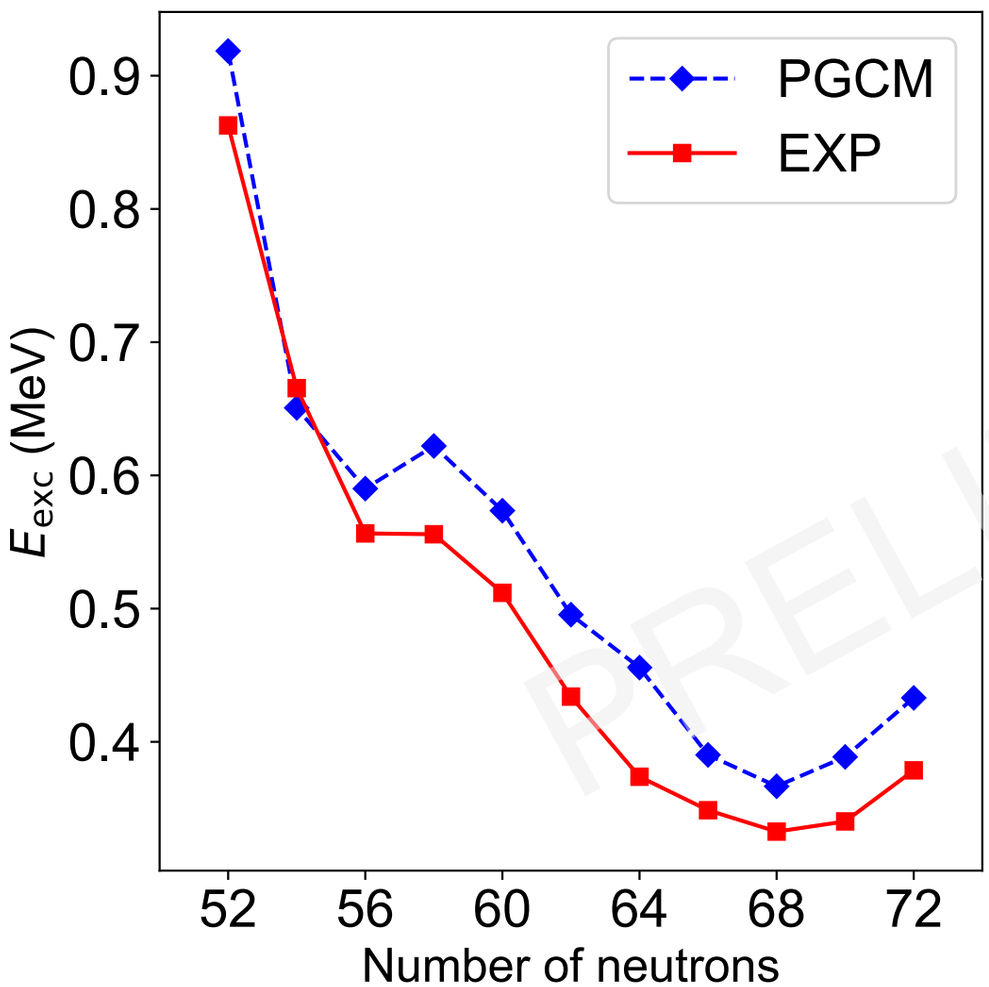

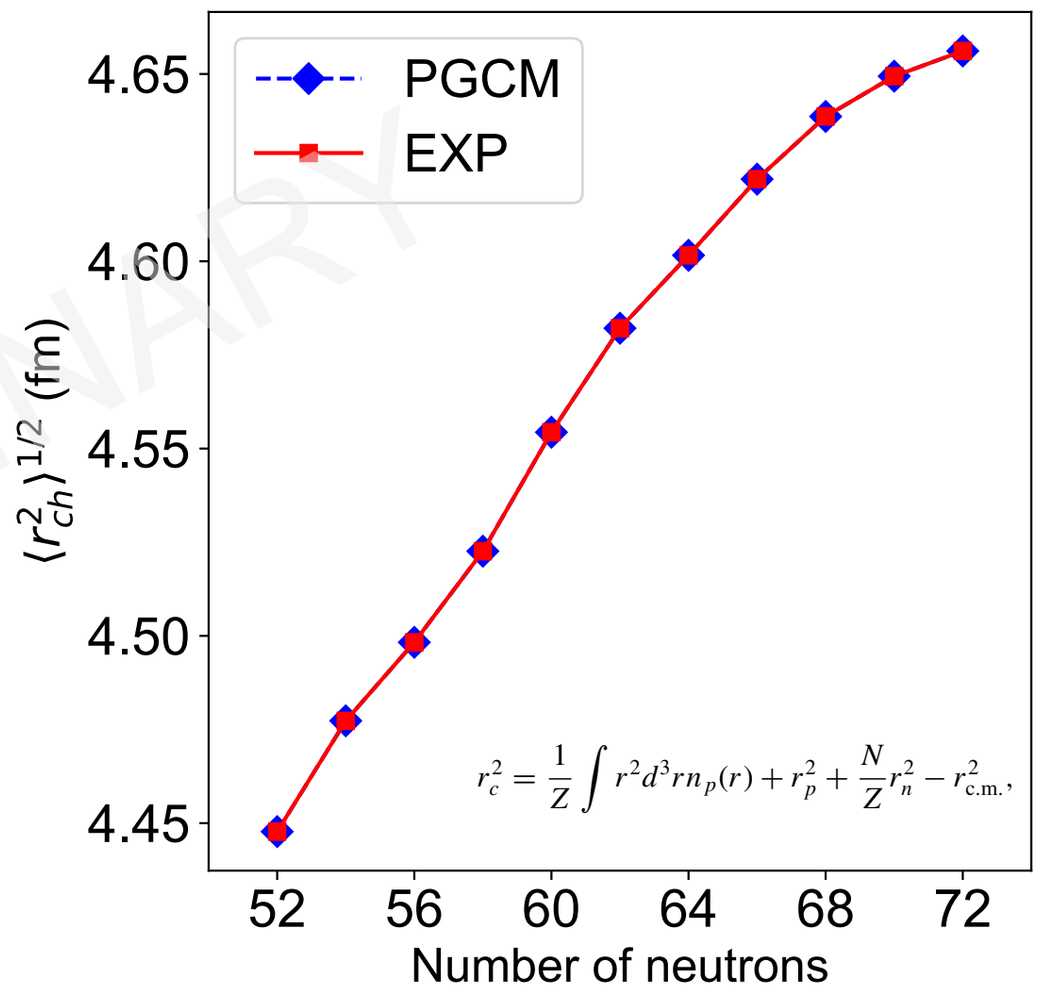

A. Ortiz-Cortes et al., in preparation

Outline

PGCM with triaxial quadrupole+cranking

- Initial intrinsic states: PN-VAP

$$E^{N,Z}[\Phi] = \frac{\langle\Phi|\hat{H}_{2b}\hat{P}^N\hat{P}^Z|\Phi\rangle}{\langle\Phi|\hat{P}^N\hat{P}^Z|\Phi\rangle} - \varepsilon_{DD}^{N,Z}(\Phi) - \lambda_{q_{20}}\langle\Phi|\hat{Q}_{20}|\Phi\rangle - \lambda_{q_{22}}\langle\Phi|\hat{Q}_{22}|\Phi\rangle - \omega\langle\Phi|\hat{J}_x|\Phi\rangle$$

cranking term!!

- Intermediate Particle Number and Angular Momentum Projected states

$$|IMK;NZ;\beta\gamma;\omega\rangle = \frac{2I+1}{8\pi^2}\int \mathcal{D}^{I*}_{KK'}(\Omega)\hat{R}(\Omega)\hat{P}^N\hat{P}^Z|\Phi(\beta,\gamma,\omega)\rangle d\Omega$$

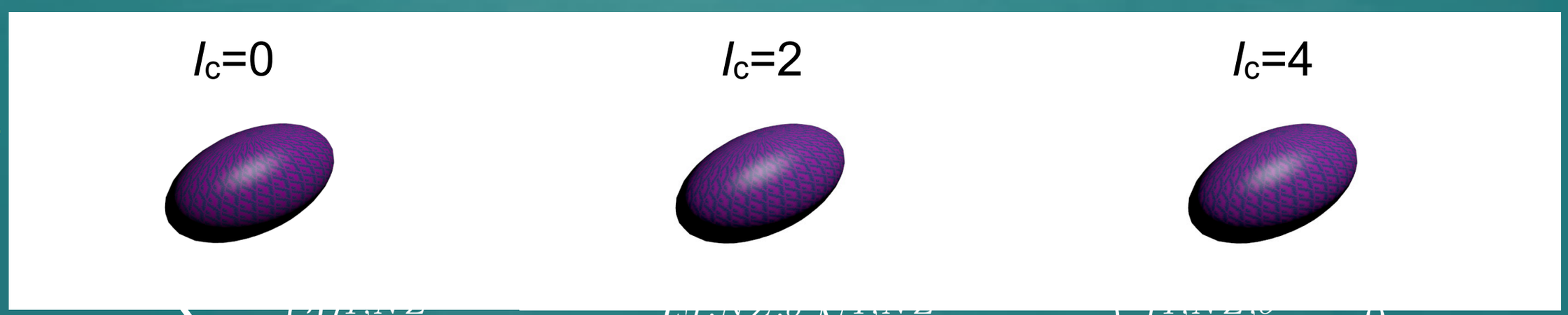

$$\sum_{K'\beta'\gamma'\omega'}\left(\mathcal{H}^{I,NZ}_{K\beta\gamma\omega;K'\beta'\gamma'\omega'} - E^{I,NZ,\omega}\mathcal{N}^{I,NZ}_{K\beta\gamma\omega;K'\beta'\gamma'\omega'}\right)f^{I,NZ,\omega}_{K'\beta'\gamma'\omega'} = 0$$

Example: ^{44}S isotope

➡ Large transition probability from $2^+ \rightarrow 0^+$ suggests the erosion of *N*=28 shell closure
(T. Glasmacher et al., Phys. Lett. B 395, 163 (1997)).

➡ Low-lying 0_2^+ state suggests shape coexistence in this nucleus
(S. Grévy et al., Eur. Phys. J. A 25, 111 (2005), C. Force et al., Phys. Rev. Lett. 105, 102501 (2010)).

➡ Very low $4_1^+ \rightarrow 2_1^+$ transition suggests a *K*=4 isomeric state in the low-lying spectrum
(D. Santiago-Gonzalez et al., Phys. Rev. C 83, 061305 (2011)).

➡ Shell Model calculations suggest that 4_1^+ is an isomeric state with *K*=4 dominance
(Y. Utsuno et al., Phys. Rev. Lett. 114, 032501 (2015)).

➡ Isomeric character of the 4_1^+ is confirmed experimentally
(J.J. Parker IV et al., Phys. Rev. Lett. 118, 052501 (2017)).

PN-VAP and PN-AM- projected energies

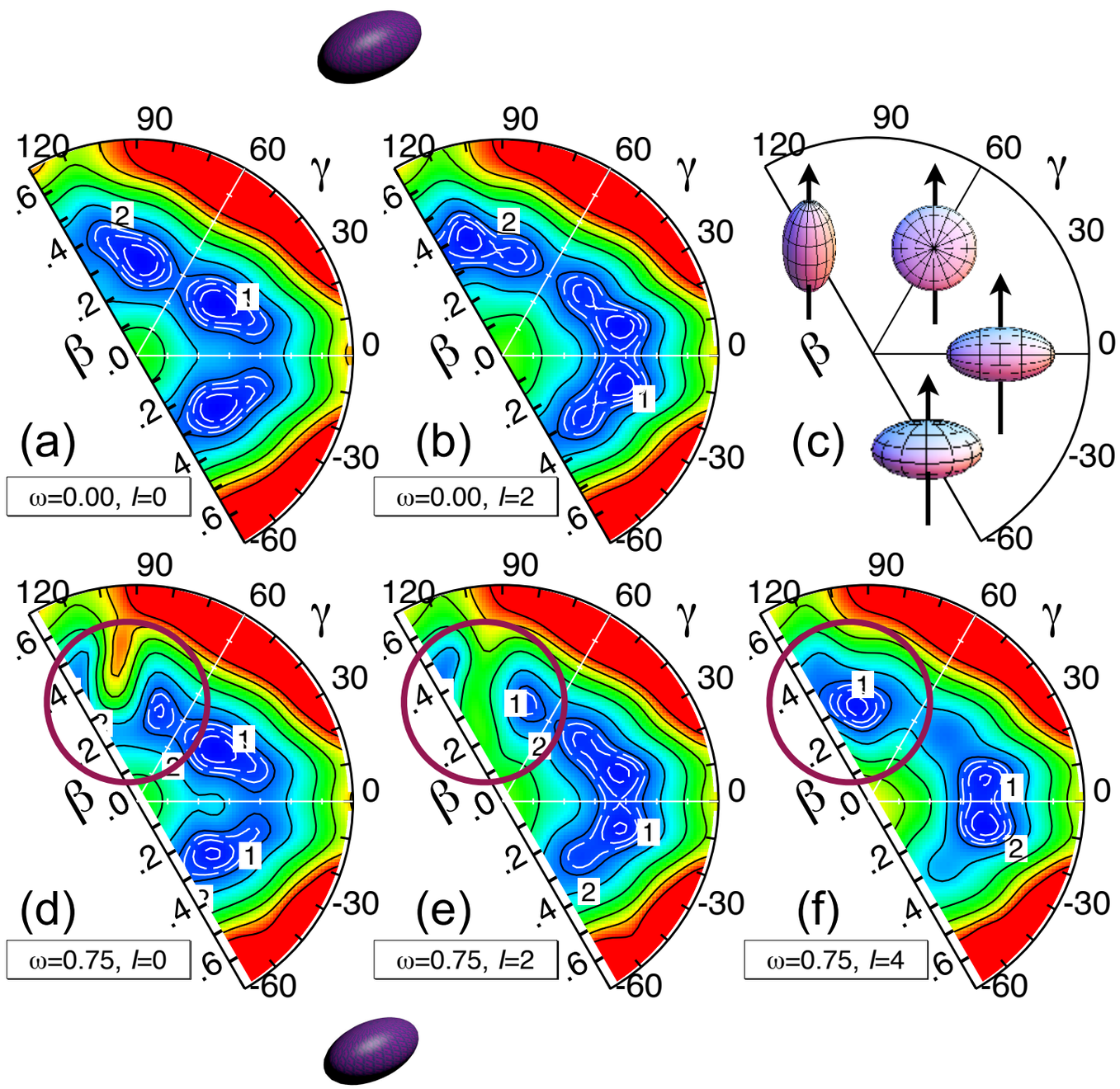

- For =0.00, we find the symmetry in the three sextants.
- For =0.75, a neutron aligned two-quasiparticle is obtained near =90º ($f_{7/2}$-$p_{3/2}$ nature, $K_x = 4$).
- Both collective and single-particle degrees of freedom can be included within this framework.

J.L. Egido, M. Borrajo, T.R.R., PRL 116, 052502 (2016)

PGCM with triaxial quadrupole+cranking

Spectrum

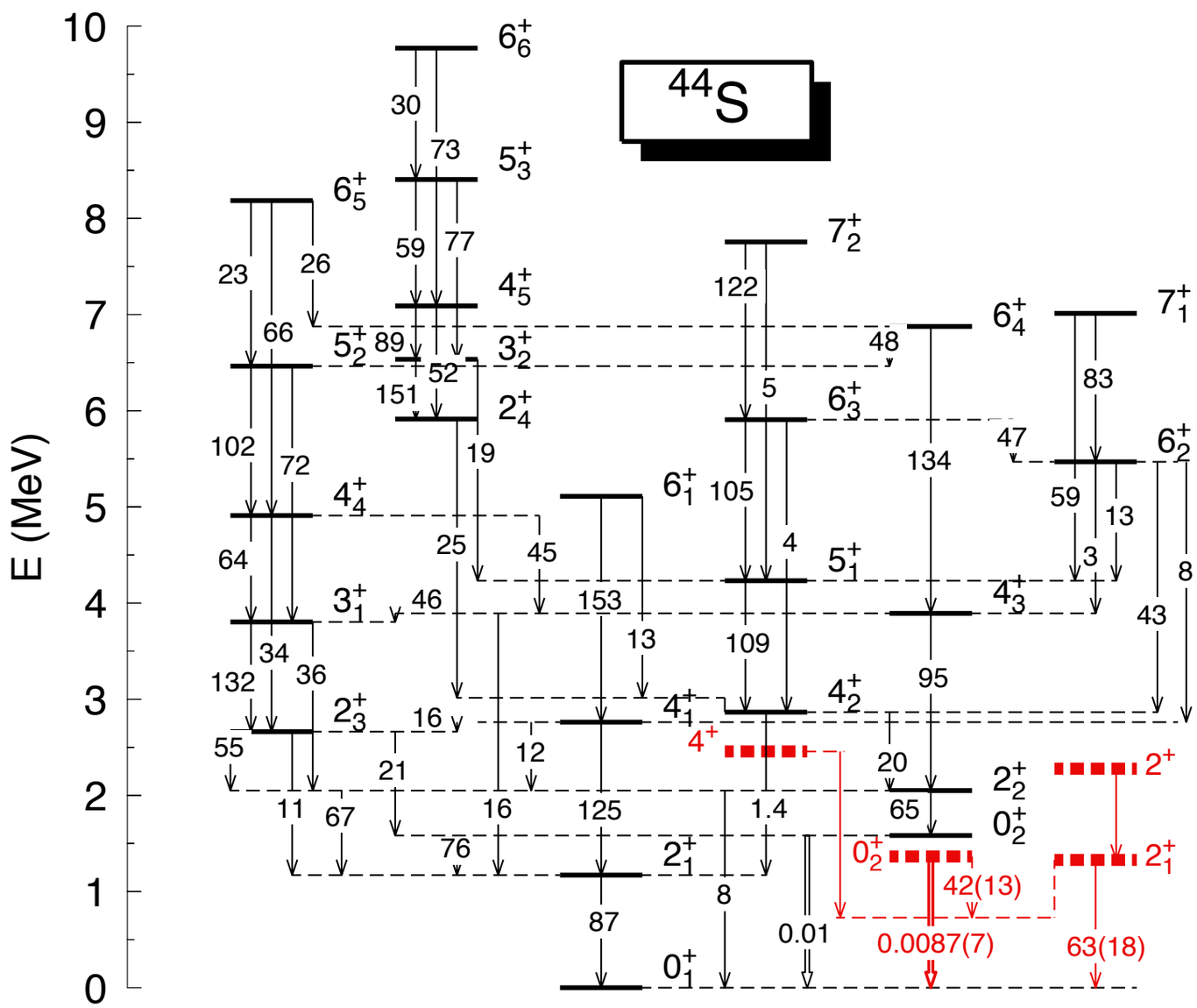

Collective wave functions

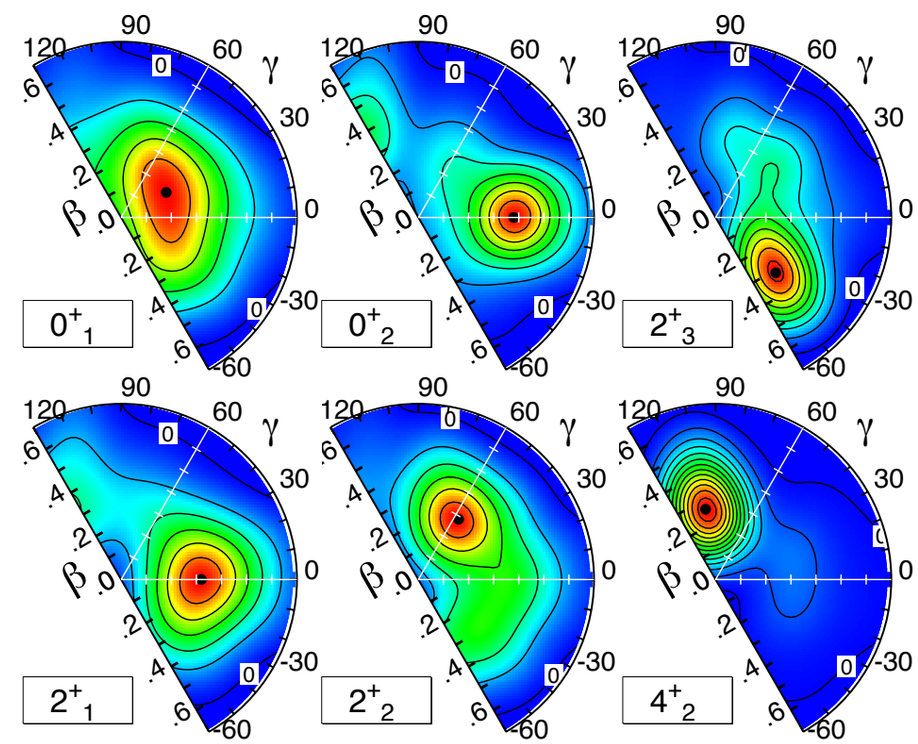

J.L. Egido, M. Borrajo, T.R.R., PRL 116, 052502 (2016)

PGCM with triaxial quadrupole+cranking

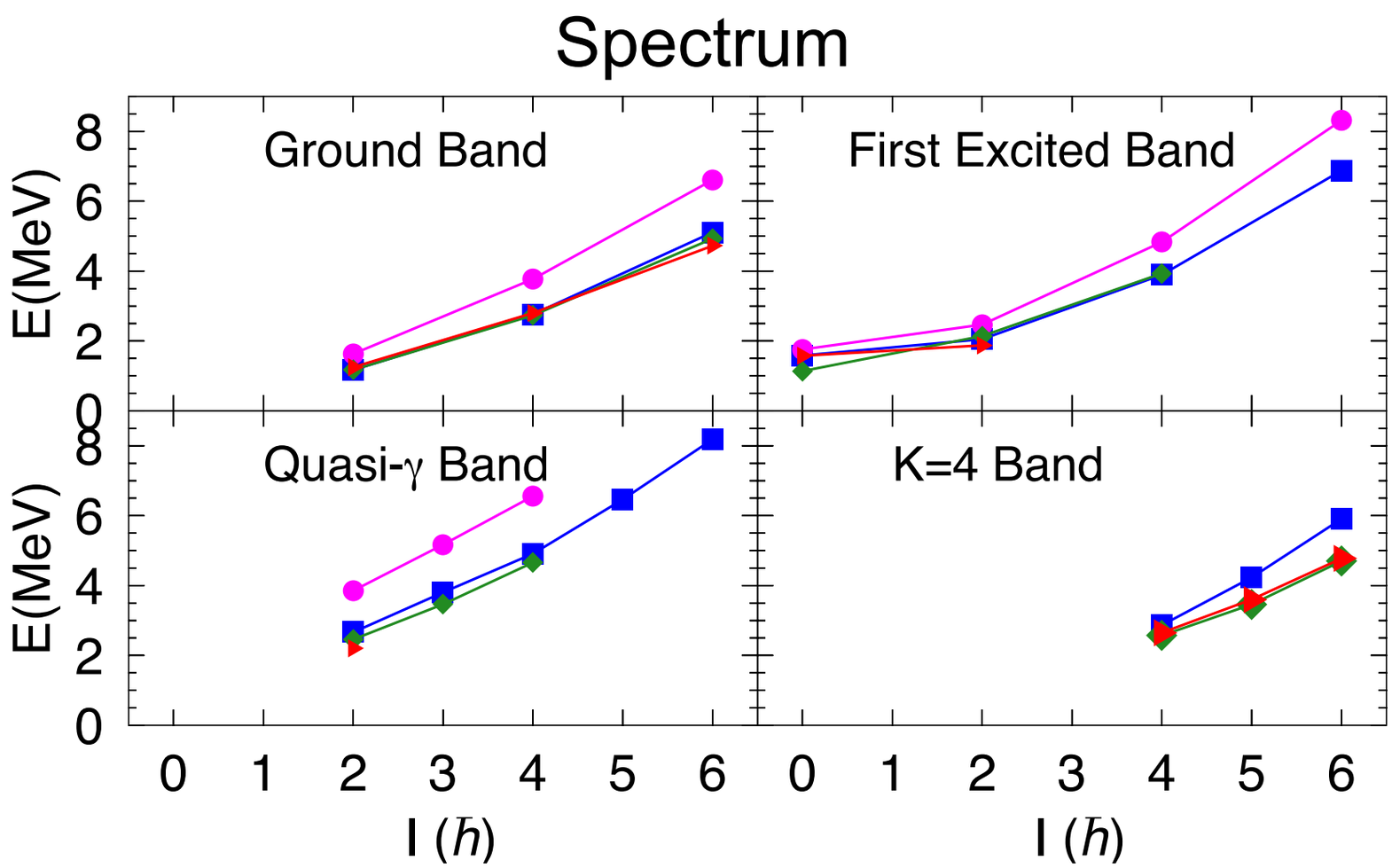

FIG. 4: (Color online) Comparison of several theories: Triangles, red lines, Tokyo group [22]; diamonds, green lines, Madrid-Strasbourg collaboration [31]; boxes, blue lines, this work; circles, magenta lines, our former work without angular frequency dependence [20].

- Very good agreement (both quantitative and qualitative) with state-of-the-art shell model calculations when cranking is taken into account.
- Quantitative agreement if only static shapes are considered.

J.L. Egido, M. Borrajo, T.R.R., PRL 116, 052502 (2016)

Compression of the spectrum I: Magnesium isotopes

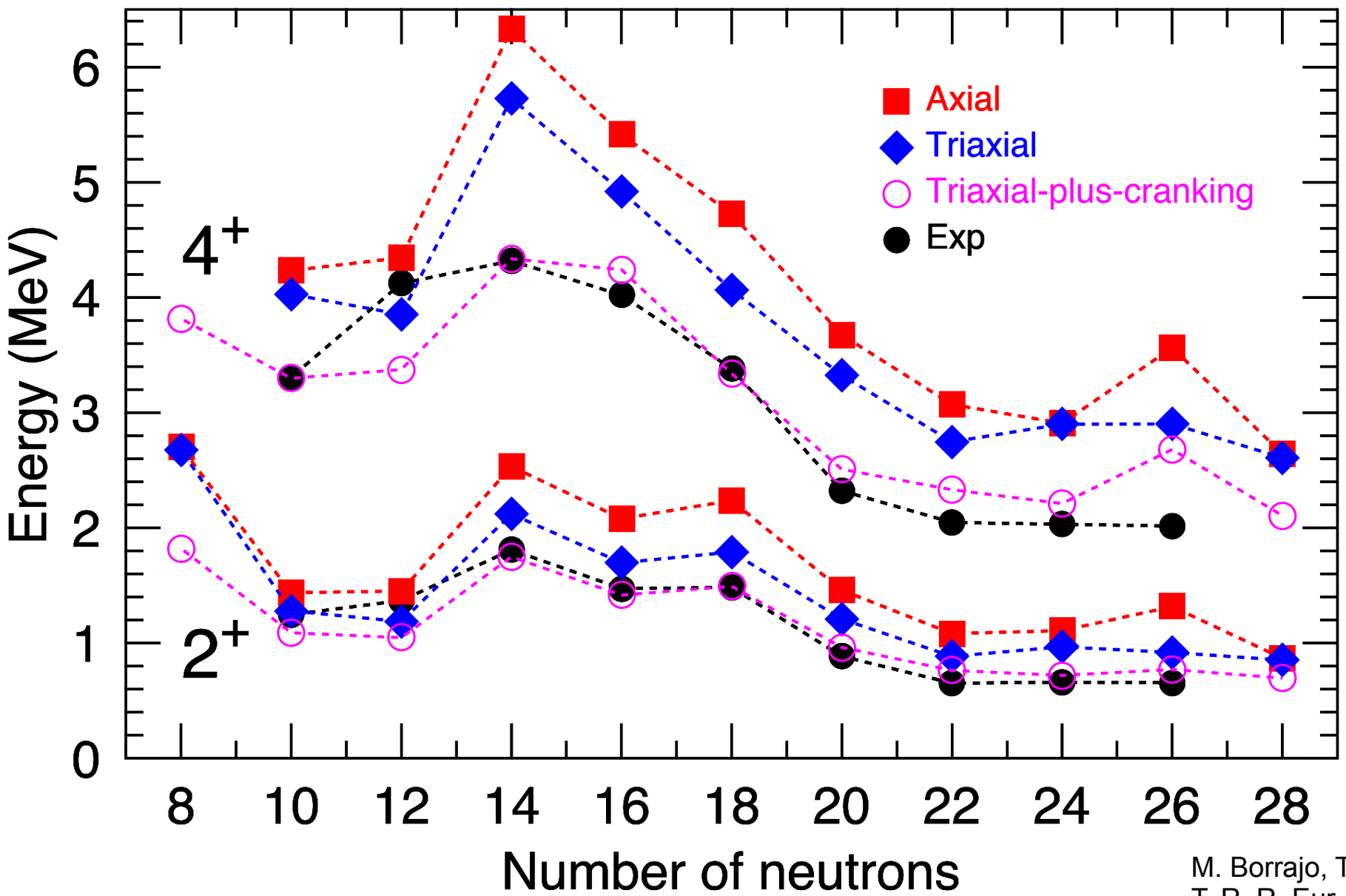

M. Borrajo, T.R.R, J.L. Egido, PLB 746, 341 (2015)
T. R. R. Eur. Phys. J. A 52, 190 (2016).

PGCM with triaxial quadrupole+cranking

Compression of the spectrum II: Calcium isotopes

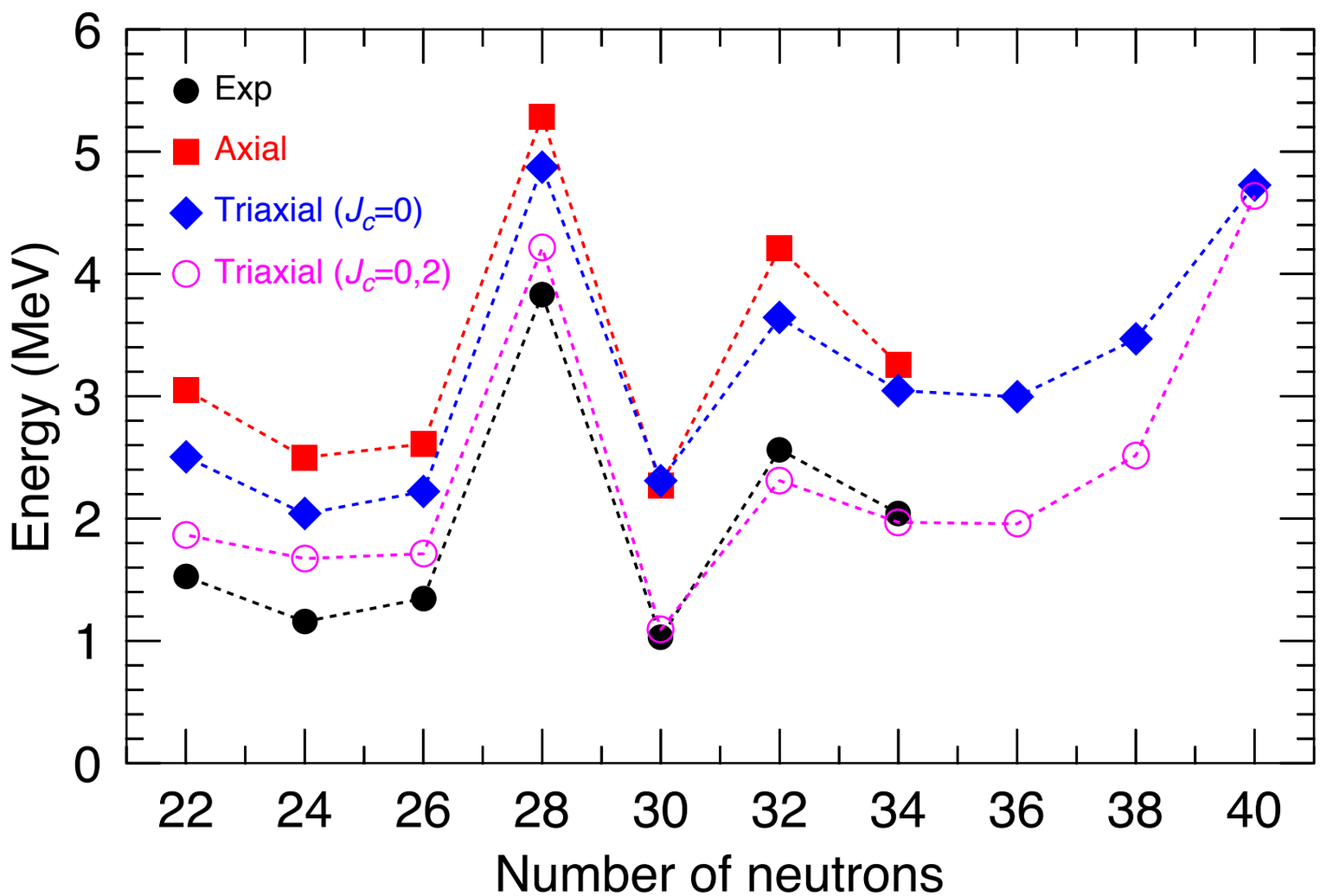

L. M. Robledo., T. R. R., R. Rodríguez-Guzmán, J. Phys. G 46, 013001 (2019)

Outline

Summary and Outlook

- PGCM methods provide a reliable description of nuclear structure observables and they provide the perfect tools to study shape transitions/ mixing/coexistence in nuclei.

- It is a very flexible method to approach exact solutions.

- Breaking of:

  - parity allows for a good description of negative parity states.

  - axial symmetry is needed to study properly shape evolution/shape coexistence in many isotopic chains.

  - time-reversal symmetry (cranking states) allows for a quantitative agreement with the experimental energy spectra.

Summary and Outlook

- Quasiparticle states:

Odd-nuclei (Bally, Bender, Heenen, Borrajo, Egido).
Single-particle excitations.

- pn pairing.
- Angular momentum projection and mixing of quasiparticle excitations.
- Generic interactions beyond Gogny (more ab initio based interactions).

* B. Bally, A. Sánchez, T. R. R., EPJA 57, 69 (2021)

Acknowledgments

L. M. Robledo
R. Bernard
J. L. Egido
P. Garrett
M. Borrajo
A. Poves
F. Nowacki
B. Bally

Thank you!